The Jordan Journal of Earth and Environmental Sciences (JJEES)

JJEES is an international peer-reviewed research journal, issued by the Deanship of Academic Research and Graduate Studies, the Hashemite University, in corporation with, the Jordanian Scientific Research Support Fund, the Ministry of Higher Education and Scientific Research.

SUBMISSION ADDRESS:

Professor **Abdul Rahim A. Hamdan**
Deanship of Academic Research and Higher Studies
Hashemite University, P.O. Box 330127, Postal Code 13133, Zarqa, Jordan.

Phone: +962-5-3903333 ext. 4151
E-Mail: jjees@hu.edu.jo , hamdan@hu.edu.jo

Hashemite Kingdom of Jordan

Hashemite University

Jordan Journal of Earth and Environmental Sciences

JJEES

An International Peer-Reviewed Scientific Journal

http:// jjees.hu.edu.jo/

ISSN 1995-6681

The Jordan Journal of Earth and Environmental Sciences (JJEES)

JJEES is an international peer-reviewed research journal, issued by the Deanship of Academic Research and Graduate Studies, the Hashemite University, in corporation with, the Jordanian Scientific Research Support Fund, the Ministry of Higher Education and Scientific Research.

Instructions to the Authors:

The Jordan journal of earth and environmental sciences (JJEES) is the national journal of Jordan in earth and environmental sciences. Indeed, it is an internationally refereed journal dedicated to the advancement and richness of scientific research. Furthermore, JJEES publishes research papers that address both theoretical and applied valuable subjects, which matters in the various fields of geosciences and environmental disciplines. JJEES is published quarterly by the Hashemite university. Academic specialists review submitted articles blindly and rigorously, and according their respected fields. The articles submitted may be authentic research papers, scientific reviews, and technical scientific notes.

Format Guide:

1. The research papers should be single sided, double-lined, and has a 30 mm space for all margins. In addition, the number of pages should not exceed 30 pages (7,500 words, font size 13). Authors should submit three copies of the paper and a floppy diskette 3.5 or a CD under (WinWord IBM) or by e-mail. The title page must list the full title and the names and affiliations of all authors (first name, middle name, and last name). Also, their addresses, including email, and their ranks/positions must be included. In addition, Authors should give the full address, including e-mail, telephone, and fax, of the author who is to check the proof.
2. The research must contain the title and abstract, keywords, introduction, methodology, results, discussion, and recommendations if necessary. Authors must use the system of international units. Furthermore, scientific abbreviations may be used; also, authors must mention them at first use in text. Include the name(s) of any sponsor(s) of the research contained in the paper, along with grant number(s).
3. Authors should submit abstracts in two languages, Arabic and English. In addition, authors should place the English abstract at the beginning of the paper, then follow it by the keywords, which must be placed before the introduction. However, Authors should place the Arabic abstract at the end of the paper, and on a separate sheet. In addition, each abstract should not contain more than 200 words.
4. Authors should number captions and tables consecutively, and according to their occurrence in the research with headings. Moreover, Authors should use the same consecutive numbers when mentioning captions and tables in the text. At the same time, they must type captions and tables on separate sheets and place it at the end of the paper.
5. The Author(s) should submit a written consent that he or she will not publish the paper in any other journal at the same time of its publication in JJEES. After the editorial board approves the paper for publication, the author does not have the right to translate, quote, cite, summarize, or use the publication in the other mass media unless the editor-in-chief submits a written consent according to the policy of JJEES. Submitted material will not be returned to the author unless specifically requested.

6. **Documentation:**

References:

a. To cite sources in the text, use the author-date method; list the last name(s) of the author(s), then the year. Examples: (Holmes, 1991); (Smith and Hutton, 1997).
b. In the event that an author or reference is quoted or mentioned at the beginning of a paragraph or sentence or an author who has an innovative idea, the author's name is written followed by the year between two brackets. Example: Hallam (1990).
c. If the author's name is repeated more than once in the same volume, alphabets can be used.
   Example: (Wilson, 1994 a; Wilson, 1994 b).
d. Footnotes may be used to solve any ambiguity or explain something as in the case of a term that requires illustration. In this case, the term is given a number and the explanation is written in a footnote at the bottom of the page.
e. If the number of authors exceeds two, the last name of the first author followed by et al. is written in the text. Example: (Moore et al.). Full names are written in the references regardless of their number.
f. Prepare a reference section at the end of the paper listing all references in alphabetical order according to the first author's last name; this list should include only works that been cited.

Books:

Hunt, J. 1996. Petroleum Geochemistry and Geology. 2nd Ed., H. W. Freeman and Company, New York.

Chapter in a book:

Shinn E. A., 1983. Tidal Flat Environment, **In:** Carbonate Depositional Environments, edited by Scholle, P. A., Bebout, D. G., and Moore, C. H., The American Association of Petroleum Geologists, Tulsa, Oklahoma, U.S.A. pp. 171-210.

Periodicals:

Sexton, P. F., Wilson, P. A.,and Pearson, P. N., 2006. Paleoecology of Late Middle Eocene Planktonic Foraminifera and Evolutionary Implication, Marine Micropaleontology, 60(1): 1-16.

Conferences and Meetings:

Huber, B. T. 1991. Paleogene and Early Neogene Planktonic Foraninifer Biostratigraphy of Sites 738 and 744, Kerguelen Plateau (Southern Indian Ocean). In: Barron, J., Larsen, B., et al. (Eds.), Proceedings of the Ocean Drilling

Program. Scientific Results, vol. 119. Ocean Drilling Program, College station, TX, pp. 427-449.

Dissertations:

Thawabteh, S. M. 2006. Sedimentology, Geochemistry, and Petrographic Study of Travertine Deposits along the Eastern Side of the Jordan Valley and Dead Sea, M. Sc. Thesis, The Hashemite University.

Unpublished:

Makhlouf, I. M. and El-Haddad, A. 2006. Depositional Environments and Facies of the Late Triassic Abu Ruweis Formation, Jordan, J. Asian Earth Sciences, England, in Press.

Illustrations:

a. Supply each illustration on a separate sheet, with the lead author's name, the figure number and the top of the figure indicated on the reverse side.
b. Supply original photographs; photocopies and previously printed material are not acceptable.
c. Line artwork must be high-quality laser output (not photocopies).
d. Tints are not acceptable; lettering must be of reasonable size that would still be clearly legible upon reduction, and consistent within each figure and set of figure.
e. Electronic versions of the artwork should be supplied at the intended size of printing; the maximum column width is 143mm.
f. The cost of printing color illustrations in the Journal may be charged to the author(s).

7. JJEES arranges its articles using editorial policy.
8. The author should submit the original and two copies of the manuscript, together with a covering letter from the corresponding author to the Editor-in-Chief.
9. The editorial board's decisions regarding suitability for publication are final. The board reserves the right not to justify these decisions.
10. In case the paper was initially accepted, it will be reviewed by two specialized reviewers.
11. The accepted papers for publication shall be published according to the final date of acceptance.
12. If the author chooses to withdraw the article after it has been assessed, he/she shall reimburse JJEES the coast of reviewing the paper.
13. The author(s) will be provided with one copy of the issue in which the work appears in addition to 20 off prints for all authors. The author(s) must pay for any additional off prints of the published work.
14. JJEES requires the submission of a statement for transferring copyright from authors to the Hashemite University before the manuscript can be accepted for publication. This procedure\re aims to enable publisher to disseminate the author's work to the fullest extent. The manuscript can be accepted for publication. A copy of the Copyright Transfer Agreement to be used (which may be photocopied) can be found in the first issue of each volume of JJEES.
15. Articles, communications, or editorials published by JJEES represent the sole opinion of the authors. The publisher bears no responsibility or liability whatsoever for the use or misuse of the information published by JJEES.

Manuscript Submission:

Submit three copies of the manuscript (including copies of tables and illustrations) to the Editor-in-Chief

Professor Abdul Rahim A. Hamdan Deanship of Academic Research and Higher Studies Hashemite University, P.O. Box 330127, Postal Code 13133, Zarqa, Jordan. Phone: +962-5-3903333 ext. 4151

E-Mail: jjees@hu.edu.jo , hamdan@hu.edu.jo Submitted manuscript should not have been previously published or submitted for publications elsewhere while they are under consideration by JJEES. Researh articles, communications, and technical notes are subject to critical review by competent refrees. Manuscript submitted in Arabic should be accompanied by abstract and keywords in English.

Copyright:

A statement transferring copyright from the authors to the Hashemite University to enable the publisher to disseminate the author's work to the fullest extent is required before the manuscript can be accepted for publication. A copy of the Copyright Transfer Agreement to be used (which may be photocopied) can be found in the first issue of each volume of JJEES.

Disclaimer:

Articles, communications, or editorials published by JJEES represent the sole opinion of the authors. The publisher bears no responsibility or liability whatsoever for the use or misuse of the information published by JJEES.

Editorial Preface

It is my great pleasure to launch this inaugural issue of the Jordan Journal of Earth and Environmental Sciences (JJEES) with the intent of providing an international forum for the researchers and scientists of the various fields of Earth and environmental sciences to publish their scientific contributions and to disseminate their knowledge. The JJEES is an International Refereed Research Journal hosted by the Hashemite University, sponsored, and approved by Jordan's Ministry of Higher Education and Scientific Research. The journal covers diverse areas of research and development in Earth and environmental sciences.

The coverage of the JJEES includes all new findings in all aspects of Earth and environmental sciences and or any closely related fields. The journal also encourages the submission of critical review articles covering advances in recent research of such fields as well as technical notes.

The Editorial Board is very committed to build the Journal as one of the leading international journals in Earth and environmental sciences in the next few years. With the support of the Ministry of Higher Education and Scientific Research and Jordanian Universities, it is expected that a valuable resource to be channeled into the Journal to establish its international reputation.

We have received a good response to the previous issue of JJEES from scientists and researchers in Jordanian universities. I am pleased by this response and proud to report that JJEES is achieving its mission of promoting research and applications in Earth and environmental sciences. In this issue, there are five interesting papers dealing with various aspects of Earth and environmental sciences.

I would like to thank all members of the editorial board and the international advisory board members for their continued support to JJEES with their highly valuable advice. I would like also cordially thank the manuscript's reviewers for providing valuable comments and suggestions to the authors that helped greatly in improving the quality of the papers. My sincere appreciation goes to all authors and readers of JJEES for their excellent support and timely contribution to this journal.

The editorial board of JJEES and me, are looking forward to receiving your valuable scientific contributions. Your support and continued contribution would be highly appreciated.

For more information about the JJEES guidelines for preparing and submitting articles, you are invited to visit the journal site http://www. jjees.hu.edu.jo

Editor-in-Chief,
Professor Abdul Rahim A. Hamdan,
Dept. of Earth and Environmental Sciences,
The Hashemite University,
Zarqa, Jordan.

JJEES

Volume 3, Number 1, June, 2010
ISSN 1995-6681
Pages 1- 16

Jordan Journal of Earth and Environmental Sciences

Lithostratigraphy and Microfacies Analysis of the Ajlun Group (Cenomanian to Turonian) in Wadi Sirhan Basin, SE Jordan

Mohamed Ka. Khalifa[a, b, *] and Abdulkader M. Abed [b]

[a] Geoscience & Petroleum Engineering Department, Universiti Teknologi PETRONAS Bandar Seri Iskandar, 31750 Tronoh, Perak Darul Ridzuan, Malaysia

[b] Department of Environmental and Applied Geology, University of Jordan, Amman, Jordan.

Abstract

The Ajlun Group of the Wadi Sirhan Basin, Jordan, of probable Cenomanian- Turonian age, consists of alternating beds of indurated marl, marly limestone and dolomitic limestone with violet friable phosphatic sandstone. The results were used to develop a new lithostratigraphic correlation of the undifferentiated Na'ur, Fuheis, Hummar and Shueib Formations and Wadi Sir Formation in the study area. The stratigraphic boundaries of these units were defined at marked changes in outcrop and borehole characteristics. They are 25.5 metres thick at outcrop of Zgaimat Al-Hasah and 147 metres in the Wadi Sirhan-2 well. Microfacies analysis indicates deposition in a near shore slightly restricted shelf lagoon (packstone-wackestone) to more restricted environment represented by pure micrite. They are arranged in four shallowing cycles of relative sea level change. The very low thickness of the Ajlun Group at Zgaimat Al-Hasah (25.5 metres compared with 100s m elsewhere in Jordan) as well as the restricted near shore environments are explained by deposition on the Bayer-Kilwa paleohigh which left little accommodation for the deposition of the Ajlun Group.

Keywords: Wadi Sirhan Basin, Jordan, Ajlun Group, lithostratigraphic correlation, petrography, microfacies analysis, Late Cretaceous, Cenomanian-Turonian and palaeogeography.

1. Introduction

This work deals with the geology of the Ajlun Group, Late Cretaceous (Cenomanian-Turonian) in the Wadi Sirhan Basin in the southeastern desert of Jordan, close to the Saudi Arabian border (Fig. 1). During the Early Cretaceous, most of the eastern Mediterranean was emergent and subjected to fluvial sandstone deposition (Powell, 1989). By the onset of the Cenomanian, the whole area was submerged by the southern continental shelf of the Tethys as a consequence of a major global eustatic sea level rise (Haq and Qahtani, 2005). Hundreds to 1000s m thick carbonates of various facies were deposited throughout the eastern Mediterranean (Bender, 1974). One of the major factors in the pattern of deposition (thickness and facies) was the ocean floor paleorelief. Basins and swells dominated the sea floor during the Late Cretaceous due to compression associated with northward movement of Arabia as part of the African Plate (Bowen and Jux, 1987). This compression is most conspicuous in what is known as "the Syrian Arc Fold System" running from northern Egypt through Sinai and into the eastern Mediterranean (Krnkel, 1924, Bowen and Jux, 1987). In Jordan, several of these basins and swells are recognized (Abed, 1994). One of the paleohighs is the Bayer-Kilwa high where Zgaimat al-Hasah is located (Fig. 1). Thicker and deeper carbonate facies can be found in the lows compared with the highs (Powell, 1989). The Ajlun Group at Zgaimat al-Hasah was studied in general works dealing with the geology of Jordan (Quennell, 1951; Bender, 1974; Powell, 1989).

The aims of this work are a) to study the microfacies of the Ajlun Group in the outcrop and subsurface, b) to deduce the depositional environments of the group and the factors controlling them, and c) to delineate the paleogeography of the Wadi Sirhan area in the Late Cretaceous.

2. Geological Setting

Integration of lineament data within the Wadi Sirhan Basin shows that the boundaries are marked by a complex of major structural features as shown in Fig. 1. The Wadi Sirhan Basin is a monocline which trends NW-SE. It is bounded on the north by the Suwaqa fault zone, which strikes S-E on Fig. 1; it seems to cross the monocline. It is a right lateral wrench system with a strong movement along the vertical down to the north margin of the Azraq Basin (Barjous, 1986). Another structural feature is the Zgaimat Al-Hasah fault zone which also trends E-W. It extends westward from Saudi Arabia for more than 250 kilometres, to the Jordan Valley (Fig. 1). It is represented by a narrow zone of discontinuous local faults. Local folding occurs in many places along this trend and the

* Corresponding author. Mohamed_kh@petronas.com.my.

  - Volume 3, Number 1 (ISSN 1995-6681)

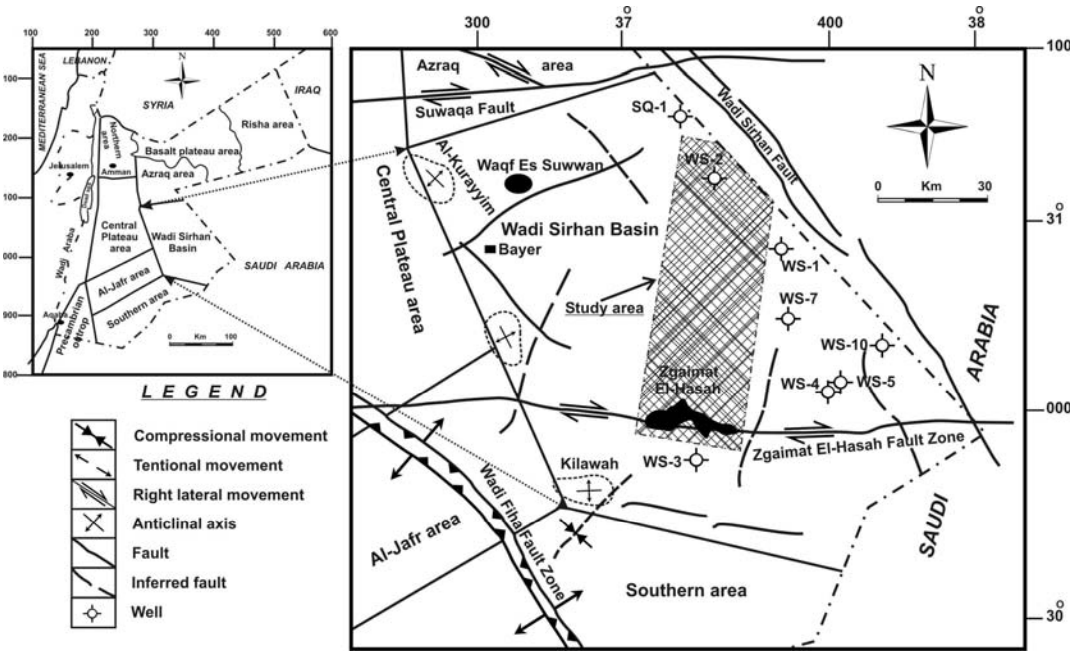

Fig. 1 Geographical location map of the study area within the Wadi Sirhan Basin (modified after Bender, 1968).

pattern of folding is indicative of (right-lateral) transcurrent movement (Holmes et al., 1989). The Zgaimat Al-Hasah outcrop is situated within one of these anticlines as an "inlier" where the Lower and Upper Cretaceous strata form its core (Qteishat, 1987; Abed and Amireh, 1999). Fig. 2 summarizes the Late Cretaceous stratigraphic framework of the Ajlun Group throughout Jordan (Wolfart, 1959; Marsi, 1963; MacDonald et al, 1965a, b; Parker, 1969; Bender, 1974; Powell, 1989; Amireh, 1997). The Ajlun Group is made of alternating limestone and marl horizons. It also thins southwards and becomes increasingly sandy in the extreme south of Jordan. It also thins eastwards and becomes sandy and phosphatic in Zgaimat Al-Hasah. The age of the group is Cenomanian-Turonian (Wetzel and Morton, 1959; Basha, 1978; Dilley, 1985).

AGE			GROUP	FORMATION	LITHOLOGY
CRETACEOUS	LATE	TURONIAN	AJLUN	Wadi Sir	Limestone, marly toward the base and massive shelly at the top increasingly sandy southwards.
				Shueib	Alternating nodular limestone with soft thinly bedded marl. Large ammonites are present.
		CENOMANIAN		Hummer	Limestone, micrite and shelly wackestone.
				Fuheis	Dominantly marly with marly limestone.
				Naur	Alternating limestone/dolomite with soft marl, increasingly sandy southwards.

Fig. 2 Stratigraphic units of the Ajlun Group throughout Jordan.

3. Lithology and Stratigraphy of the Ajlun Group

Following is a description and correlation of the Ajlun Group units at the Zgaimat Al-Hasah outcrop in the south Sirhan Basin and the Wadi Sirhan-2 well (WS-2) further north.

4. Zgaimat Al-Hasah Outcrop

The outcrop of Zgaimat Al-Hasah is approximately 90 kilometres south of the WS-2 (Fig. 1). The total thickness of the Ajlun Group in the measured outcrop is 25.5 metres. The lithostratigraphic units are summarized in Table 1.

Table 1. Lithostratigraphic units distribution of Ajlun Group sequence in the studied section of Zgaimat Al-Hasah.

Age	Group	Formation	Thickness (metres)		Main Lithology	Remarks
Turonian	Ajlun Group	Wadi Es Sir Formation	5.5 metres		Formation consists mainly of phosphatic sandstone sequence occasional thin sandstone interbeds.	Mainly of violet friable phosphatic sandstone
		Undifferentiated Na'ur, Fuheis, Hummar and Shueib Formation	20 metres	9 metres	Unit consists mainly of marly limestone with interbedded limestone, yellowish-grey, medium- grained, massive; fossils: mollusc fragments. The marls are thin, light yellowish-grey, unstratified.	The unit is yellowish in colour. The centre has a thick bed of molluscan-rich coquinoidal limestone. The gastropods and pelecypods are abundant throughout Yellowish unit, with few ostracods.
Cenomanian				11 metres	Unit consists mainly of marl and marly limestone, with scattered grey, buff and tan, dolomitic limestone. Thin levels of secondary gypsum crystals are also found.	Common in the unit is white lithology. This unit is rich in fauna, in particular; echinoids, gastropods, cephalopods and pelecypods.

The Ajlun Group here can be divided into two units; the lower part of the section is composed of undifferentiated Na'ur, Fuheis, Hummar and Shueib Formations as one formation, with a thickness of about 20 metres, shown in Fig. 3. This formation clearly overlies the varicoloured Kurnub Sandstone Formation of Early Cretaceous age. This lower unit is most probably the equivalent of the marl, marly limestone, and limestone with a few dolomitic limestones in north and central Jordan. In other words, they are equivalent to Na'ur, Fuheis, Hummar and Shueib Formation, with greatly reduced thickness.

The upper unit of the section is believed to be equivalent to Wadi Es Sir Formation with a thickness of 5.5 meters (Fig. 3, Table 2). It consists of friable phosphatic sandstone to sandy phosphorite.

5. Wadi Sirhan-2 well

The Wadi Sirhan-2 is situated in the eastern part of the Wadi Sirhan Basin (Fig. 1), 45 kilometres northeast of the outcrop at Zgaimat Al-Hasah. The report on the Wadi Sirhan-2 well (Qteishat, 1987) indicated that the Ajlun Group, Cenomanian to Turonian, extended from depths of 643 to 790 metres. However, the total thickness of the Ajlun Group in the measured section is 147 meters (Fig. 3). The undifferentiated Na'ur, Fuheis, Hummar and Shueib Formations at Wadi Sirhan-2 well are difficult to define in its boundaries and distribution. However, these descriptive undifferentiated formations can be resolved into a three intervals (Table 2). In the Wadi Sirhan-2 well, Wadi Es Sir Formation overlies undifferentiated Na'ur, Fuheis, Hummar and Shueib Formation, and it is overlain conformably by the lower part of the Belqa Group, the Amman Formation (B_2) (MacDonald, 1965a) (Fig. 3, Table 2).

6. Correlations with Other Areas

When correlating the Ajlun Group in the WS basin with two localities some 150 km further west (Fig. 4), the following points are evident:

1. The highly reduced thickness of the group in the WS basin, 25 meters in the former compared with around 450 meters in the latter. We did not see any erosional unconformities in the Zgaimat Al-Hasah outcrop. Thickness reduction might be non-depositional, or else a slower sedimentation rate will appear.
2. Despite the reduction in thickness, the lithology of the lower Zgaimat Al-Hasah unit is essentially the same as those in the west; i.e. fossiliferous marl, marly limestone and limestone. However, the upper unit is phosphatic in Zgaimat Al-Hasah compared with limestone in the west.

7. Petrography and Sedimentary Facies Analysis

The Aljun Group has been studied petrographically in outcrop of Zgaimat Al-Hasah (ZH series) and Wadi Sirhan-2 well (WS series). Standard microfacies types (SMF) have been established according to Wilson (1975) and Flugel (1982). The classification of limestone is that of Dunham (1962) and sandstone rocks of Pettijohn et al. (1973). Fig. 5 shows the MF types at Zgaimat al-Hasah outcrop while Fig. 11 is for the WS-2 well.

8. Microfacies and Depositional Environments of the Zgaimat al-Hasah Outcrop

Twenty thin-sections were studied from Zgaimat al-Hasah section (Fig. 5), 16 thin sections from the lower part, while the upper unit is represented by 4 thin sections. The description of these microfacies is shown in Table 3 and Figs 6 and 9.

  - Volume 3, Number 1 (ISSN 1995-6681)

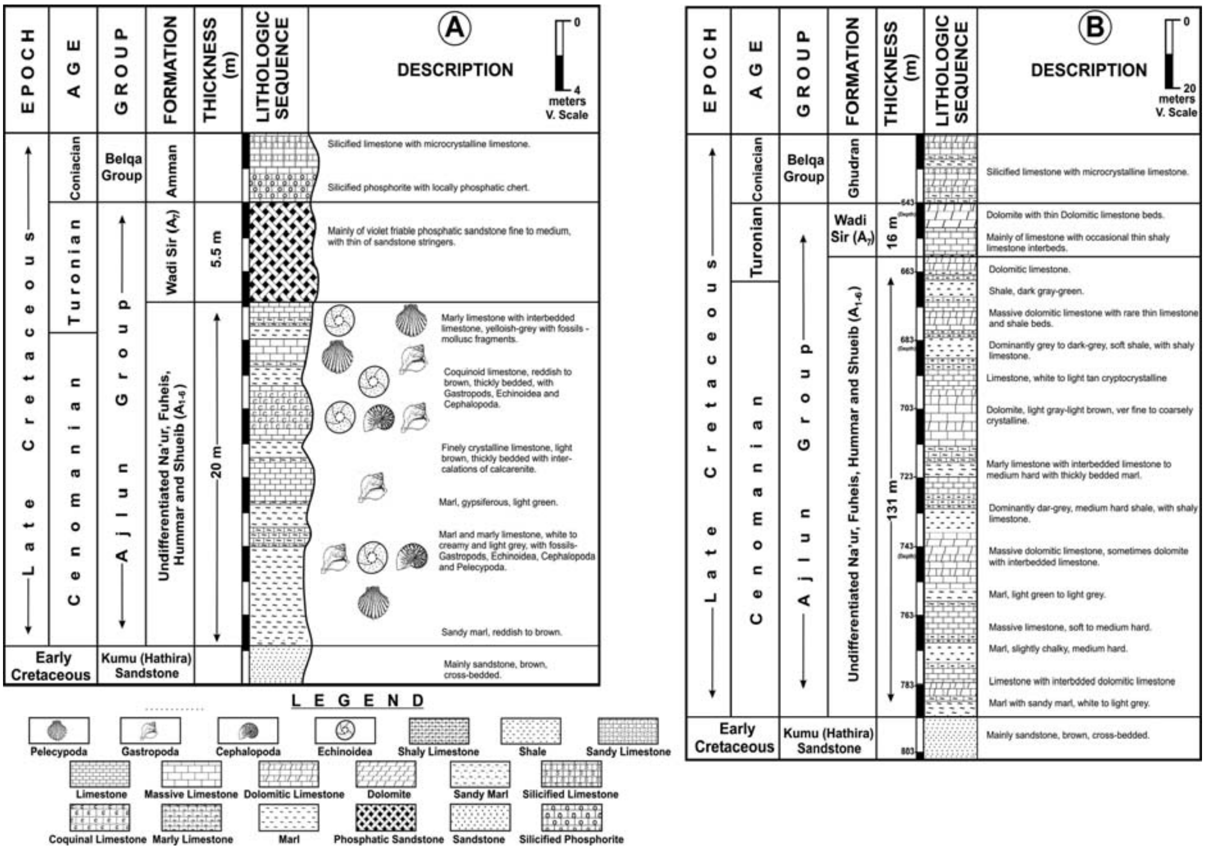

Fig. 3 Simplified lithostratigraphic column of Ajilun Group sequence in this study. **A** Representative measured section of the outcrop of Zgaimat Al-Hasah. **B** Representative measured section of the Wadi Sirhan-2 Well. (See Fig. 1 for column section location).

Table 2. Lithostratigraphic units distribution of Ajlun Group sequence in the studied section of Wadi Sirhan-2 well.

Age	Group	Formation	Thickness (metres)		Main Lithology	Remarks
Turonian	------------------ Ajlun Group ------------------	Wadi Es Sir Formation	16 metres		Depths (643-659 metres) represent this formation. The upper formation consists of fine-crystalline dolomites with minor amounts of dolomitic limestone beds. Thin shale interbeds are rare. The lower formation consists mainly of a thick bedded to massive, hard, crystalline limestone.	The dolomite is often vugular, sometimes with few fractures filled with calcite or dolomite. The lower part of the formation is sometimes sandy indicating a local mixing with underlying sands and, quartz grains are found in the basal centimeters.
Cenomanian		Undifferentiated Na'ur, Fuheis, Hummar and Shueib Formations	---------131 metres ---------	28 metres	This upper undifferentiated formations from 659-687 meters depth is composed of shale with minor dolomitic limestone and very scattered thinly bedded shaly limestone.	The shale occurs in thin interbeds and is gray to green, soft, and calcareous.
				45 metres	This middle undifferentiated formations from 687-732 metres depth and consists of limestones, slightly-medium hard, fine crystalline, medium crystalline in part, massive crystalline dolomitic limestones and dolomite.	Thin interbeds of marly limestones are common especially in the lower of the interval.
				58 metres	The lower undifferentiated formations extend from 732-790 metres depth and consist predominantly of shale with thin limestone or dolomite and dolomitic limestone interbeds, from hard to soft.	Slightly marl at its base.

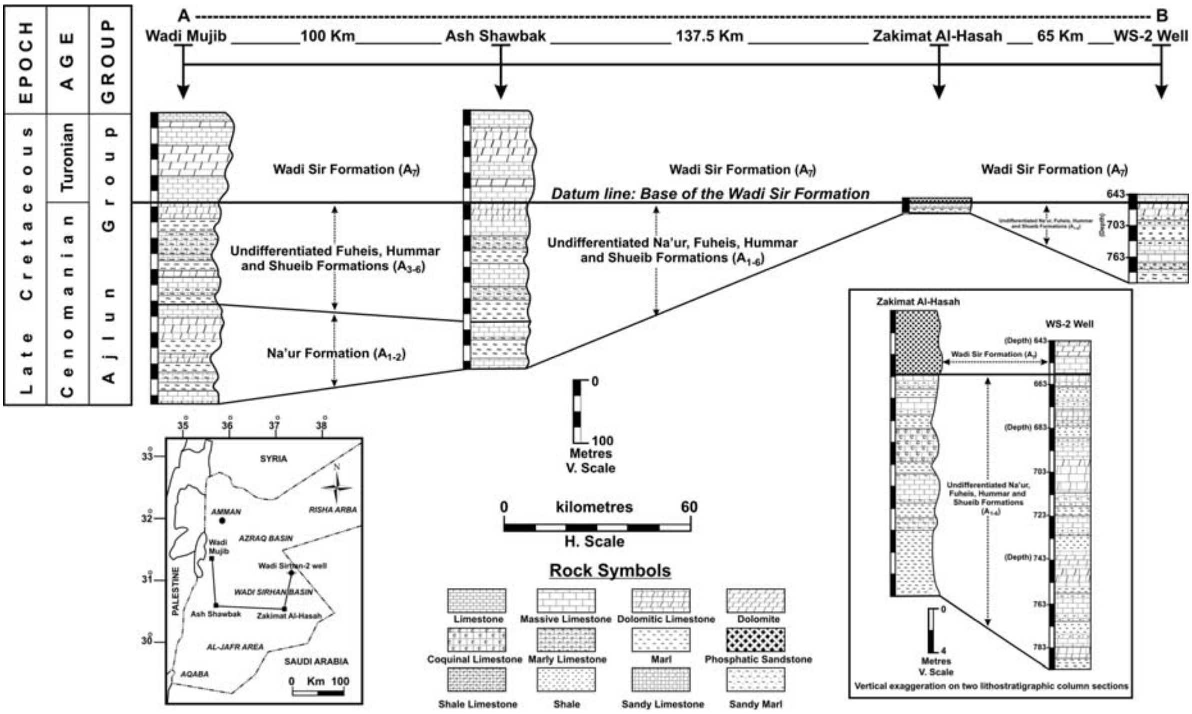

Fig. 4 Generalized lithostratigraphic columns of the Ajlun Group sequence between the Wadi Sirhan Basin (eg. outcrop of Zgaimat Al-Hasah and WS-2 well), Ash Shawbak and Wadi Mujib areas, showing the distribution of lithology, sedimentology and thickness from different lithostratigraphic units.

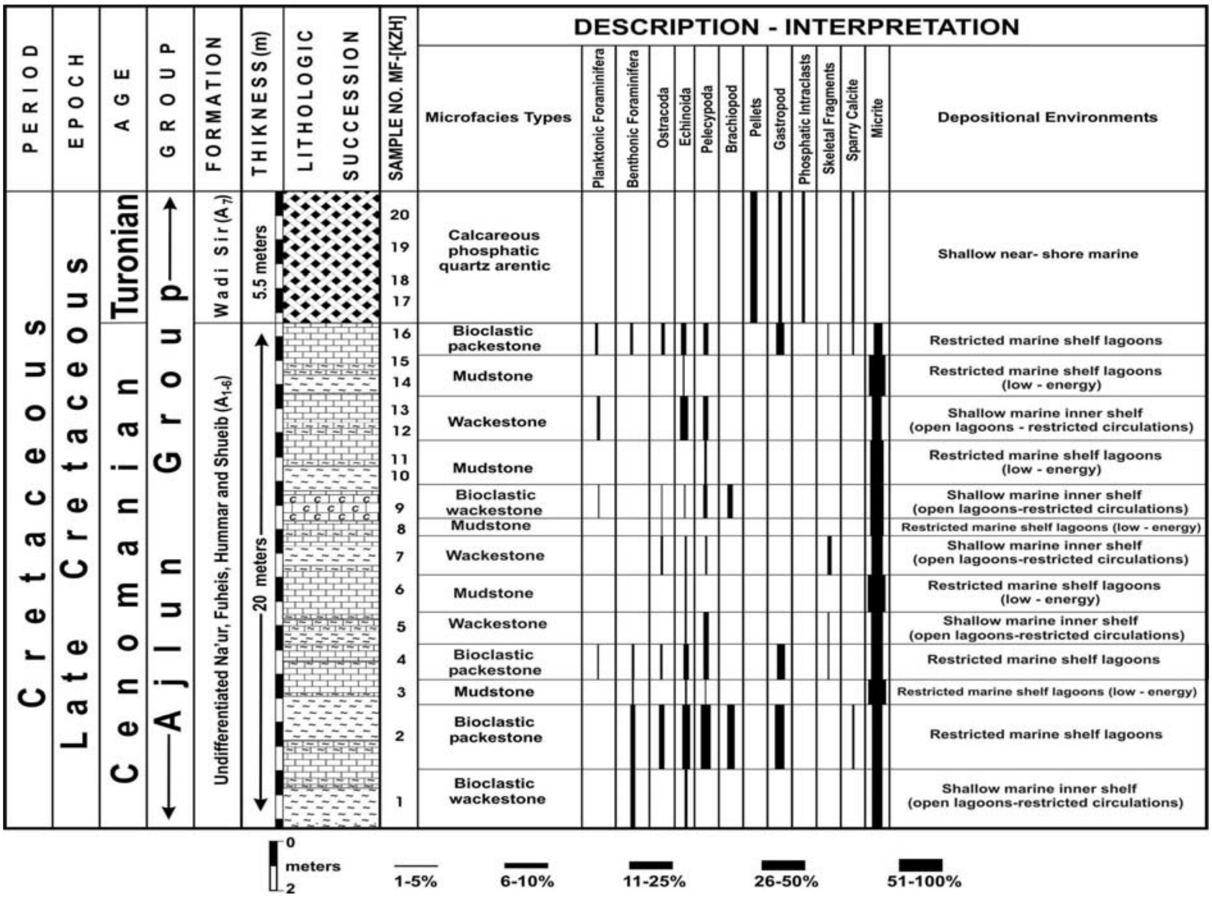

Fig. 5 Stratigraphic column of the undifferentiated Na'ur, Fuheis, Hummar and Shueib Formations and Wad Sir Formation in the outcrop of Zgaimat Al-Hasah showing microfacies types, particles and depositional environment distribution.

Table 3. Summary of the characteristics of the petrography for the Zgaimat Al-Hasah section.

Formation	Thin-section	Description	Standard microfacies types
Wadi Es Sir Formation	ZH-17, 18, 19 & 20	*Microscopically this general thin-section is composed of 36% detrital quartz rounded to subrounded quartz grains (Fig. 8e). Phosphorite particles are about 21% (Fig. 8f) and are made of brown-coloured pellets anisotropic fish debris (bone fragments). Other minerals occur as accessory components including glauconite, heavy minerals such as tourmaline, and minor amount of rock fragments (chert). The chief cement component about 39% (Figs. 10a & 10b) in this rock is calcite occurring as recrystallized blocky grains within the detrital minerals. The calcite cement corrodes the detrital quartz grains. Other cements, as quartz overgrowth is also present in very small amount. Locally the calcite cement is growing at the expense of quartz overgrowth and the detrital quartz.*	MF (ZH-17, 18, 19 & 20) ~ calcareous phosphatic quartz arenite microfacies
Undifferentiated Na'ur, Fuheis, Hummar and Shueib Formations	ZH-2	This thin-section show different sizes of grains. This thin section is composed mainly of shell fragments of echinoids 29%, pelecypods 20%, gastropods 15% and brachiopods 14%, very limited of shell fragments of ostracods 10%, benthonic foraminifers 8% and dasycladcean algae 4% (Fig. 6b). Shell fragments embedding in matrix of micrite (Fig. 7a) and may be micritized skeletal fragments. It contains also some sparry calcite cement 4% (Fig. 7b).	MF (ZH-2, 4 & 16) ~ bioclastic packstone microfacies is similar to Wilson's belt 7 or 8, SMF 18 and 19.
	ZH-4	This thin-section similar to thin-section (ZH-2), but here it contains few amount of very fine detrital quartz 5% shown in Figs. 6c and 7d.	
	ZH-16	It is similar to samples (ZH-2 and 4), but without brachiopod fragments. It contains also, a few detrital quartz small ranging from 0.3-0.1 mm in diameter.	
	ZH-3	This thin-section is pure micritic limestone without fossils (Fig. 7c), sometimes a few ostracods 2%. It has same sparry calcite filling the fractures.	MF (ZH-3, 6, 8, 10, 11, 14 & 15) ~ mudstone microfacies is similar to Wilson's belt 7, 8 or 9, SMF 19, 21 and 23.
	ZH-6	This thin-section is made up of pure micrite (Fig. 7f) with about 1% of small amount of echinoids, matrix in fine-grained micrite lime mud.	
	ZH-10	This thin-section is composed of pelecypod shell of fragments and few amount of algae, mixture of carbonate mud sediment and sparry calcite 7% (Fig. 10e). Skeletal algal and pelecypod fragments are often micritization.	
	ZH-11	The thin-section characteristically consist specialized thin-section pure micrite and skeletal debris is not as abundant (e.g. foraminifers and gastropods) and some channels porosity are present in the section. Several channels are filled partially with calcite.	
	ZH-14	It is similar to thin-sections (ZH- 3, 6, 8, 11 and 14), but in this sample the micrite shows recrystallization processes, also contains few amount 3% of detrital quartz, small ranging from 0.05-0.1 mm in diameter. The sample (ZH- 8) without echinoids and ostracods fragments.	
	ZH-7	This thin-section is composed mainly of shell fragment of gastropods and foraminifers present and scattered embedded in fine grain matrix. Most of the section is made of micritized skeletal fragments shown in Fig. 8a.	MF (ZH-7, 12 & 13) ~ wackestone microfacies is similar to Wilson's belt 7 or 8, SMF 19.
	ZH-12	It thin-section with abundant shell debris and larger pelecypod and gastropod fragments and few amount of algae, and some of it reach detrital quartz that are embedded in a matrix of micrite. The micrite is recrystallized. Several channels are filled partially with calcite and few amount of silica are present in microfacies.	
	ZH-13	Microscopically, this thin-section is composed mainly of shell debris and larger echinoids 34% pelecypods 19% and benthonic foraminifers 9%, with detrital quartz 7%, particles embedding in matrix of micrite (Fig. 9b). Sometimes particles are micritized shells. In addition, fractures are filled with calcite.	

	ZH-1	Microscopically, this thin-section is consists mainly of shell fragments jumbled of echinoids 63%, some miliolids of foraminifers 37%, and few amount 6% of detrital quartz shown in Fig. 6a. Quartz-size ranging commonly from 0.2-0.6 mm in diameter that is embedded in micritic matrix.	MF (ZH-1 & 9) ~ bioclastic wackestone microfacies is similar to Wilson's belt 7 and 8, SMF 9 and 19.
	ZH-9	This thin-section is dominated by shell of fragments pelecypods 42%, ostracods 28%, and echinoids 20% with some fragments of fenestrate bryozoans shown in Fig. 9a. Shell fragments embedding in matrix of micrite, the micrite is recrystallized (Figs. 8b and 8c). The In some sparry calcite cement fills the chambers and the surrounding sediment is micrite with a few thin ostracods and echinoidsd.	

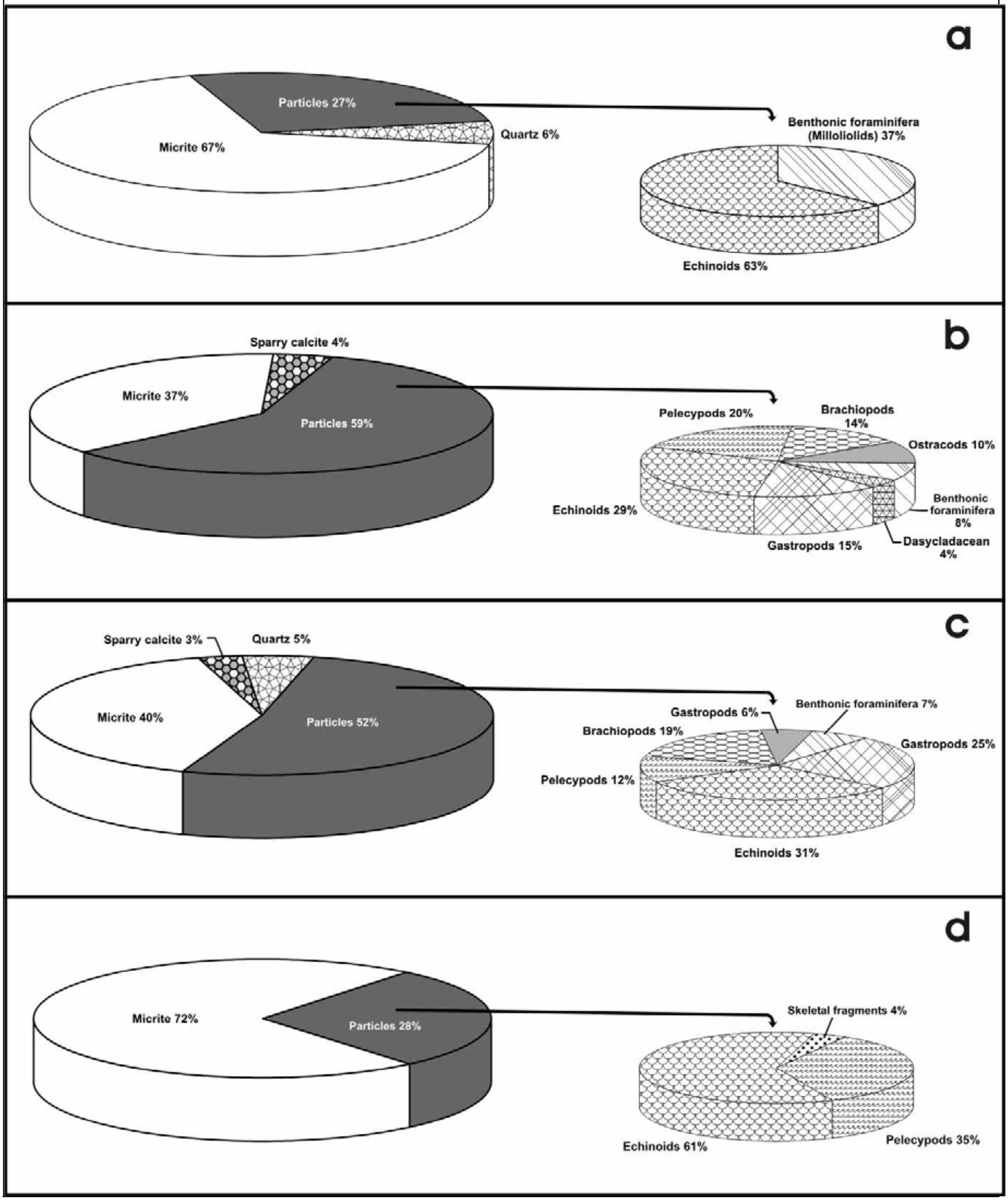

Fig. 6 Quantitative composition of the microfacies types within the outcrop of Zgaimat Al- Hasah. **A** MF (KZH-1): Bioclastic wackstone. **B** MF (KZH-2): Bioclastic packstone. **C** MF (KZH-4): Bioclastic wackstone. **D** MF (KZH-5): Wackstone.

Photomicrographs are shown in Figs. 7, 8 and 10. Four major microfacies types are recognized at the Zgaimat al-Hasah outcrop. These are (1) bioclastic wackestone/ wackestone microfacies; (2) bioclastic packstone microfacies; (3) mudstone microfacies; and (4) calcareous phosphatic quartz arentic microfacies.

Table 4. Summary of the characteristics of the petrography for the Wadi Sirhan-2 well.

Formation	Thin-section	Description	Standard microfacies types
Wadi Es Sir Formation		-- No thin-sections -- --	
Undifferentiated Na'ur, Fuheis, Hummar and Shueib Formations	WS-1	*This thin-section from depth 768 metres indicate the presence mainly of planktonic foraminifers 29%, benthonic foraminifers 21%, ostracods 15% and pelecypods 21% debris fragment, and few grains of glauconite and detrital quartz, embedded in a matrix of micrite (Fig. 9c). In some places, it is dolomitized, in other places recrystallized to sparry calcite.*	MF (WS-1) ~ foraminifera wackestone microfacies is similar to Wilson's belt 7 or 8, SMF 16, 18 and 19.
	WS-2	Microscopically this thin-section is best represented by depth 764 metres, which mainly consists of shell fragments (pelecypod and echinoid). Some foraminifers also present, dolomitization processes are also took place within this thin-section.	MF (WS-2 & 4) ~ wackestone microfacies is probably equivalent to the microfacies used as a similar to Wilson's belt 7 or 8, SMF 8, 9, 10, 17 and 19.
	WS-4	This thin-section about depth 763 metres and is represented by shell fragments of pelecypod 42% and echinoids 37%, and few benthonic foraminifers 21% (Fig. 9d). The matrix also contains some grains of quartz and glauconite. The matrix have been affected by two major processes, the first one is the recrystallization into sparry calcite, the other is the transformation of microsparrite into obvious dolomite grains (dolomitization), the last processes appears to be less obviously (Figs 10c and 10d).	
	WS-3	This thin-section is pure micrite limestone, without any fossils content. Small amount of quartz grains are present. Dolomatization has been detected but lesser, thin-section (WS-3), about 764 metres.	MF (WS-3 & 5) ~ mudstone microfacies is similar to Wilson's belt 8 or 9, SMF 23.
	WS-5	Microscopically, this thin-section similar to thin-section (WS-3), but matrix darker, about depth 762 meters.	

Interpreted depositional environment: this microfacies represents a shallow marine inner shelf (open lagoons-restricted circulation) environment. This is supported by presence in the sediment of fragments of diverse organisms. Wilson (1975) believed that these organisms may occur locally in great abundance in such facies. This microfacies occurs in an environment similar to Wilson's (1975) facies belt 7 or 8, SMF 8, 9 and 19.

9. Bioclastic Packstone Microfacies

This facies is composed mainly of marly limestone, light brown to dark grey, with yellow to cream, thin-medium bedded, interbedded with yellow marl. This belt has abundant bioclastic packstone textures that comprise 10-30% of the undifferentiated Na'ur, Fuheis, Hummar and Shueib Formations within of the Zgaimat Al-Hasah section.

Here macrofossils are restricted to only a few thin beds. The macrofossils present as whole shells; echinoids, cephalopods and gastropods are the most important fossil groups in this facies.

Microscopically, this section shows abundant bioclasts of brachiopods, echinoids, ostracods, mollusca (gastropods and pelecypods) all, dasycladacean algae, few benthonic foraminifers, and some detrital quartz, embedded in a matrix of micrite. The cement is mostly blocky sparry calcite and constitutes less than 10%. Fig. 5 shows the results of microscopic investigations of this microfacies bioclastic packstone were also given in thin-sections MF (ZH- 2, 4 and 16).

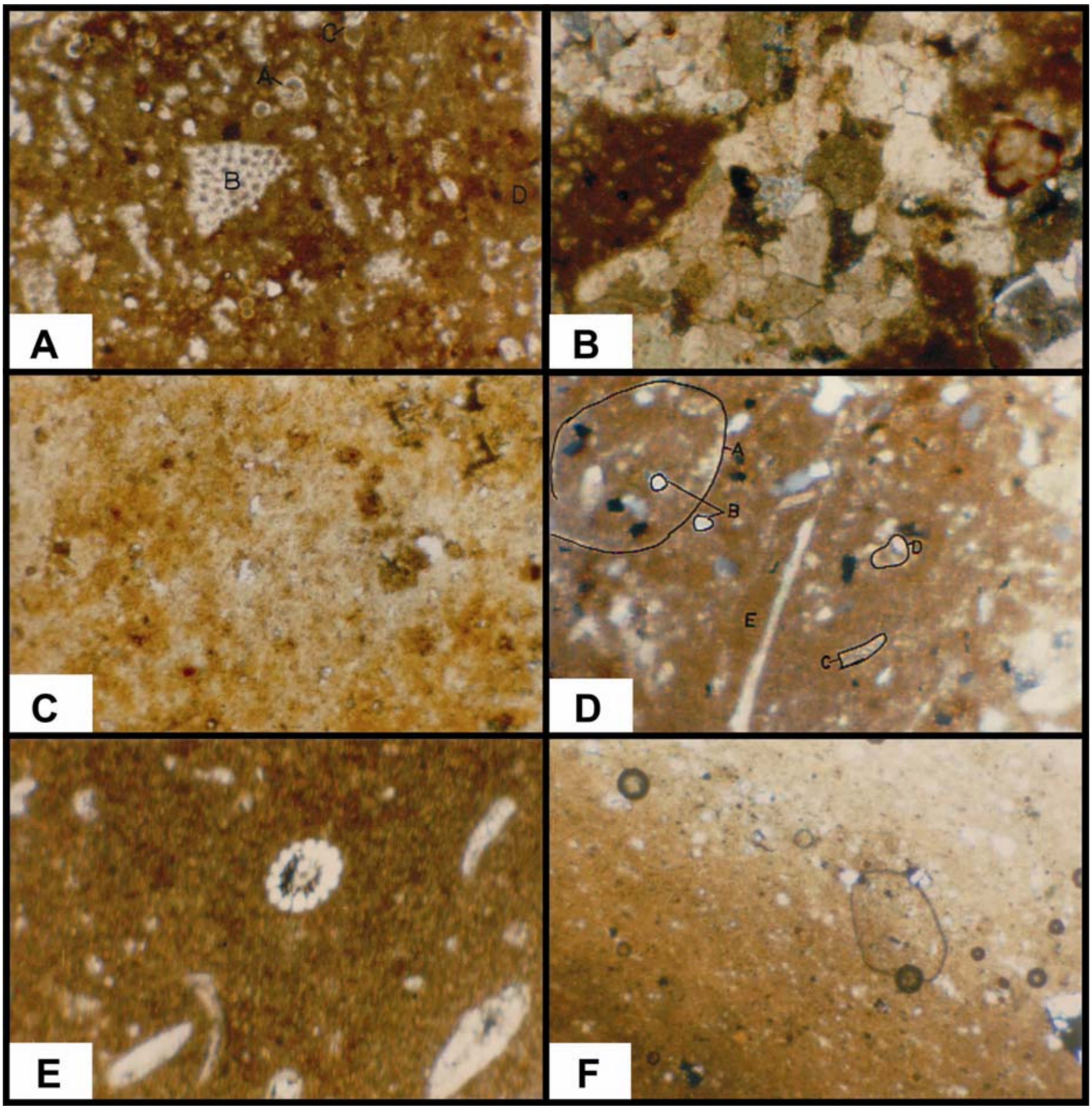

Fig. 7 Thin-section photomicrographs within the outcrop of Zgaimat Al-Hasah. **A** Bioclastic packstone showing benthonic foraminifera (*A*), dasycladcean algae (*B*), gastropod (*C*) and matrix of micrite - magnification X10/ XPL. **B** Bioclastic packstone with abundant blocky calcite cements - magnification X10/XPL. **C** Pure mudstone - magnification X10/XPL. **D** Bioclastic packstone shows gastropod (*A*) fossil filled with detrital quartz (*B*), pelecypod fragments (*C*), foraminifera (*D*) and matrix of micrite (*E*) - magnification X10/ XPL. **E** Wackstone shows echinoid spine and pelecypod (shell fragments) embedding in micrite - magnification X10/ XPL. **F** MF (KZH-6) is made up of pure micrite - magnification X10/ XPL.

Interpreted depositional environment: this microfacies is similar to SMF-19 of Wilson (1975), indicating a restricted marine shelf lagoon environment. This is supported by the very limited whole fossils, mainly cephalopods, echinoids and gastropods, which indicate a quiet environment, and the presence of shell debris of ostracods, brachiopods, mollusca (pelecypods and gastropods), dasycladcean algae and benthonic foraminifera is abundant. The detrital quartz possibly was originated from a sand bar producing this shelf lagoon (Selley, 1988).

10. Mudstone Microfacies

This facies contains marls, white to yellowish, with associated light brown, marly limestone and minor coarse shell debris. The facies is dominated by mudstone textures which comprise 40% or more of the total thickness of the undifferentiated Na'ur, Fuheis, Hummar and Shueib Formation in Zgaimat Al-Hasah section.

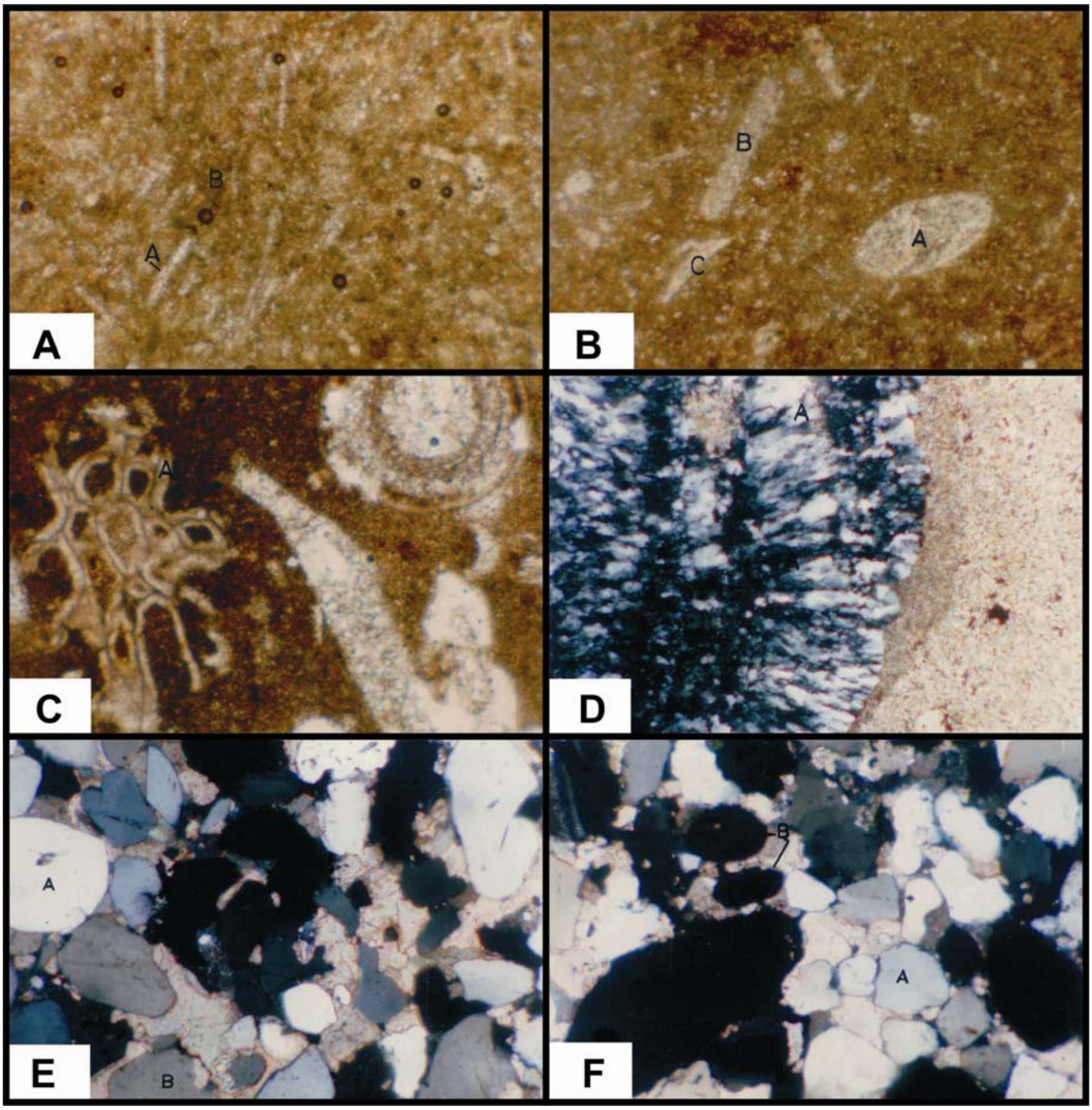

Fig. 8 Thin-section photomicrographs within the outcrop of Zgaimat Al-Hasah. **A** Wackstone microfacies shows micritized shell fragments (*A*) micrite (*B*) - magnification X10/ XPL. **B** Bioclastic wackstone with abundant fragments including ostracods (*A*), pelecypods (*B*) and echinoids (*C*) embedding in micrite - magnification X10/ XPL. **C** Typical sample of MF (KZH-9), showing effect of micritization on bryozoans (*A*) - magnification X10/XPL. **D** Mudstone shows fracture filled with silica (*A*) - magnification X10/XPL. **E** Calcareous phosphatic quartz arentic microfacies shows detrital quartz rounded (*A*) and corrosive quartz grain due to calcite cement (*B*) - magnification X10/XPL. **F** Calcareous phosphatic quartz arentic microfacies with common detrital quartz subrounded (*A*) and rounded and subrounded phosphate particles (*B*) - magnification X10/ XPL.

The mudstone microfacies is recognised at several horizons, and is represented by the following by MF (ZH-3, 6, 8, 11, 14 and 15), as shown schematically in Fig. 5. The mudstone microfacies comprises a range of sedimentary constituents in which carbonate mud is dominant. Microscopically, this microfacies is a pure mudstone locally, very fossiliferous in places; individual pellets are smeared or coalesced, giving rise to patches of apparently homogeneous micrite. That represented by this microfacies which consists on unfossiliferous mudstone partly of completely recrystallized phenomenon. Fossiliferous mudstone has usually less than 10% particles, with fossils constituting one of more of the following types: echinoids, pelecypod fragments, ostracods and small foraminifers.

Interpreted depositional environment: these sediments were deposited in a low-energy lagoonal environment (cf. Rohl et al., 1991). This microfacies is interpreted as indicating the presence of a restricted marine shelf lagoon environment similar to Wilson (1975) facies belt 8 or 9, SMF 23 (?) and Flugel (1982).

11. Calcareous Phosphatic Quartz Arenite Microfacies

The facies consists mainly of phosphatic sandstone, typically violet, medium hard to friable, always massive, with sandstone occurring locally. This facies is recognized only in the Wadi Es Sir Formation at Zgaimat Al-Hasah section.

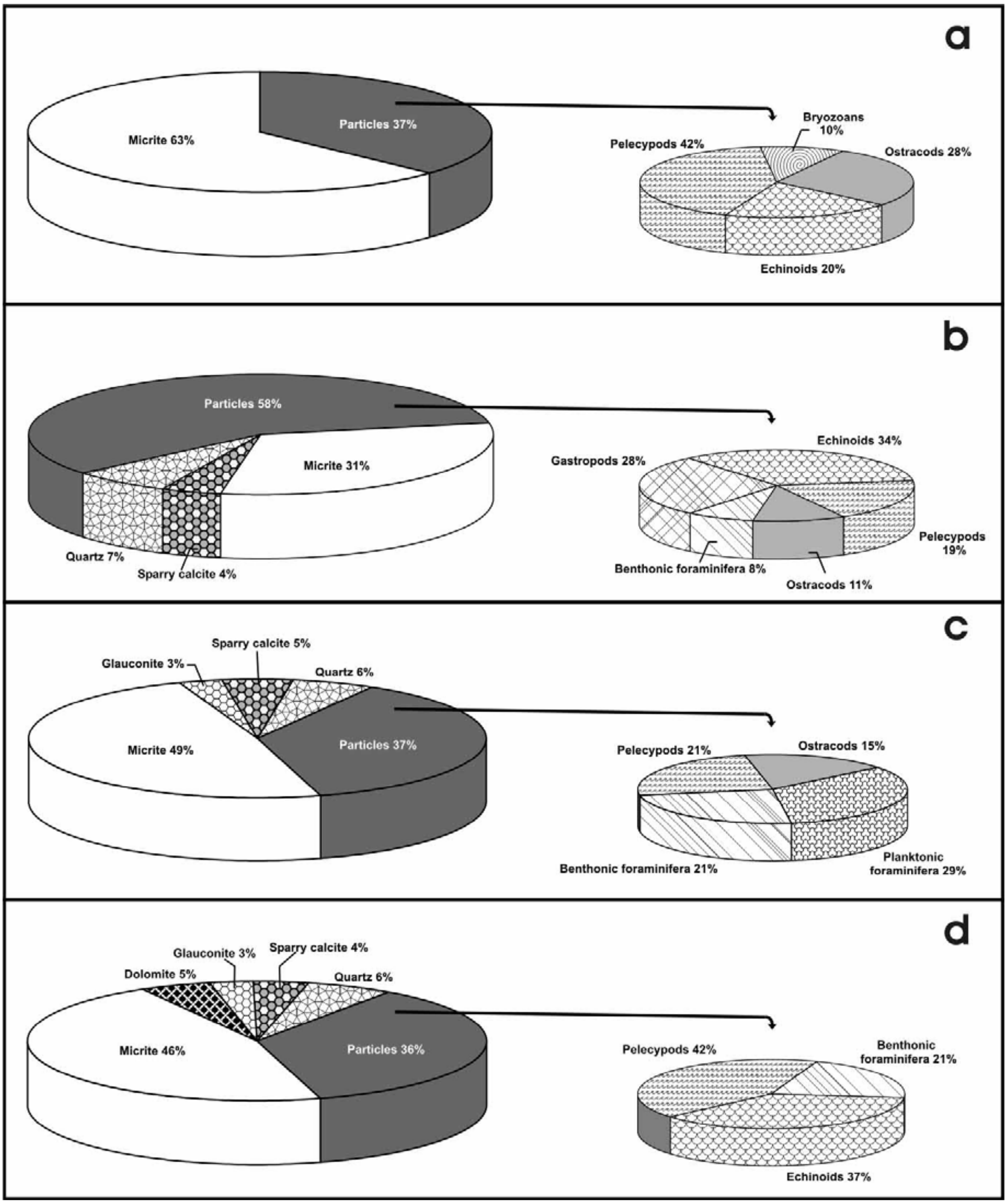

Fig. 9 Quantitative composition of the microfacies types within the outcrop of Zakimat Al-Hasah and Wadi Sirhan-2 Well. **A** MF (KZH-9): Bioclastic wackstone. **B** MF (KZH-13): Bioclastic wackstone. **C** MF (KWS-1): Foraminifera wackstone. **D** MF (KWS-4): Wackstone.

This microfacies consists of detrital quartz and rounded to subrounded phosphatic particles. It also, contains few glauconitic grains and is slightly dolomitic with the calcite cement. Microscopically, this section shows abundant detrital quartz and phosphatic particles including skeletal fragments (bones and teeth) and some intraclasts, and it is suggested that thin-sections MF (ZH-17, 18, 19 and 20) mostly represent calcareous phosphatic quartz arenite microfacies.

Interpreted depositional environment: the presence of phosphorite particles and glauconitic grains indicates that this sand is a marine sand with near-shore deposition for the supply of the abundant detrital quartz. The microfacies and sedimentological analysis suggest that this shallow near-shore marine depositional environment is restricted to the Wadi Es Sir Formation at the Zgaimat Al-Hasah section, and has only a relatively limited geographic distribution. It is probably equivalent to the depositional environment used as a similar facies by Wilson (1975); Southgate (1986).

12. Microfacies and Depositional Environments for the Wadi Sirhan-2 well

Thin-section studies show that the lower part of the Aljun Group in Wadi Sirhan-2 is represented by undifferentiated formations (Fig. 11). One core sample with a thickness of about 9 metres was cut in the undifferentiated Na'ur, Fuheis, Hummar and Shueib Formation from a depth of 643-790 metres. Four thin sections are made (Fig. 11). No core samples were cut in the Wadi Sir Formation in Wadi Sirhan-2. The summary of the undifferentiated formations as recognised in thin-sections is represented by the following WS-1, 2, 3, 4 and 5 (Table 4).

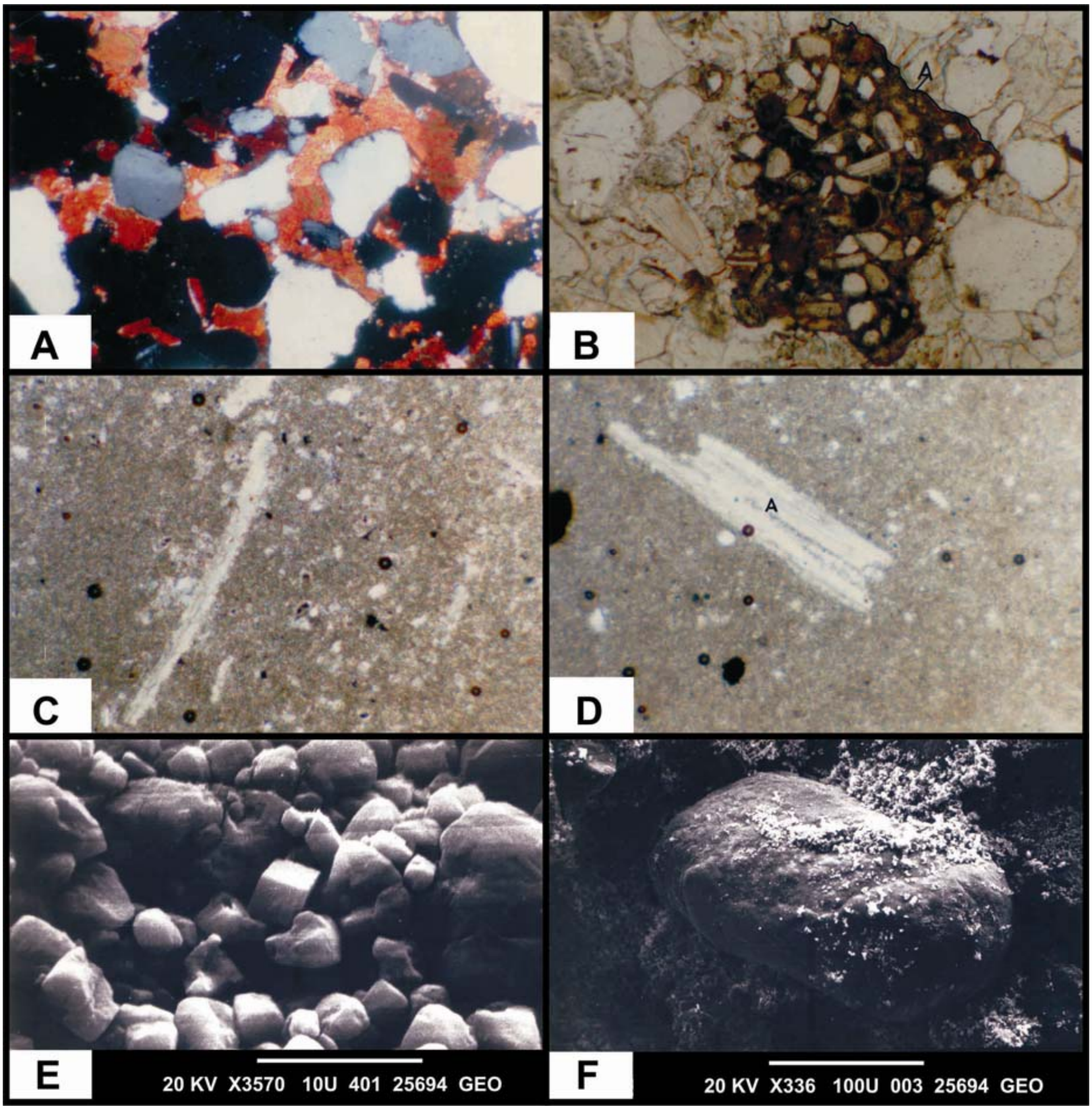

Fig. 10. Thin-section photomicrographs within the outcrop of Zgaimat Al-Hasah and Wadi Sirhan-2 Well. **A** Calcareous phosphatic quartz arentic microfacies shows calcite cements, phosphate particle brown-coloured pellets anisotropic fish debris - magnification X10/XPL. **B** Thin-section shows phosphate intraclasts (*A*) - magnification X10/ XPL. **C** Wackestone with numerous shell fragments embedding in micrite - magnification X10/ XPL. **D** Thin-section show pelecypod (shell fragment) - magnification X10/XPL. **E** SEM photomicrograph for MF (KZH-10) shows the crystal calcite. **F** SEM photomicrograph for Calcareous phosphatic quartz arentic microfacies show detrital phosphorite.

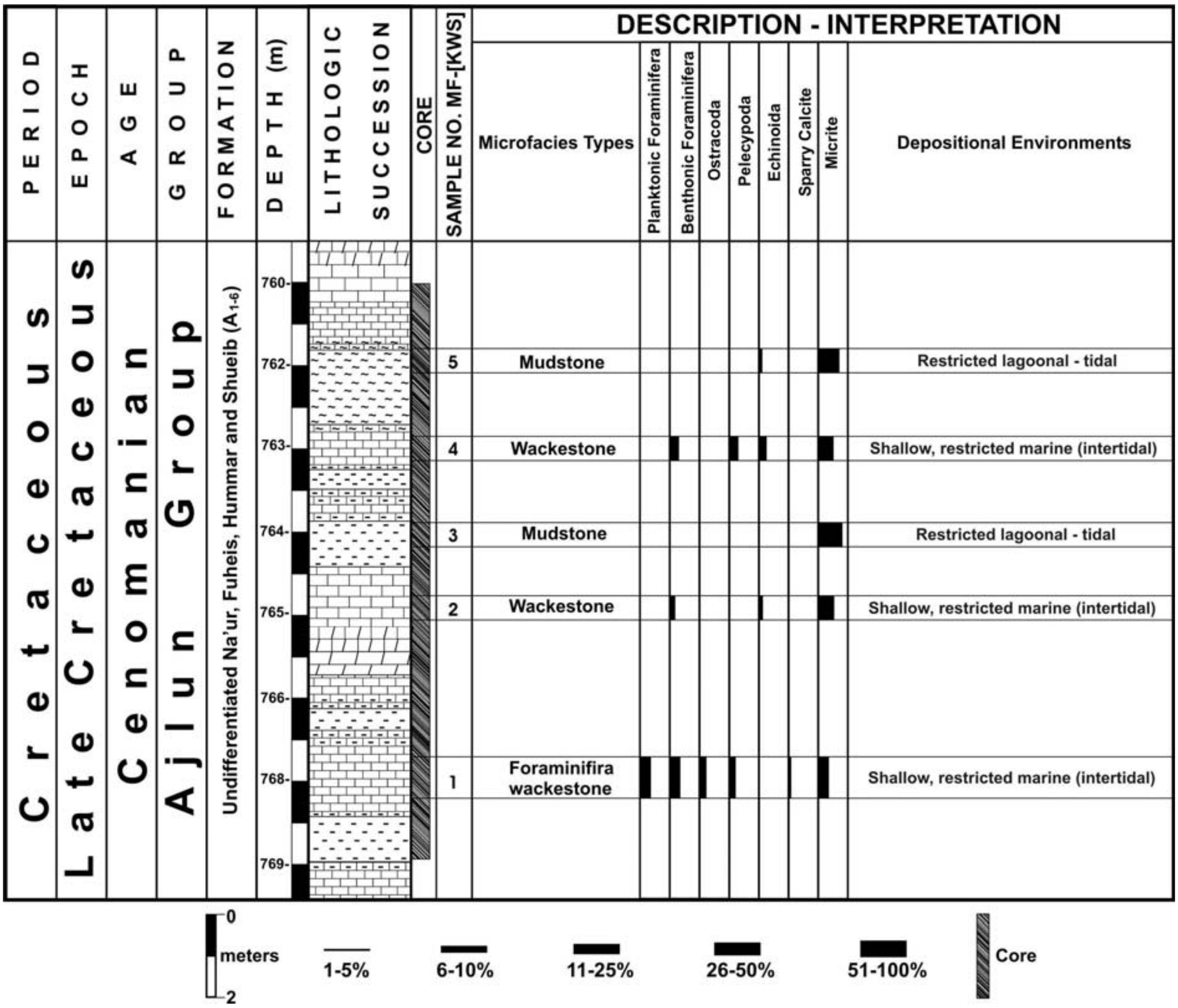

Fig. 11 Stratigraphic column of the undifferentiated Na'ur, Fuheis, Hummar and Shueib Formations in the Wadi Sirhan-2 well showing microfacies types, particles and depositional environment distribution.

Two microfacies analyses are recognized in this well. These microfacies belts and paleodepositional environments are discussed in ascending order below and the characteristics inherent to each facies are summarized in Fig. 4. They are subdivided into two major microfacies as follows: (1) foraminiferal wackestone/wackestone microfacies; and (2) mudstone microfacies.

13. Foraminiferal Wackestone/ Wackestone Microfacies

This facies consists mainly of shale to shaly limestone with a few levels of limestone. The shale is greenish grey to dark grey, locally red-brown, and limestone is cream to dark brown. In some shale beds a few foraminifers, ostracods and pelecypods are present. This belt is composed mainly of wackestone to foraminiferal wackestone textures in the Wadi Sirhan-2 well (Fig. 11).

The criterion for this microfacies is the abundance of generally well preserved debris fragments of echinoids, ostracods, pelecypods and foraminifers. Throughout the thin-section other fossils are present in smaller numbers, such as brachiopod etc. and few detrital quartz that are embedded in a micritic matrix. The results of microscopic investigations of this microfacies were also in thin-sections MF (WS-1, 2 and 4), as shown schematically in Fig. 11.

Interpreted depositional environment: this microfacies is highly diverse and its distribution pattern indicates deposition in intertidal environments (Flugel, 1982). The suggested environment for this facies is a shallow, restricted marine environment.

14. Mudstone Microfacies

This belt is dominated by shales, which comprise 70% or more of the Wadi Sirhan-2 well (Fig. 11). The shale is dark grey grading to greenish grey locally shaly limestone.

Microscopically, the term "lime mudstone microfacies" is used here in the manner suggested by Dundam (1962) to indicate rocks made up of pure lime mud. Microscopically, this microfacies is pure mudstone, for the most part without fossils, sometimes a few shell fragments of pelecypod, echinoids and foraminifers are present. Unfossiliferous mudstone consists completely of micrite which often shows dolomitization processes; see thin-sections MF (WS-3 and 5).

Interpreted depositional environment: this microfacies is believed to have been deposited in restricted lagoonal to tidal environments (cf. Flugel, 1982).

  - Volume 3, Number 1 (ISSN 1995-6681)

15. Discussion

The Ajlun Group, Cenomanian-Tutonian, is present throughout Jordan in except the extreme south where it was eroded as a consequence of the recent uplift associated with formation of the Dead Sea Transform (DST) in the Middle Miocene (Bender, 1974; Powell, 1989). It crops out fully in many wadis throughout the western mountain range forming the eastern shoulder of the DST. It becomes subsurface in the Jordanian plateau further east except for certain "inliers" like the Zgaimat Al-Hasah (Fig.1).

Typically, the group is made of alternating limestone and marl horizons ranging in thickness from 50 to 150 meters. However, sand starts to invade the group from central Jordan southwards until it becomes almost completely a marine sandstone in the south. The southwards increase of sand is explained by the proximity to the Palaeozoic Nubian sandstone facies. The abundant sandstone brought to the southerly localities seems to have diluted the carbonate facies or interfered seriously with the carbonate factory.

On the other hand, the group thickness decreases in the same direction of sand increase; i.e. southwards. In a distance of 350 km along the western mountain range, the thickness varies from around 600 meters in NW Jordan, 400-500 meters central Jordan to in the south. Also, the thickness decreases in a W-E direction, but more rapidly to 25 meters at Zgaimat Al-Hasah in a distance of <150 kilometres. (Fig. 12). We believe that the reason for the drastic decrease in the group thickness at the Zgaimat Al-Hasah is the presence of a paleohigh or arch called the Bayer-Kilwa Arch. This high decrease seems responsible for the non-deposition of the whole Triassic and Jurassic periods (Powell, 1989). With the onset of the major Cenomanian transgression, the Bayer-Kilwa high was submerged, thus creating some accommodation for the deposition of the Ajlun Group.

Such a setting would allow the deposition of Ajlun Group within the inner shelf not far way from the shore lines of the Neotethys further south east. Small changes in relative sea level, partly associated with low rate of uplift of the Jordanian plateau, can explain the changes in the microfacies and depositional environments described above. Four shallowing cycles are shown in Fig. 4. They consist of the slightly restricted shelf lagoon represented by the bioclast wackestone – packestone at the base changing into the more restricted micrite facies. The fourth cycle, consisting of phosphatic quartz arenite, indicates that the Zgaimat Al-Hasah became more proximal to the sand source area; i.e. shallowest.

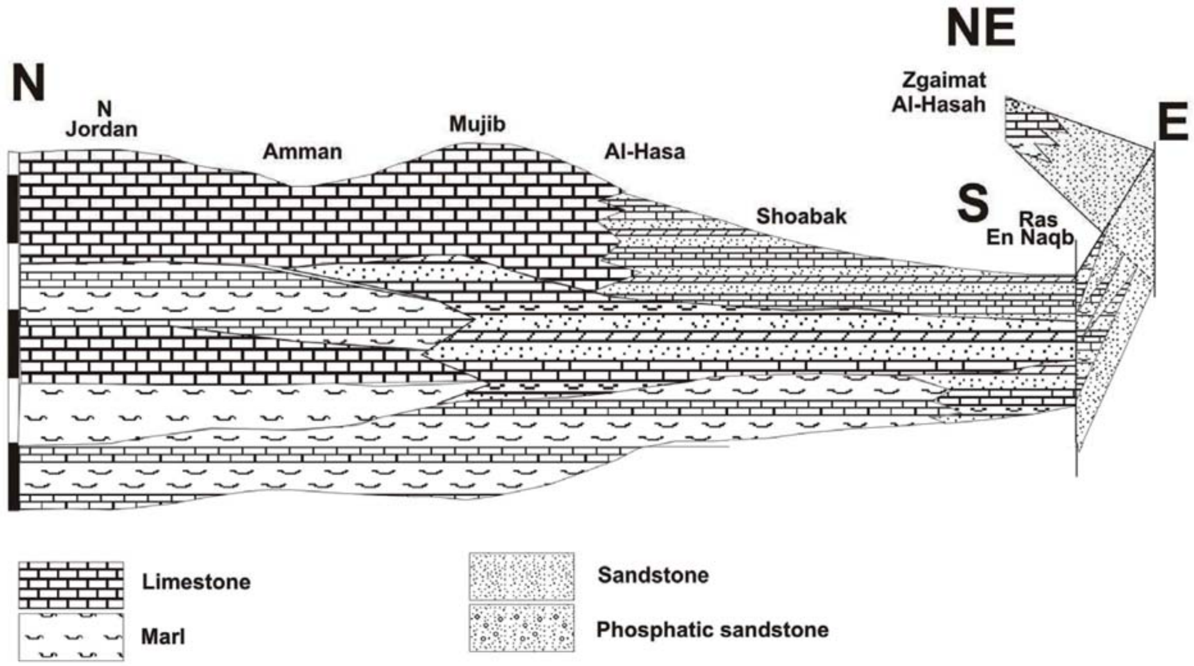

Fig. 12 A generalized fense diagram showing the lithological and thickness changes throughout Jordan.

16. Conclusions

1. Zgaimat Al-Hasah formed part of the Bayer-Kilwa paleohigh during most of the Mesozoic with the non-deposition of the Triassic and Jurassic periods.
2. Zgaimat Al-Hasah was submerged since the early Cenomanian as a consequence of a major global eustatic sea level rise, carbonate sedimentation commenced.
3. Changes in relative sea level associated with low rate of uplift in the Jordanian plateau did not allow much accommodation for sediments to accumulate, thus restricting them to 25 meters for the whole Ajlun Group compared with a 10-20 folds thickness in the western mountain range.
4. Microfacies analysis indicates near shore depositional environments of slightly restricted (wackestone/packstone) to more restricted shelf lagoon (micrite) arranged in 4 cycles of sea level changes. The 4th cycle contains phosphatic sandstone where accommodation is nearly closed.
5. The Sirhan Basin deepened northwards because the Bayer-Kilwa paleohigh is subdued in that direction or the basin is plunging in the same direction.

Acknowledgements

This work was supported principally by University of Jordan in collaboration with the Petroleum Geology Division of the Jordanian Natural Resources Authority as part of MSc thesis. I am grateful to Dr Grant-Mackie (The University of Auckland) for the review of the final version and his many suggestions and useful amendments.

References

Abed AM (1994) Shallow marine phosphorite-chert-palygorskite association, Late Cretaceous, Amman Formation, Jordan. In: Siliceous, pf the Tertiary and Mesozoic (Eds Jijima A, Abed AM, Garrison R), VSP, Zeist, Netherlands, pp. 205-324.

Abed A, Amireh BS (1999) Sedimentology, geochemistry, economic potential and palaeogeography of an upper Cretaceous phosphorite belt in the southeastern desert of Jordan. Cretaceous Research 20: 199-133.

Abed A, El Hiyari M (1986) Depositional environment and palaeogeography of the Cretaceous Gypsum Horizon in West-Central Jordan. Sed. Geol. 47: 109-123.

Abed AM, Schneider W (1982) The Cenomanian Nodular Limestone Member of Jordan, from subtidal to supratidal environment N. JB. Geol. Palaeontol Monatsh 9: 513-522.

Amireh BS (1997) Sedimentology and palaeogeography of the regressive-transgressive Kurnub Group (Early Cretaceous) of Jordan. Sed. Geol. 112: 69-88.

Barjous MO (1986) The Geology of Siwaqa, Map Sheet No. 3252 IV. Geological Mapping Project Bull. 4. Natural Resources Authority of Jordan, Amman.

Basha SH (1978) Foraminifera from the Ajlun Group of east Jordan. Jour. Geol. Soc. Iraq 11: 67-91.

Bender F (1974) Geology of Jordan. Borntraeger, Berlin, pp 196.

Bowen R, Jux U (1987) Afro-Arabian Geology. Chapman and Hall, London.

Dilley FC (1985) Cretaceous correlations in the Hamza Wells No. 1 to 5. Palaeontology Report No. 6. Natural Resources Authority of Jordan, Amman.

Dunham RJ (1962) Classification of carbonate rocks according to depositional texture. In: Classification of Carbonate Rocks. A Symposium (Ed. Ham WE), AAPG Mem. 1: 108-121.

Flugel E (2004) Microfacies Analysis of Limestone. Springer Verlag, Berlin, pp 1-975.

Haq BU, Qahtani AM (2005) Phanerozoic cycles of sea-level changes on the Arabian Platform. GeoArabia, 10: 27-160.

Holmes MJ, Harland WB, Suleiman AL (1989) The geology and seismic interpretation for Wadi Sirhan Area ‘A’. Natural Resources Authority of Jordan, Amman.

Krenkel E (1924) Der Syriasche Bogen. Zentralbulletin fur Mineralogie Geologies and Palaontologies, 9: 274-281; 10: 301-313.

Masri M (1963) The geology of the Amman-Zerqa Area. The Central Water Authority of Jordan, Amman.

MacDonald, SM, Partners (1965a) East Bank Water Resources. The Central Water Authority of Jordan, Amman, volume 6.

MacDonald SM, Partners (1965b) Bank Water Resources. Hydrogeological Survey of the Madaba-Maan area. The Central Water Authority of Jordan, Amman, volume 3.

Parker DH (1969) The hydrogeology of the Mesozoic-Cainozoic aquifers of the Western Pighlands and Plateau of East Jordan. UNDP/FAO 212.

Pettijohn EJ, Potter PE, Siever R (1973) Sand and sandstone. Springer, Berlin.

Powell J (1989) Stratigraphy and sedimentation of the Phanerozoic rocks in central and south Jordan, part B: Kurnub, Ajlun and Belqa Groups. Bulliten, vol. 11. Geology Directorate, Natural Resources Authority of Jordan, Amman, pp 130.

Qteishat A (1987) Wadi Sirhan Basin evaluation. Natural Resources Authority of Jordan, Amman.

Quennell AM (1951) The Geology and Mineral Resources of (former) Transjordan. Colonial Geology and Mineral Resources 2: 85-115.

Rabadi NR (1986) Final geological report on Wadi Sirhan-2 (WS-2). Natural Resources Authority of Jordan, Amman.

Rohl U, Dumont T, Von Rad, U, Martini R, Zaninete L (1991) Upper Triassic Tethyan carbonates off Northwest Australia (Wombat Plateau, ODP Leg 122). Facies 25: 211-252.

Selley RC (1988) Applied Sedimentology. Academic Press.

Southgate PN (1986) Cambrian phoscrete profiles, coated grains and microbial processes in phosphogenesis, Georgina Basin, Australia. J. Sed. Petrol. 56: 429-441.

Wetzel R, Morton DM (1959) Contribution a la geologie de la Transjordanie. Notes et Memoirs sur le Moyen Orient 7: 95-191.

Wilson JL (1975) Carbonate Facies in Geologic History, Springer, Berlin, pp 471.

Wolfart R (1959) Geology and hydrogeology of the Irbid District (Hshemite Kingdom of Jordan). Bundesanstalt fur Bodenforschung. Hannover.

JJEES

Volume 3, Number 1, June, 2010
ISSN 1995-6681
Pages 17- 24

Jordan Journal of Earth and Environmental Sciences

Column Flotation of Non-Slimed Jordanian Siliceous Phosphate

Salah Al-Thyabat

Faculty of Engineering /Al-Hussein Bin Talal University –Jordan

Abstract

In phosphate flotation, it is a standard practice to remove (deslime) fine particles before conducting flotation. Since phosphate matrix is friable, agitating, scrubbing, or grinding causes a significant loss in valuable phosphate; this has an economic and ecological impact on phosphate industry. The aim of this study is to minimise the loss of phosphate slime by conducting column flotation without desliming. Fractional factorial experimental design was used to evaluate flotation performance of non-slimed siliceous phosphate in flotation column. The effect of gas flow rate, feed size (P_{80}), and sodium silicate dosage were statistically evaluated. The results showed that gas flow rate followed by feed size were the most significant parameters. The general trend in flotation results was poor flotation recovery and concentrate grade. However, concentrate grade and flotation recovery were slightly improved when fine feed was used which may be due to the increase in phosphate particles liberation.

Keywords: Column Flotation, Sedimentary Phosphate Flotation, Phosphate Slime, Jordan.

1. Introduction

Using column flotation in minerals industry has been increased in recent years. Conventional mechanical flotation cells have been replaced by column cells in several mines especially in cleaning circuits. The main advantages of column flotation can be summarised as follows (Yahyaei et al, 2008; Finch and Doby,1991;Tao et al, 2000; Ityokumbul,1992; Oliveira et al,2007; Hacifazlioglu ,and Sutcu,2007; Guimaraes and Peres,1999; Fortes et al,2007; Delvillar et al,1999; Abdel-Khalek et al, 2000).

- Cleaner concentrate which reduces cleaning and re-cleaning circuits.
- Reducing energy consumption because of less mechanical parts compared with mechanical flotation cells.
- Less maintenance costs due to less mechanical parts.
- High capacity to size-ratio compared to mechanical flotation cell, which may reduce capital costs.

Extensive research has been done in order to identify the important operating parameters that affect column flotation performance in order to maximise flotation recovery and concentrate grade. To mention some, Patile et al (1996) used factorial experimental design to study the effect of gas flow rate, wash water, and froth height on column flotation of Indian siliceous phosphate. Using Sodium Oleate as phosphate collector and sodium silicate as silica depressant, the authors obtained concentrate grade containing 31% P_2O_5 with more than 94 % recovery.

* Corresponding author: salah.thyabat@ahu.edu.jo; althyabat@yahoo.co.uk

El- Shall et al (2003) studied the use of column flotation to upgrade Florida coarse phosphate (850-425 μm) feed. The authors used different types of frothers to investigate the effect of collector –frother interaction on flotation recovery and concentrate grade. They obtained a concentrate assaying 31% P_2O_5 with more than 96% recovery.

Ityokumbul et al (2003) evaluated the effect of amine dosage and airflow rate on phosphate rougher flotation in a pilot- plant column cell. The authors mentioned that collector dosage used in column flotation was less than that used in conventional mechanical cell. In addition, the authors claimed that flotation water didn't significantly affect flotation efficiency if its pH, and turbidity were kept under a certain level.

Recently, Fortes et al (2007) used bench- scale column flotation to separate siliceous gangue from Brazilian phosphate ore. Using alkali amine as silica collector and cornstarch as phosphate depressor, the authors obtained concentrate with less than 8% SiO_2 and more than 90 % P_2O_5 recovery.

In most of phosphate flotation reported in the literature, flotation feed is usually deslimed i.e. fine fraction, less than 100 μm , is removed. This is due to the deteriorating effect of slimes on flotation recovery and concentrate grade. Phosphate particles are friable; so agitating, scrubbing or grinding followed by desliming may cause an economic loss where considerable amount of phosphate is lost. This work is an attempt to evaluate the possibility of separating valuable phosphate from siliceous gangue by column flotation without desliming. Flotation performance was statistically evaluated by laboratory scale column flotation using different feed size (P_{80}), depressant dosage, and gas flow rate.

2. Experimental set up

Phosphate feed used in this work was obtained from Eshydia mine in south of Jordan. The feed (-1mm) was dried in 70c oven for 24 hours then separated into two parts: feed 1 is (-1000+355 μm) while feed 2 is (-355 μm). No further desliming was conducted on both feeds. Chemical analysis of flotation feed, concentrate and tailing were conducted by Induced coupled Plasma-spectroscopy (ICP). Tables 1 and 2 show the chemical and physical analysis of these feeds.

Table 1 Chemical analysis of flotation feed.

Content	%wt	
	Feed1	Feed 2
P_2O_5	23.6	21.2
SiO_2	34.4	41.7
CaO	35.6	31.8
Fe_2O_3	0.66	0.49
Al_2O_3	0.65	0.37
MgO	0.2	0.14
LOI	3.56	2.94

Table 2 Size distribution of flotation feeds (feed 1 and 2).

Upper size (micron)	% Undersize	
	Feed 1	Feed 2
1000	100.00	*
710	82.61	*
500	50.35	*
355	*	100.00
255	*	57.37
180	*	31.40
125	*	16.22
90	*	5.71
63	*	2.73
45	*	1.05

Flotation tests were conducted by column flotation as shown in Figure 1. For each test, 3kg of the feed was conditioned with the required amount of collector in 45 L tank at 50 % solids for 10 minutes. The pulp was then diluted to 10 % solids and frother was added. Slurry was then pumped into the column until the pulp level reached the required height (froth height 1 m).

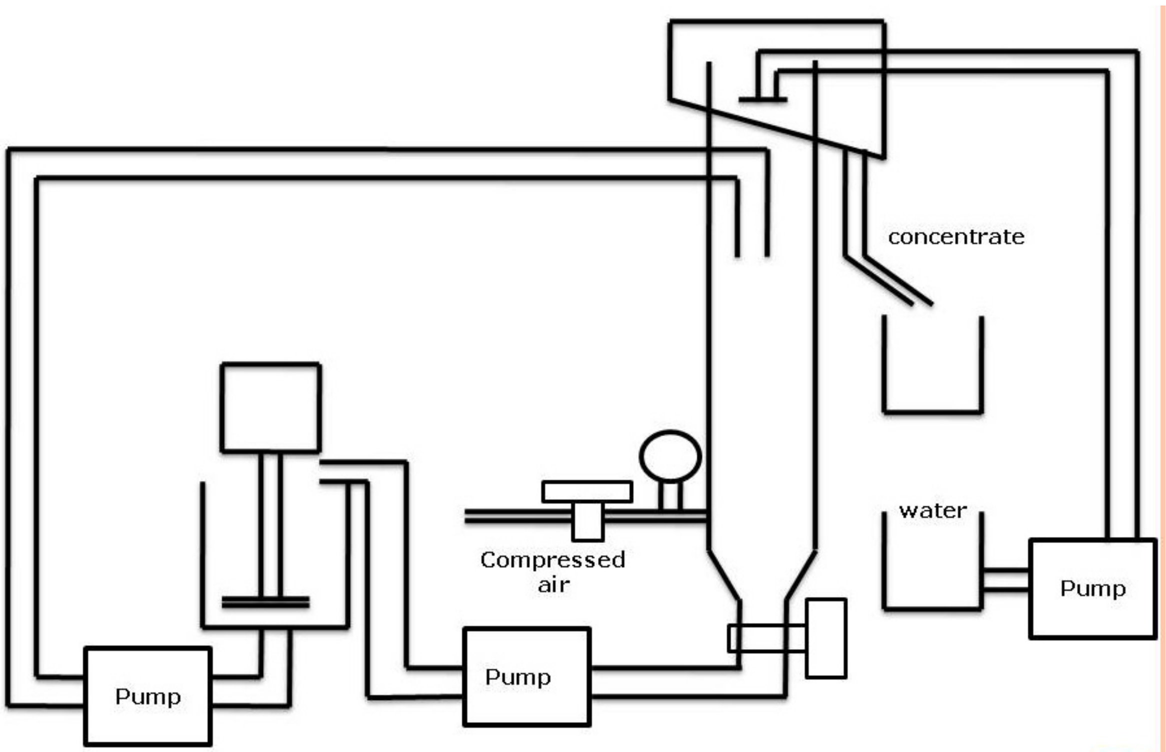

Figure 1. Schematic diagram of flotation column

Slurry pumping rates were calibrated to keep pulp level at 2m. Air was then introduced to the cell for 10 minutes. Concentrate was collected and the slurry left in the column and tanks were collected as flotation tailing. Flotation and conditioning parameters shown in Table 3 were held constant throughout the test unless otherwise is stated. Chemicals used in flotation tests were oleic acid as phosphate collector, sodium silicate as silica depressor, Dowfroth200 as frother, and sodium hydroxide as pH modifier. All these chemicals were used in their reagent grade.

Table 3 Constant parameters of conditioning and flotation

Conditioning		Flotation	
Parameter	value	Parameter	value
Solids %	50 %	Solids %	10
Time	10 minutes	Flotation time	10 minutes
pH	9.5	Wash water	0.2 L/min (0.019cm/s)
Impeller speed	750 RPM	Collector dosage/(g/t)	1200 (4.2×10^{-3} M)
Solids charge	3000 g	Froth height	1000 mm
Water type	Tap water	Frother dosage (MIBC)	80 PPM

Two level fractional factorial experimental design (2^3) with one replicate was used to evaluate flotation performance on different set of parameters. These parameters and their values are shown in Table 4. Flotation recovery, concentrate grade, and amount of water reported to concentrate were measured for each test.

Table 4 Variable conditioning and flotation parameters

Parameter	Values	
	Low	High
Feed size(FS) (P80,micron)	300	700
Sodium silicate(S.S) (g/t)	0	100
Air flow rate(J_g)(cm/s)	1	1.5

3. Results and discussion

3.1. The effect of flotation parameters on recovery and concentrate grade

The results of flotation experiments and their replicates are shown in Table 5.The table shows that fractional factorial design was used to evaluate of the studied flotation parameters and their interactions on flotation recovery and grade.

Statistical analysis (analysis of variance, ANOVA) was conducted on previous results in order to statistically evaluate the effect of these parameters as shown in Tables 6 and 7.

Table 5 Flotation experimental results

Exp No.	FS micron	S.S g/t	J_g cm/s	Replicate 1		Replicate 2	
				Recovery %	P_2O5 %	Recovery %	P_2O5 %
1	L	L	L	29.60	28.12	29.35	27.71
2	H	L	L	16.84	28.61	16.71	28.26
3	L	H	L	13.32	27.89	13.46	27.25
4	H	H	L	30.84	26.87	30.29	26.53
5	L	L	H	62.53	28.69	62.97	28.10
6	H	L	H	26.60	24.70	24.96	25.30
7	L	H	H	77.81	27.28	77.92	27.29
8	H	H	H	29.02	24.74	28.93	24.82

Table 6 ANOVA analysis of flotation recovery

Source	Sum Sq.	d.f	Mean Sq.	F	Prob>F
FS	1713.96	1	1713.96	2088.25	0
S.S	68.89	1	68.89	88.93	0
J_g	2754.68	1	2754.68	3356.24	0
FS*S.S	85.66	1	85.66	104.36	0
FS*J_g	2078.45	1	2078.45	2532.34	0
S.S*J_g	112.57	1	112.57	137.16	0
FS*S.S*J_g	409.05	1	409.05	498.38	
Error	6.57	8			
Total	7229.82	15			

Table 7 ANOVA analysis of concentrate grade

Source	Sum Sq.	d.f	Mean Sq.	F	Prob>F
FS	7.3712	1	7.3712	19.11	0.0024
S.S	3.0102	1	3.0102	7.81	0.0234
J_g	4.4944	1	4.4944	11.65	0.0092
FS*S.S	0.2162	1	0.2162	0.56	0.4755
FS*J_g	6.5025	1	6.5025	16.86	0.0034
S.S*J_g	0.2025	1	0.2025	0.53	0.4894
FS*S.S*J_g	0.6241	1	0.6241	1.62	0.2391
Error	3.0858	8	0.385725		
Total	25.507	15			

Table 6 showed that all the flotation parameters (feed size, sodium silicate dosage, and gas flow rate) and their interactions were significant for flotation recovery. However, a comparison between F- values showed that gas flow rate (Jg) has the most significant effect followed by the interaction between feed size and gas flow rate. On the other hand, sodium silicate has the least significant effect; even less than the third interaction between feed size, gas flow rate and sodium silicate. Feed size (P_{80}) was the third significant parameter but its interaction with gas flow was more significant. This emphasizes the role of interactions between parameters in flotation.

Increasing feed size with the same amount of collector reduced the amount of particles reported to concentrate by true flotation since coarser particles require larger area coverage by the collector to be attached strongly enough to the rising air bubbles. On the other hand, fine feed increased the recovery of both gangue and valuable particles due to either entrapment in froth or by entrainment with the rising swarm of bubbles. Increasing gas flow rate encouraged such entrainment but has more effect on flotation of fine particles .These results are in agreement with those obtained by Patil et al (1996) who stated that bubble- particle collection rate is linearly proportional to gas flow rate. On the other hand, the addition of sodium silicate improved the selectivity of the collector by depressing silica and stabilizing the froth. Further increase of sodium silicate increased the bulk precipitation of sodium silicate on both of apatite and silicate surface, which affect the selectivity and apatite recovery (Dho and Iwasaki, 1990).

Table 7 shows that concentrate grade was less sensitive to the change on flotation parameters. Feed size followed by the interaction between gas flow rate and feed size were the most significant parameters. On the other hand, feed size and sodium silicate interactions, sodium silicate and gas flow rate interactions, as well as the third interaction between feed size, sodium silicate and gas flow rate were not significant. This may be due to the non-selectivity in flotation of this type of non-slimed feed where phosphate particles may report to concentrate by other means than true flotation (bubble–particle attachment) such as entrainment. The improvement of concentrate grade when using finer feed and higher gas flow rate supports this claim.

3.2. The relation between water recovery and flotation performance

Table 8 shows the results of water flow rate (J_w) reported to concentrate normalised by the cell cross section while Table 9 and 10 show ANOVA analysis of water recovery. Separation efficiency (SE) was calculated by equation 1.

$$SE = (P_2O_5 \text{ recovery} \times silica\ \ removal\ )*100\% \tag{1}$$

Table 8 Flotation experimental results

Exp No.	FS micron	S.S g/t	J_g cm/s	Replicate 1		Replicate 2	
				J_w (cm/s)	SE %	J_w (cm/s)	SE %
1	L	L	L	0.0399	26.48	0.0418	23.27
2	H	L	L	0.0397	15.58	0.0346	16.10
3	L	H	L	0.0626	13.04	0.0625	10.92
4	H	H	L	0.0644	24.95	0.0641	27.78
5	L	L	H	0.1530	48.81	0.1530	47.20
6	H	L	H	0.0762	19.97	0.0746	21.03
7	L	H	H	0.1355	54.78	0.1409	55.22
8	H	H	H	0.1461	22.89	0.1367	21.04

Table 9 ANOVA analysis of separation efficiency (SE)

Source	Sum Sq.	d.f	Mean Sq.	F	Prob>F
FS	761.48	1	761.48	400.78	0
S.S	9.27	1	9.27	4.90	0.0582
J_g	1102.57	1	1102.57	580.3	0
FS*S.S	80.01	1	80.01	42.11	0.0002
FS*J_g	1085.37	1	1085.37	571.25	0
S.S*J_g	29.32	1	29.32	15.43	0.0044
FS*S.S*J_g	209.53	1	209.53	110.28	0
Error	15.2	8	1.9	1	
Total	3292.77	15			

Table 10 ANOVA analysis of water recovery

Source	Sum Sq.	d.f	Mean Sq.	F	Prob>F
FS	0.00146	1	0.0015	155.86	0
S.S	0.0025	1	0.0025	267.02	0
J_g	0.02298	1	0.0230	2454.75	0
FS*S.S	0.00186	1	0.0017	198.41	0
FS*J_g	0.00131	1	0.0013	139.97	0
S.S*J_g	0	1	0	0.15	0.7052
FS*S.S*J_g	0.00142	1	0.0014	151.81	0
Error	0.00007	8	0.00001		
Total	0.03161	15			

As shown in previous tables, gas flow rate, feed size and their interactions were the most significant parameters on separation efficiency and water recovery. Gas flow rate effect was very significant in water recovery, even higher than the effect of feed size. This shows that gas flow rate increases particle entrainment by increasing water recovery. This was more apparent in flotation of the finer feed.

In all previous results, the general trend was low recovery and concentrate grade, which may be due to poor liberation of phosphate particles in this non-slimed feed. So to investigate the effect of feed liberation on flotation performance, the previous +1 mm run of mine feed were wet grinded by rod mill for 10 minutes to (P_{80}=280 μm) (feed 3). Flotation results for this non-slimed feed are given in the following section.

3.3. The effect of feed size on flotation performance

Size distribution and chemical analysis of feed 3 are given in Tables 11 and 12 while flotation parameters and results are given in Table 13.

Table 11 Size distribution of flotation feed (feed 3).

Upper size (micron)	% Undersize
500	100.00
355	90.61
255	75.80
180	48.02
125	29.54
90	12.42
63	6.36
45	3.12

Table 12 Chemical analysis of flotation feed (feed 3)

Content	Feed 3(%)
P_2O_5	27.6
SiO_2	23.6
CaO	41.8
Fe_2O_3	0.6
Al_2O_3	0.65
MgO	0.25
LOI	3.56

Table 13 Flotation experimental results (feed3)

Collector dosage :1200 g/t ,wash water :200 ml/min, gas flow rate :1.5 cm/s						
Exp No.	Frother (ppm)	S.S g/t	P_2O_5 %	P_2O_5 Recovery %	Silica removal %	Separation Efficiency %
1	40	160	29.8	67.4	76.1	51.21
2	80	160	30.4	56.3	83.0	46.71
3	40	320	30.2	53.7	83.6	44.90
4	80	320	30.4	55.9	83.6	46.71

A comparison between the results shown in Table 13 with those in Table 5 showed an improvement in both of concentrate grade and recovery. This indicates an increase in the percentage of particles reported to concentrate by true flotation other than non-selective entrainment. According to Peng and Gu (2005), about 85 % of Florida phosphate particles are liberated at (P_{100}=300 μm). By interpolation of Peng and Gu data, phosphate feed need to be ground to at least (P_{100}=150 μm) to obtain 95% liberation.

4. Conclusions

Based on previous results, the following conclusions can be drawn:

- Factorial experimental design used in this work showed that the interaction between flotation parameters was significant on flotation recovery and concentrate grade. The order of significance was gas flow rate, feed size, and sodium silicate dosage.
- Agitating and scrubbing of flotation feed was very significant on flotation recovery and concentrate grade especially with no grinding because of low phosphate particles liberation. The effect of slimes (fines) generated by such process on flotation performance can be reduced by using column flotation.

References

Abdel-Khalek, N.,Hassan , F., and Arafa, M.,2000. Separation of valuable fine phosphate particles from their slimes by column flotation, Separation Science and Technology, 35(7):1077–1086.

Delvillar ,R., Grigoire ,M., and Pomerleau,A.,1999. Automatic control of a laboratory flotation column, Minerals Engineering, 12(3): 291-308.

Dho,H., and Iwasaki, I., 1990.Role of sodium silicate in phosphate flotation, Minerals and Metallurgical Processing, 11:215-221.

El-Shall., A Abdel-Khalek;N., and El-Mofty,S.,2003. Role of frothers in column flotation of coarse phosphates, Minerals and Metallurgical Processing, 20 (4): 199-205.

Finch, J.A., and Doby, G.S., 1991.column flotation: A selected review –Part V, International Journal of minerals processing, 33:343-347.

Fortes, M., Silva, A., Rogerio, C., Guimaraes, R., Ataıde, C., and Barrozo, M., 2007. Pre-separation of Siliceous Gangue in Apatite Flotation, Industrial Engineering and Chemistry Research 46:7027-7029.

Guimaraes,C., and Peres,A.,1999. Interfering ions in the flotation of a phosphate ore in a batch column, Minerals Engineering, 12(7): 757-768.

Hacifazlioglu ,H., and Sutcu,H.,2007.Optimization of some parameters in column flotation and a comparison of conventional cell and column cell in terms of flotation performance, Journal of the Chinese Institute of Chemical Engineers, 38: 287–293.

Ityokumbul; M.T., Brooks; G., Yensco; M., Ellington, J.T., 2003. Pilot-plant evaluation of amine flotation of rougher phosphate concentrate, Minerals and Metallurgical Processing 20(1): 52-56.

Ityokumbul, M.T., 1992. A new approach to flotation column design, Minerals Engineering, 5(6): 685-691.

Oliveira,M., Queiroz,G., Guimaraes,R., Ataıde,C.,and Barrozo ,M.,2007. Selectivity in phosphate column flotation, Minerals Engineering 20 : 197–199.

Peng,F., and Gu,Z., 2005 Processing Florida dolomitic phosphate pebble in a double reverse fine flotat, Minerals and Metallurgical Processing, 22(1): 23-30.

Tao, D., Luttrell, G.H., Yoon, R.H., 2000. A parametric study of froth stability and its effect on column flotation of fine particles, International Journal of Minerals Processing 59: 25–43.

Yahyaei ,M., and Banisi ,S., and ,.Javani ,H.,2006. Replacing Mechanical Flotation Cells by a Flotation Column at the Pilot Plant of the Sarcheshmeh Copper Mine, Separation Science and Technology, 41: 3609–3617.

JJEES

Volume 3, Number 1, June, 2010
ISSN 1995-6681
Pages 25- 36

Jordan Journal of Earth and Environmental Sciences

Paleostress Analysis of the Cretaceous Rocks in Northern Jordan

Nuha Al Khatib [a], Mohammad atallah [a], Abdullah Diabat [b,*]

[a] Department of Earth and Environmental Sciences, Yarmouk University Irbid-Jordan

[b] Institute of Earth and Environmental Sciences, Al al-Bayt University, Mafraq- Jordan

Abstract

Stress inversion of 747 fault- slip data was performed using an improved Right-Dihedral method, followed by rotational optimization (WINTENSOR Program, Delvaux, 2006). Fault-slip data including fault planes, striations and sense of movements, are obtained from the quarries of Turonian Wadi As Sir Formation , and distributed over 14 stations in the study area of Northern Jordan. The orientation of the principal stress axes (σ_1, σ_2, and σ_3) and the ratio of the principal stress differences (R) show that σ_1 (SHmax) and σ_3 (SHmin) are generally sub-horizontal and σ_2 is sub-vertical in 9 of 15 paleostress tensors, which are belonging to a major strike-slip system with σ_1 swinging around NNW direction. Four stress tensors show σ_2 (SHmax), σ_1 vertical and σ_3 are NE oriented. This situation is explained as permutation of stress axes σ_1 and σ_2 that occur during tectonic events. The new paleostress results show three paleostress regimes that belong to two main stress fields. The first is characterized by E-W to WNW-ESE compression and N-S to NNE –SSW extension. This stress field is associated with the formation of the Syrian Arc fold belt started in the Turonian. The second paleostress field is characterized by NW-SE to NNW-SSE compression and NE-SW to ENE-WSW extension. It is related to Middle Miocene – Recent sinistral movement along the Dead Sea transform and the opening of the Red Sea.

Keywords: Paleostress, Turonian- Miocene, Northern Jordan.

1. Introduction

The major structures in the Levant are the Dead Sea transform (DST) and the Syrian Arc belt (SAB). The Dead Sea transform extends from the Gulf of Aqaba in the south to the Taurus mountains in Turkey in the north. It separates the Arabian plate from Sinai sub-plate and connects the Red Sea spreading center with the Alpine orogeny in the north (Fig. 1). The DST was formed as a result of the northward sinistral movement of the Arabian plate associated with the opening of the Red Sea. The movement started in the Miocene and is still active in the present times. The Syrian arc is a system of fold belts extending from Sinai in the southwest to central Syria in the northeast (Fig. 1). This folding was formed in two phases. The first phase formed in the Turonian-Maestrichtian and the second phase in the Oligocene. The structural pattern of Jordan was affected since the Late Cretaceous by the movement along the DST and the formation of the SAB . The regional tectonics of the continental part of the Arabian plate including Jordan has been studied through macrostructures by many authors (e.g., Burdon 1959; Bender 1968; Mikbel and Zacher 1981; Quennell 1983; Mikbel 1986; Atallah 1992). Few analyses have been focusing, however, on the regional tectonics based on mesostructures in Jordan (e.g., Salameh and Zacher 1982; Diabat 1999, 2002; Zain Eldeen et al.,2002; Diabat et al., 2003., 2004; Diabat and Masri 2005). The relative motion across the DST has been estimated both by regional plate motion models and local slip rate considerations. The regional plate motion studies used the fault orientation , additional local observations, and constraints from the motion of neighboring plates to estimate 5- 10 mm/ yr of relative motion across the DST (e.g., Garfunkel, 1981; Joffe and Garfunkel, 1987; Chu and Gordon, 1998). Local geologic and seismic studies, which estimate the slip rate across the DST, yielded a wider range of relative motion estimates, from 1 to 10 mm/ yr (e.g., Freund et al., 1968 ; Mckenzie et al., 1970; Ben Avraham et al., 1979; Shapira and Hofstetter, 1993; Klinger et al., 2000a, 2000b). Generally, seismic estimates show a rate of only 1- 4 mm/ yr, geomorphologic estimates are in the range of 3- 7 mm/ yr, whereas long-term geological estimates are in the range of 6- 10 mm/ yr. Space geodetic technologies, in particular GPS, providing the first direct estimates of current plate motion in the eastern Mediterranean, estimated the current slip rate across the DST as 3.3 +- 0.4 mm/ yr.

Mesostructures are considered to be accurate indicators of the paleostress and strain orientation (Angelier, 1979, 1989, 1994; Delvaux et al., 1995, 1997).

Horizontal stylolites in Jordan were measured and described for the first time by Salameh and Zacher (1982), when they studied the relationship between stylolites and

* Corresponding author. abdullahdiabat@yahoo.ca

paleostresses. Zain Eldeen et al (2002) studied the tectonic evolution of the Wadi Araba segment (the southern part of the DST), based on fault slip data. Diabat (1999) and Diabat et al. (2004) studied the paleostresses at the eastern rim of the DST. The study represents the first results of the paleostresses in Jordan based on fault slip data (Slickenside analysis). Their results summarize the stress field east of the DST in two compression stress systems; the NNW-SSW Dead Sea system (DSS), and the Syrian Arc system (SAS).

The area of investigation is located in the northern part of Jordan (Figs1,2 and 3). It includes Al Husn, Shatana, Kitim, Deyr Yusif, Eshtafaina, and Thaghret Asfour, where Upper Cretaceous (Turonian) rocks are well exposed in many quarries. This gives a good opportunity for measuring fault slip data.

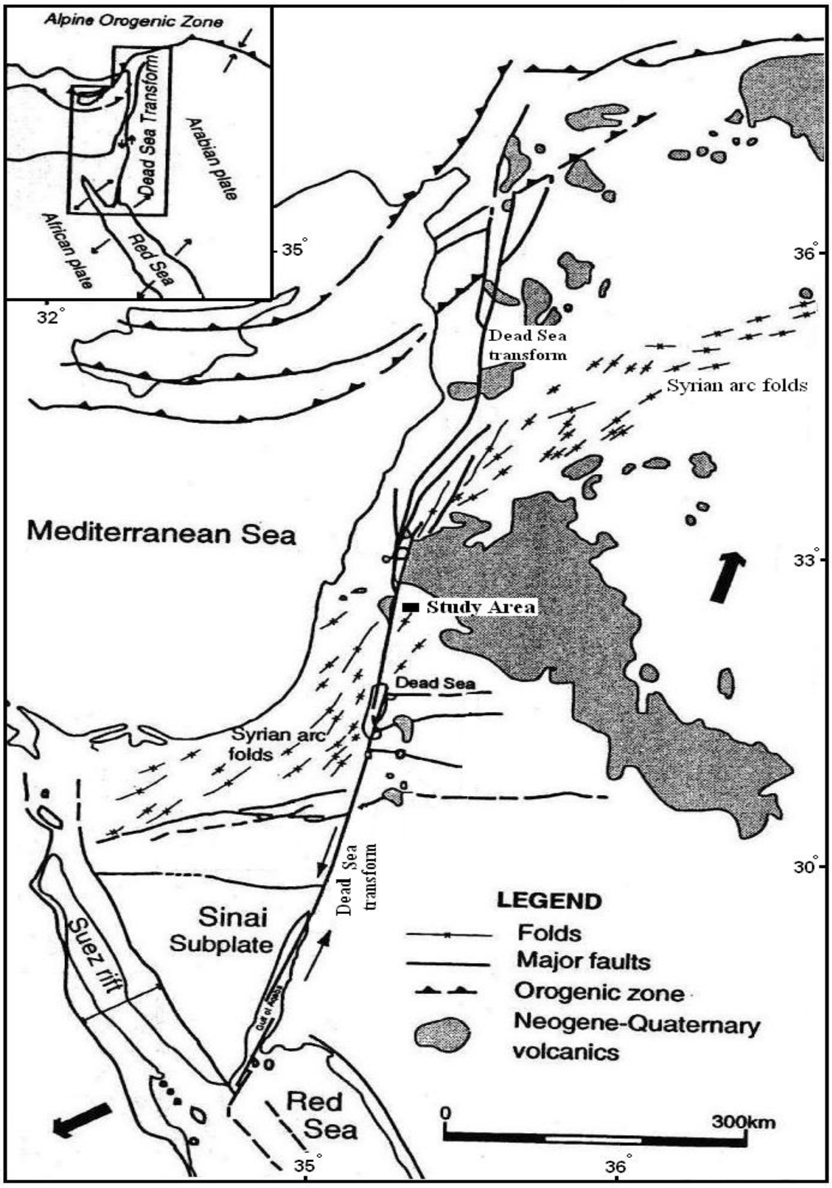

Fig. 1. Tectonic setting of the Dead Sea transform and the Syrian Arc, showing the study area (modified after Garfunkel, 1981).

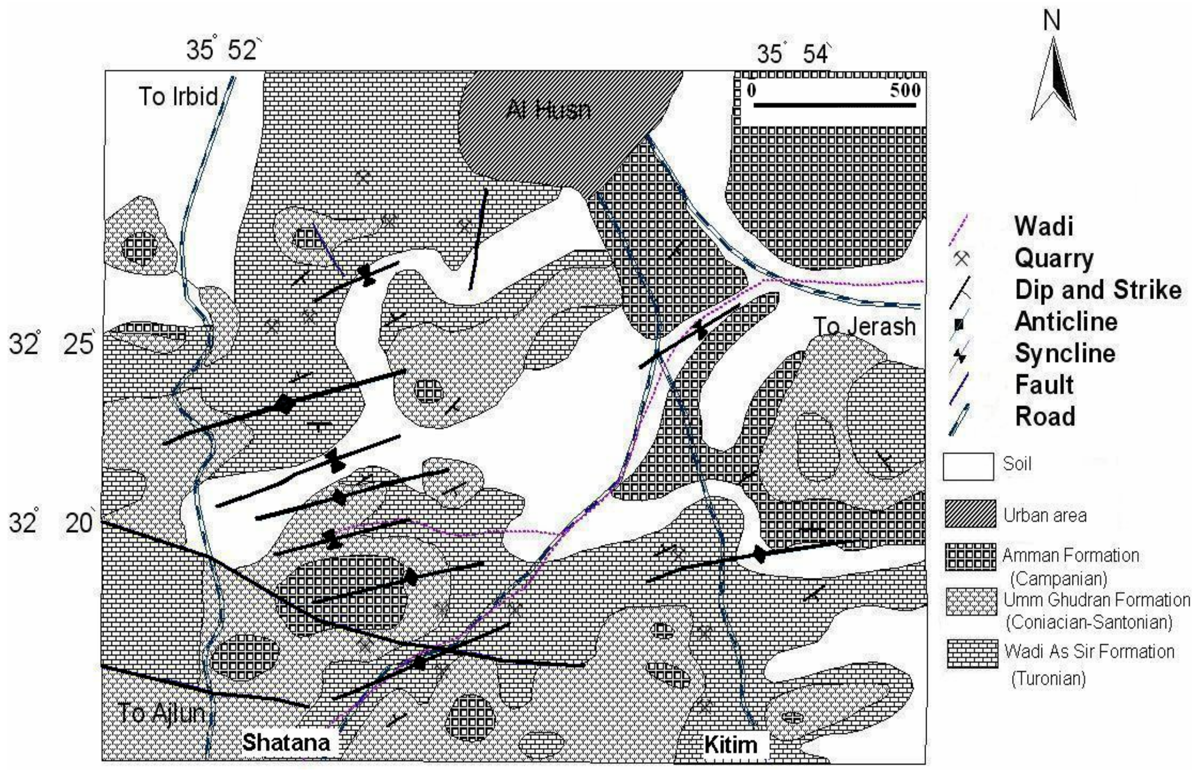

Fig. 2.a (1): Geological map of Al Husn area.

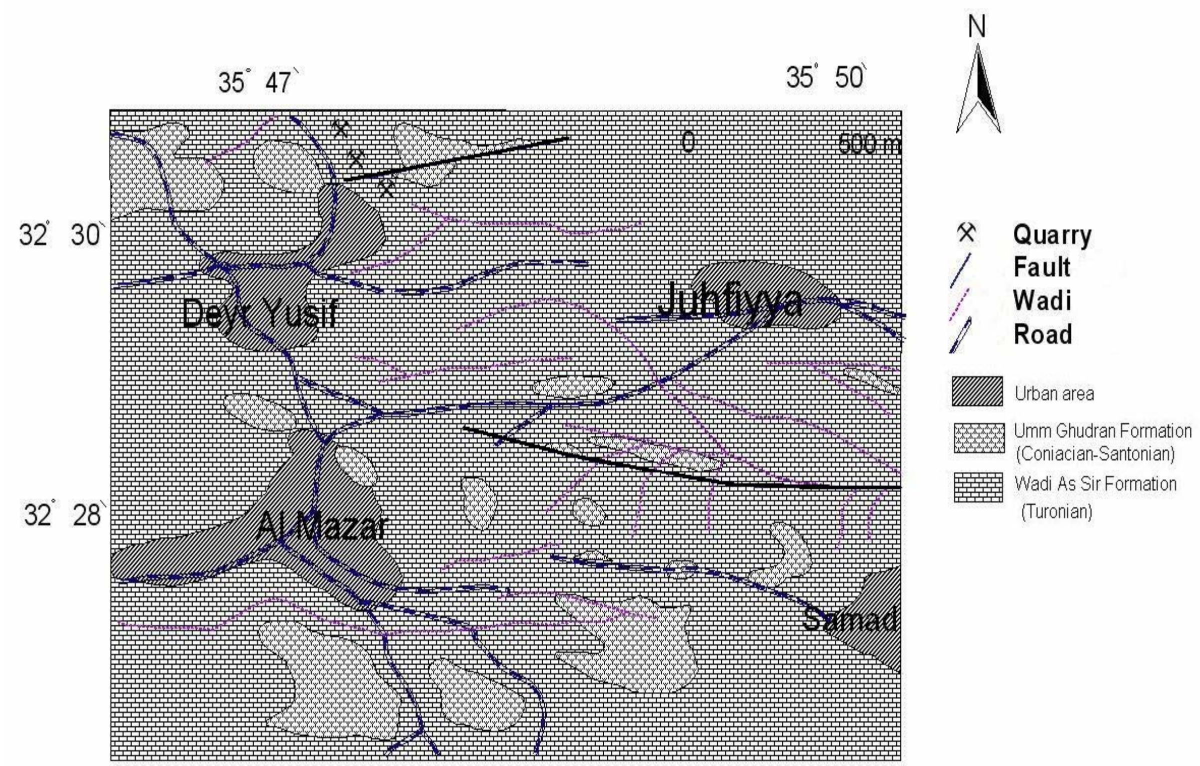

Fig. 2.a (2): Geological map of Deyr Yusif area.

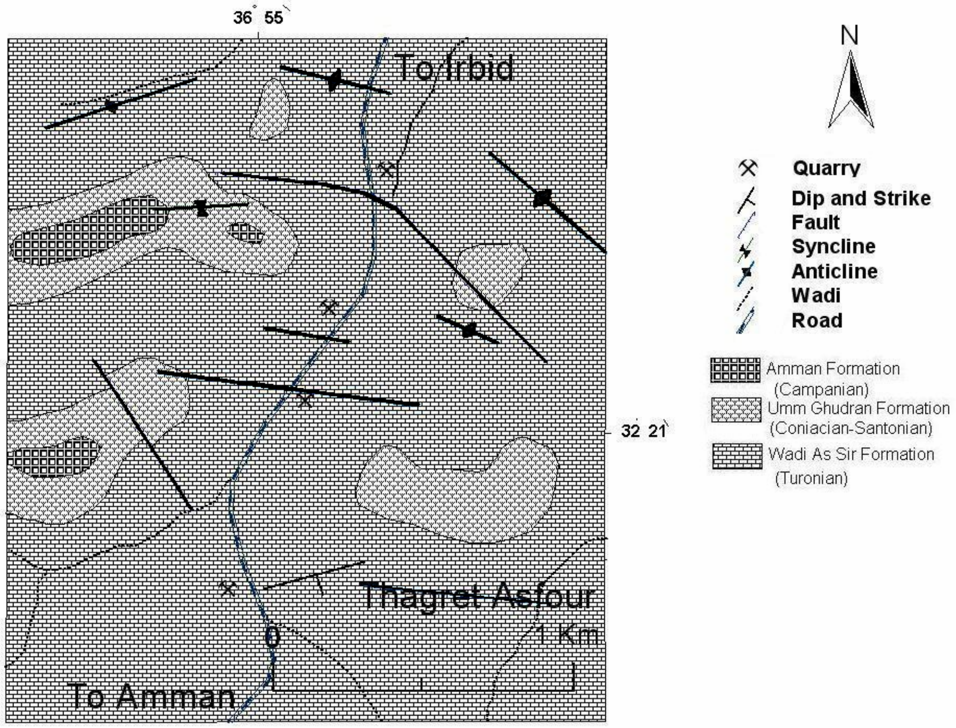

Fig 2. b (1) : Geological map of Thagret Asfour area.

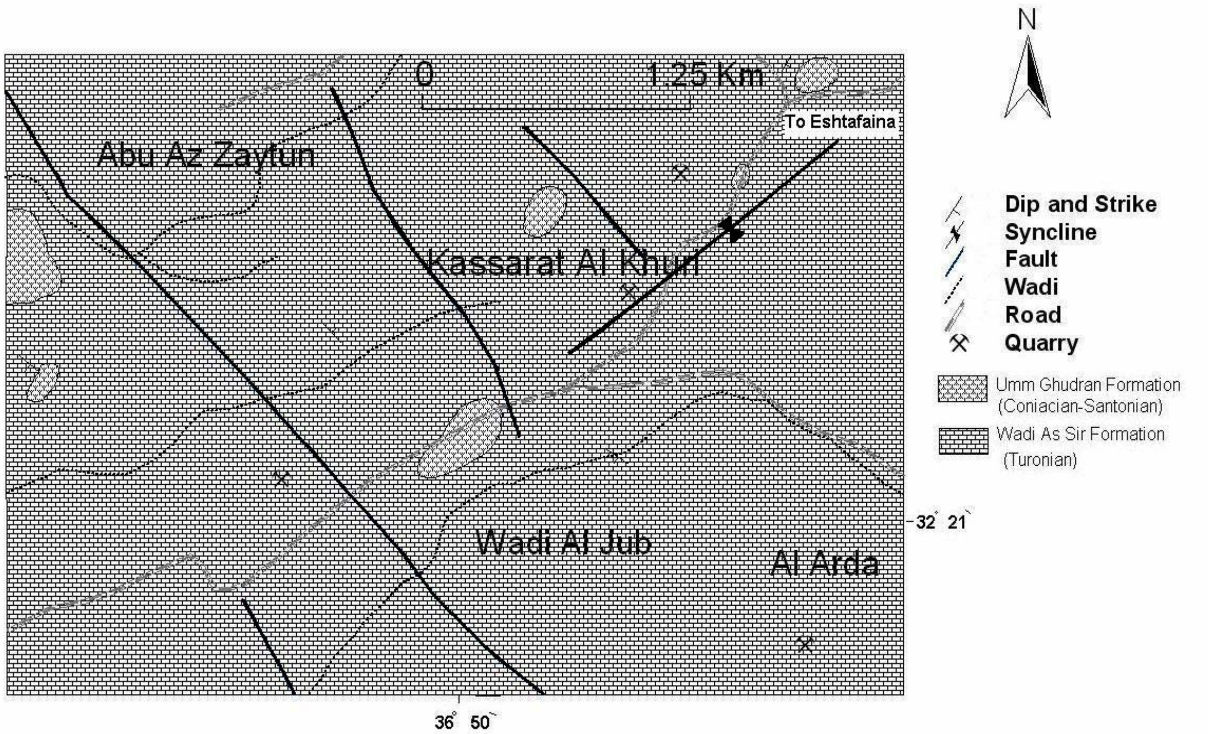

Fig 2. b (2) : Geological map of Eshtafaina area

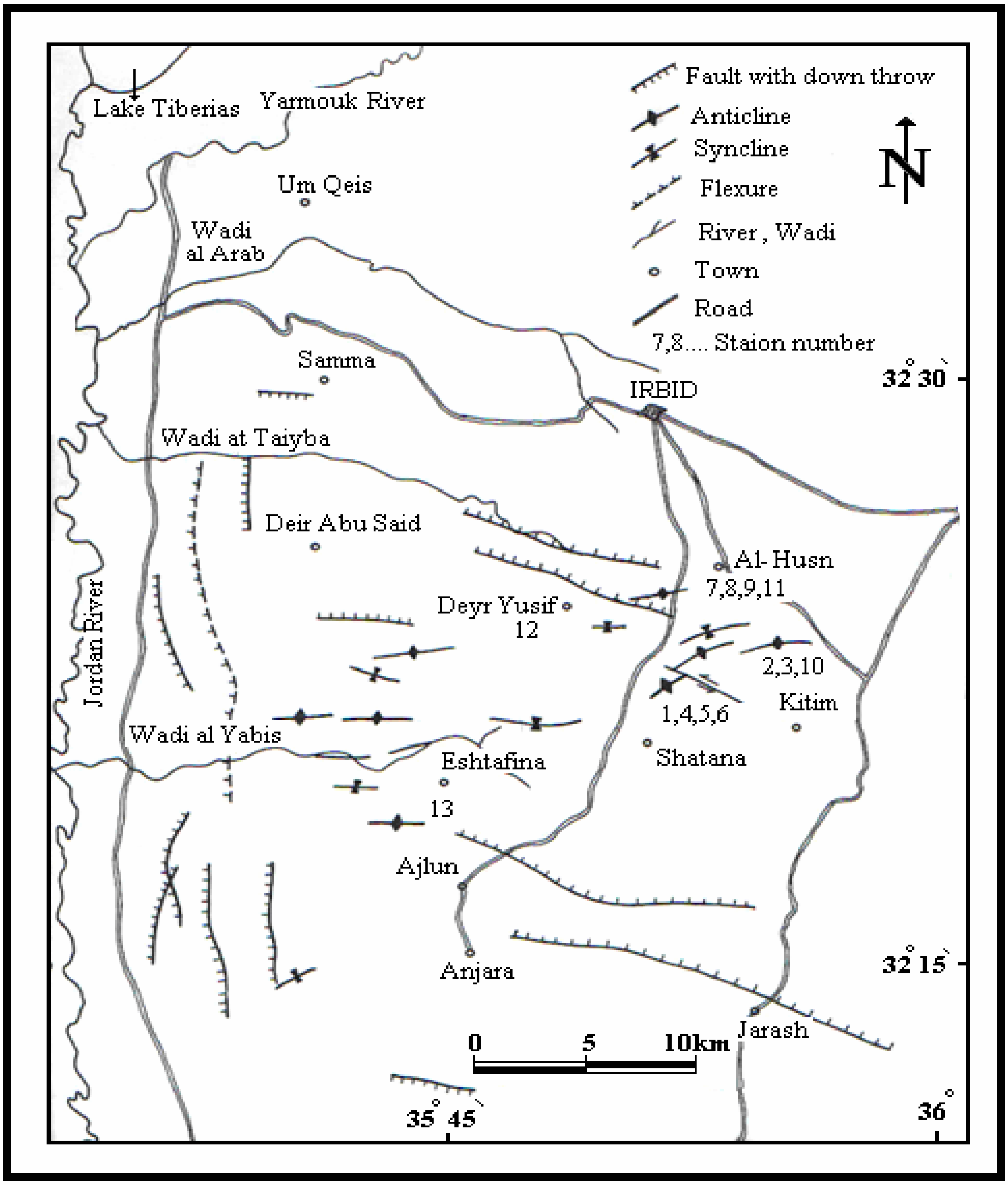

Fig.3. Major structures in northern Jordan, showing stations of fault slip data measurements.

2. Geological Setting

The outcropping rocks in the study area are of Upper Cretaceous age (Fig. 2). The oldest and most exposed rocks are the Wadi As Sir Formation of Turonian age. It is composed mostly of three distinctive parts, the lower part consists of dolomite, dolomitic limestone and/or recrystallized limestone, the middle part consists of relatively soft marly limestone and limestone, and the upper part consists almost totally of thick, bedded to massive limestone. The average thickness of this formation in the study area is 120 m (Abdelhamid, 1993). This formation is overlain by the Um Ghudran Formation of Coniacian-Santonian age, composed mainly of massive chalk at the base and intercalations of chalk and limestone at the top with chert beds and concretions. The thickness of this formation is about 30 m. The youngest rocks are the Campanian Amman Formation. It is composed of alternating beds of chert and limestone. In the study area most of this formation was eroded and remnants of fractured rocks were preserved at the top of hills.

The area of North Jordan is characterized by the presence of ENE-WSW trending Al Husn and Thaghret Asfour fold belts (Atallah and Mikbel, 1992). These fold belts occur as gentle parallel anticlines and synclines. Another prominent structure in northern Jordan is the Ajlun structure (Abed, 200. The area is cut by many faults mostly of strike slip and normal types. The general strike of these faults is WNW-ESE (Figs 2 and 3).

3. Paleostress analysis

3.1. Field Measurements

The fault slip data were collected by measuring the attitude (strike and dip) of the fault planes and the attitude (trend and plunge) of the slickenlines (lineated slickensides) on these faults. The measurements took place in 14 stations. 860 fault slip data were collected from horizontal and subhorizontal strata in the limestone quarries of the Turonian Wadi As Sir Formation. The stations are distributed in six areas in northern Jordan. Each station in most cases is one quarry, but in the case of few measurements two or more adjacent quarries were considered as one station. The attitude of slickenlines in addition to the associated features as mineral steps and tension gashes has been used to determine the orientation of slip and the sense of relative motion along the fault planes. The faults on which slickenlines were measured are generally high angle and are of normal, reverse and strike slip nature. Figure 4 shows the major trends of the fault strikes. Normal faults have two major trends: NE-SW and NW- SE, reverse faults strike NNE-SSW, dextral faults have three major trends: NE-SW, WNW- ESE, and NNW- SSE, and the sinistral faults have also three trends: NNE-SSW, E-W, and NNW- SSE.

3.2. Stress inversion method

Fault plane and slickenline orientations, including slip senses are used to compute the four parameters of paleostress tensors (σ_1, σ_2, σ_3 and R): the principal stress axis σ_1 (maximum compression), σ_2 (intermediate compression) and σ_3 (minimum compression) and the ratio of principal stress difference $R = (\sigma_2 - \sigma_3)/ (\sigma_1 - \sigma_3)$. These four parameters are determined using an improved version of the Right Dihedron method of Angelier and Mechler (1977), using the WINTENSOR computer program developed by Delvaux (2006). Paleostress inversion techniques have been used by various workers for more than 30 years. They are based upon the work of Wallace (1951) and Bott (1959), who assumed that slip on a plane occurs in the direction of the maximum resolved shear stress. The slip direction on the fault plane is inferred from slickenside lineation and calcite steps. The data used for the inversion are the fault plane, slip line orientation whereas the sense of movement was derived from slickolites and mineralization along steps for each fault plane. Stress tensors can be reconstructed by using tension and compression structures (Delvaux et al., 1995), in addition to fault planes with slip lines. Quartz veins, plume joints and dykes are considered as tension joints, developing perpendicular to the least compressive stress axis (σ_3). Fracture cleavages are considered as compression joints, developing perpendicular to the maximum compressive stress axis (σ_1). For them, the resolved normal stress magnitude is either minimized or maximized. During the rotational optimization, different functions can be optimized according to the nature of tectonic structure used. For faults, the angular deviation between observed slickensides and computed shears is minimized, together with the maximization of friction coefficients for each fault plane. Fault planes with slip lines can not only be used for the reconstruction of stress tensors, but also for tension and compression structures (Delvaux et al., 1995). The TENSOR procedure optimizes the appropriate function by progressive rotation of the tested tensor around each of its axes, and by testing different values of R. The amplitude of rotation angles and values of R ratio tested are progressively reduced, until the tensor is stabilized. Separation of fault populations resulting from successive tectonic regimes is based on interactive kinematic separation and progressive stress tensor optimization, to obtain homogeneous subsets, representing different stress regimes. Their chronological succession is established as a function of microstructural and geological criteria and in relation with known regional tectonic events (for details see Delvaux, 1993; Delvaux et al., 1995, 1997). Critical considerations on the accuracy of stress inversion methods are given in Dupin et al. (1993) and Pollard et al. (1993). They concluded that uncertainties in stress tensor determination due to geological and mechanical factors generally fall in the range of measurement errors.

The stress regime is defined by the nature of the vertical stress axes:

1) Normal faulting when σ_2 is the maximum horizontal stress axes (σ_2 SHmax) and σ_1 is vertical, 2) strike- slip faulting when $\sigma 1$ is the maximum horizontal stress axes ($\sigma 1$ SHmax) and when $\sigma 2$ is vertical and 3) thrust/ reverse faulting when $\sigma 1$ is the maximum horizontal stress axes ($\sigma 1$ SHmax) and $\sigma 3$ is vertical. The stress regimes also vary as a function of the stress ratio R: radial extension ($\sigma 1$ vertical, $0 < R < 0.25$), pure extension ($\sigma 1$ vertical , $0.25 < R < 0.75$), trans-tension ($\sigma 1$ vertical , $0.75 < R < 1$ or $\sigma 2$ vertical , $1 > R > 0.75$), pure strike- slip ($\sigma 2$ vertical , $0.75 > R > 0.25$), transpression ($\sigma 2$ vertical , $0.25 > R > 0$ or $\sigma 3$ vertical, $0 > R > 0.25$), pure compression ($\sigma 3$ vertical, $0.25 < R < 0.75$), and radial compression ($\sigma 3$ vertical , $0.75 < R < 1$) (Delvaux *et al.,* 1997).

The orientation of the principal stresses and the stress difference ratio (R) were determined by selecting those measurements of small faults with obvious sense of movement (i.e. slickolites and mineral steps).

The fourteen established stations are located on exposures of Wadi As Sir Formation. 113 measurements out of 860 were omitted because they are incompatible with slip deviations and show unreasonable results. This may be due to measurement error in the field or to local block rotation around fault blocks. Table 1 shows the number of fault- slip data used for stress tensor determination; plunge and azimuth of the principal stress axes; stress ratio; the orientation of maximum horizontal compressive stress and the deformation geometry (tensor type). Examples of stress inversion results in different sites of the study area are presented in Figure 5. Some sites like station 1 exhibit more than one tensor, indicating multiple movements (displacement) and superimposed stress states.

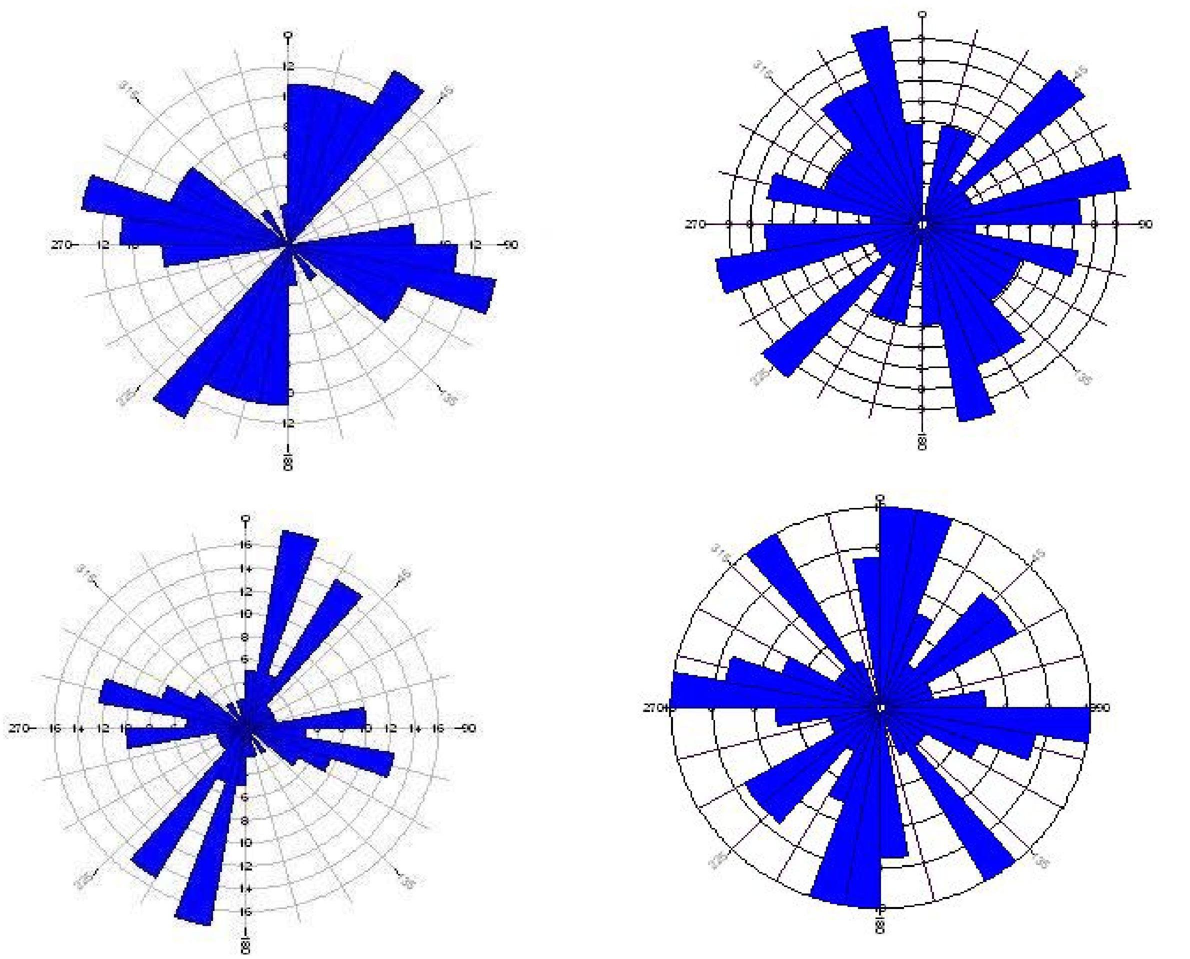

Fig. 4. General trends of fault strikes in the study area (1) normal faults (2) dextral faults (3) reverse faults and (4) sinistral faults.

4. Results

Fourteen stations have been studied in which 747 fault slip data were used in calculation. Shatana area is represented by 4 stations (1, 4, 5 and 6) , Kitim area by 3 stations (2, 3, and 10), Al-Husn area by 4 stations (7, 8, 9, and 11), and the following 3 areas by 1 station each: Deyr Yusif (station 12), Eshtafaina (station 13), and Thagret Asfour (station 14) (Figs 2 and 3).

The following is a representation of the results in each station:

4.1. Station 1

One hundred and ninety five measurements were carried out in Shatana quarries of the study area (Fig. 3 and Table 1). Two stress tensors were obtained from the whole fault population: the first stress tensor (59 measurements) gives the maximum principal stress axis (σ1) 00/ 273, the intermediate principal stress axis (σ2) 04/ 183, and the minimum principal stress axis (σ3) 85/ 315; with stress ratio(R) equals 0.21. The tensor belongs to compressive strike- slip regime. It indicates E- W compression and N- S extension. This tensor produced the conjugated WNW dextral and NNE sinistral strike- slip faults.

The second stress tensor (136 measurements) is characterized by σ1: 05/ 167, σ2: 84/ 308 and σ3: 04/ 082 with R= 0.7. This tensor belongs to pure strike- slip regime, and indicates NNW-SSE compression and ENE-WSW extension. It is responsible for the conjugated N-S sinistral and ESE dextral strike- slip faults.

4.2. Station 2

Seventy- six fault slip data were carried out in a quarry located in Kitim of the study area (Fig. 3 and Table 1). The calculated stress tensor is characterized by σ1: 25/ 065, σ2: 64/ 269 and σ3: 06/ 160 with R= 0.35. It belongs to extensive strike-slip regime and indicates ENE compression and NNW extension. This tensor show local counterclockwise rotation of the principal stress axes.

4.3. *4.3. Station 3*

Fifteen fault slip measurements have been carried out in a quarry of this station (Fig. 3 and Table 1). The resulted stress tensor is characterized by σ1: 01/ 086, σ2: 82/ 186 and σ3: 08/359 with R= 0.18. It belongs to compressive strike- slip regime and indicates E- W compression and N-S extension. This tensor produced the conjugated NE dextral and NW sinistral strike- slip faults.

4.4. Station 4

Two hundred and forty fault- slip measurements were carried out in a quarry of this station (Fig. 3 and Table 1). The stress tensor deduced from these measurements is characterized by σ1: 05/155, σ2: 80/036 and σ3: 09/243 with R= 0.52. It belongs to pure strike- slip regime and indicates NNW compression and ENE extension.

Table .1: Results of the reduced paleostress tensors from the fault-slip data

Station No.	Nt.	R	Principal Stress axis			Tensor type	S_{Hmax}
			σ_1	σ_2	σ_3		
1	59	0.21	00/273	04/183	85/315	Pure compression	273
1	136	0.7	05/167	84/308	04/082	Pure strike slip	167
2	76	0.35	25/065	64/269	06/160	Extensional strike slip	70
3	15	0.18	01/086	82/186	08/359	Compression Strike slip	89
4	240	0.52	05/155	80/036	09/243	Pure strike slip	156
5	87	0.26	03/156	22/247	68/059	Pure compression	156
6	90	0.42	11/319	78/115	04/225	Pure strike slip	135
7	35	0.65	16/155	74/316	06/068	Pure strike slip	154
8	7	0.67	03/283	85/054	09/193	Pure strike slip	103
9	15	0.7	08/091	73/201	16/000	Pure strike slip	89
10	14	0.53	81/162	05/282	04/191	Pure extension	89
11	36	0.35	71/191	09/309	16/041	Pure extension	113
12	85	0.65	77/248	16/053	03/323	Pure extension	053
13	27	0.74	70/202	11/325	24/060	Pure extension	145
14	25	0.65	03/113	83/355	06/207	Extensional strike slip	117

Nt. = net Number of measurements representing the tensor; R = stress ratio $(\sigma_2 - \sigma_3)/(\sigma_1 - \sigma_3)$; S_{Hmax} = Horizontal maximum principal stress axis.

The tensor is responsible for the WNW- trending dextral faults and the N-S sinistral faults.

4.5. Station 5

Eighty- seven fault- slip data have been carried out in this station (Fig. 3 and Table1). The tensor is characterized by σ1: 03/ 156, σ2: 22/ 247 and σ3: 68/ 059 with R= 0.26. It indicates NNW compression and belongs to pure compression regime. The tensor produced the N- S sinistral strike- slip faults and \ or the NE reverse faults at least in this station.

4.6. Station 6

Eleven fault- slip data were carried out in a quarry located in the northernmost part of the study area (Fig. 3 and Table 1).The stress tensor is characterized by σ1: 10/ 112, σ2: 76/ 247 and σ3: 10/ 020 with R= 0.45. It indicates WNW compression and NNE extension and belongs to pure strike- slip regime. This tensor is responsible for the NE- E dextral strike-slip faults.

4.7. Station 7

Ninety fault- slip measurements were carried out in this station of the study area (Fig. 3 and Table 1). The tensor is characterized by σ1: 11/ 319, σ2: 78/ 115 and σ3: 04/ 225 with R= 0.42. It indicates NW compression and NE extension and belongs to pure strike- slip regime. The tensor related with the conjugated E-W and N- S trending strike-slip faults.

4.8. Stations 8 and 9

Twenty- two fault- slip measurements were carried out in these stations (7 from station 8 and 15 from station 9). The two stress tensors are similar in the four parameters in which σ1 oriented E- W and σ3 N-S with R= 0 .7. They belong to the pure strike- slip regime (Fig. 3 and Table 1). The tensors are responsible for the conjugated ENE sinistral and WNW dextral strike-slip faults .

4.9. Station 10

Fourteen measurements were used in calculation of this station(Fig. 3 and Table 1). The resulted stress tensor is characterized by σ1: 81/ 162, σ2: 05/ 282 and σ3: 04/ 191 with R= 0.53.It indicates N- S extension and belongs to pure extension regime. This tensor is responsible for E- W trending normal faults in the study area.

4.10. Station 11

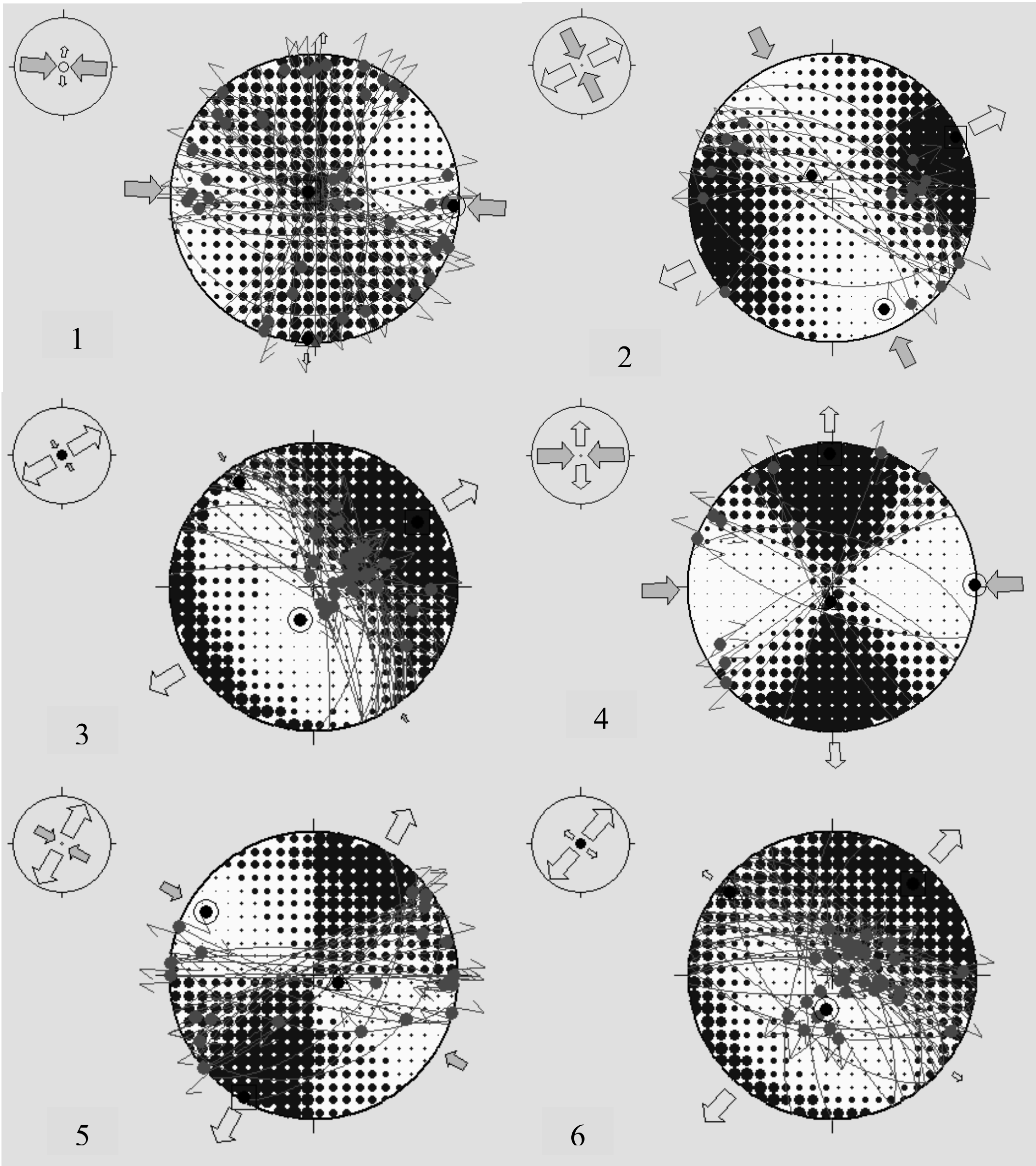

Fig. (5) Examples of stress inversion results in the different areas. (1) Shatana, (2) Kitim, (3) Deyr Yusif, (4) Al Husn, (5) Thagret Asfour, and (6) Eshtafaina.

Thirty- six were used in calculation of this station (Fig. 3 and Table 1). The resulted stress tensor is characterized by σ1: 71/ 191, σ2: 09/ 309 and σ3: 16/ 041 with R= 0.35. It indicates NE-SW extension and belongs to pure extension regime. This tensor is responsible for NW trending normal faults in the study area.

4.11. Station 12

Eighty- five fault- slip measurements were carried out in this station(Fig. 3 and Table 1). The calculated stress tensor is characterized by σ1: 77/ 248, σ2: 16/ 053 and σ3: 03/ 323 with R= 0.65. It indicates NW-SE extension and belongs to pure extension regime. This tensor shows a contra verse result.

4.12. Station 13

Twenty- seven fault- slip measurements were carried out in this station. The calculated stress tensor is characterized by σ1: 70/ 202 σ2: 11/ 325 and σ3:24/ 060 with R= 0.74. It indicates ENE extension and belongs to pure extension regime. This tensor is responsible for N- S to NNW trending normal faults in the study area (Fig. 3).

4.13. Station 14

Twenty- five fault- slip measurements were carried out in this station (Fig. 3 and Table 1). The calculated stress tensor is characterized by σ1: 03/ 113 σ2: 83/ 355 and σ3: 06 / 207 with R= 0.65. It indicates ESE compression and NNE extension. It belongs to extensional strike-slip regime. This tensor is responsible for E- W dextral strike-slip faults and to WNW trending normal faults in this station.

The above results with all parameters of the reduced stress tensors are provided in Table 1 and Fig. 5

5. Discussion and Conclusions

The data in Table 1 and Figure 5 show that, nine out of the fifteen stress tensors belong to strike -slip regime (pure strike- slip, compressive strike- slip and extensive strike-slip). The tensors that show strike slip-dominated regimes are shown in stations 1, 2, 3, 4, 6, 7, 8, 9, and 14.

The calculated results indicate that σ1 (SHmax) and σ3 (SHmin) are generally sub-horizontal and σ2 is sub-vertical in all the previous stress tensors, which belong to a major strike-slip system with σ1 swinging around N to NW direction in stations 1, 4 ,6,and 7. These stress tensors are mainly responsible for the conjugated E- W dextral and NNW sinistral strike- slip faults in the study area. Stations 1, 3, 8, 9 ,on the other hand, show tensors with σ1 (SHmax) swinging around E- W direction. These stress tensors are mainly responsible for NNE reverse faults and conjugated NE dextral with NW sinistral faults. Four stress tensors in stations 10, 11, 12, and 13 show σ2 (SHmax), σ1 vertical and σ3 is NE oriented except station 12 shows NW extension. This situation can explain as permutation of stress axes σ1 and σ2 that occur during tectonic events and partitioned strike slip deformation. Such changes from predominantly strike- slip to predominantly normal faulting modes (σ1/ σ2 permutation) frequently occur during a single stage and a distinct stress field. Results show that both normal and strike- slip faulting have relatively stable orientation of σ3 axis, while σ1and σ2 axes may change place at a single tectonic events at spatially different regions. Two tensors in stations 1 and 5 show pure compression. The first one shows σ1 (SHmax) swinging around E- W direction, and the other shows σ1 (SHmax) swinging around NNW- SSE direction. This means that they belong to two different stress systems and are compatible with the regional known stress fields in the region.

Figure 5 and Table 1 show the reduced stress tensors with the orientation of both the horizontal maximum stress axes (Sh_{max}) and the horizontal minimum stress axes (Sh_{min}). The orientation of stress tensors in the different areas can be summarized in the following trends:

1. Six stations show a NW to NNW compression and NE to ENE extension. These tensors related with the Dead Sea stresses during the Miocene and the later stages.
2. Three stations show an E-W to ESE compression and N-S to NNE extension. These tensors are related with the Syrian Arc Stress field and responsible for the formation of the associated conjugated ENE- WSW dextral and NW-SE sinistral strike-slip faults in the study area.
3. Two stations show orthogonal pure compression (E- W and NNW- SSE). These tensors explained as the reactivation of the Syrian Arc related structures by the Dead Sea stresses on Post- Miocene times.
4. Three stations have a NE-SW extension. These stress tensors may be responsible for the formation of the local E-W and ESE- WNW normal faults in the study area. These stress tensors include three paleostress regimes, one with predominantly strike slip faulting (strike slip regime) and the two others with predominantly dip slip either normal faulting (extensional regime) or dip slip reverse faulting (compression regime).

There are some paleostress studies in the region. The work of Eyal and Reches (1983), Ron and Eyal (1985), Eyal (1996), and finally Eyal et al (2001) west of the DST show that, there are two main stress fields acting on the area since the Late Cretaceous, the oldest is the E-W to ESE-WNW compression. According to these authors, this stress is responsible for the formation of the Syrian Arc belt and they call this stress the Syrian Arc System (SAS). The second younger stress system is the N-S to NNW-SSE compression, and is responsible for the 105 km sinisitral displacement along the DST and the opening of the Red Sea since the Miocene, it is called the Dead Sea System (DSS). East of the rift , the work of Diabat (1999), Diabat et al (2004), and Zain Eldeen et al (2002) found almost the same above mentioned stress systems in addition to other local stresses. In the present study, the most dominating stress system is the NW to NNW compression, this stress system is compatible with the DSS. The second stress is the E-W to ESE compression, which is compatible with the SAS. The stations which have N-S and NE-SW extension are characterized by vertical σ_1. These stress tensors may be responsible for the formation of the E-W and the ESE- WNW normal faults shown on the map of Figure 3.

References

Abed, A. 2000. Geology of Jordan. Publication of Jordanian Geologists Association.

Abdelhamid, GH. 1993. Geological map of Jerash, scale 1: 50000. Geological mapping division, NRA, Jordan.

Angelier, J. 1979. Determination of the mean principal stresses for a given fault population. Tectonophysics 56: T17-T26.

Angelier, J. 1989. From orientation to magnitudes in paleostresses determinations using fault slip data. J. Struct. Geol. 11:37-50.

Angelier, J. 1994. Fault slip analysis and paleostress reconstruction. In Hancock , P. (ed): continental deformation. Pp: 53-100, Pergamon Press Oxford.

Angelier, J. and Mechler, P. 1977. Sur une method graphique de recherché des contraintes principals egalement utilizable en techtonique et en seismologie: la method de diedres droils. Bull. Soc. Geol. Fr. 7: 1309-1318.

Atallah, M.,1992. On the structural pattern of the Dead Sea Transform and its related structures in Jordan. Abhath Al-Yarmouk (Pure Sciences and Engineering) 1, 127-143.

Atallah, M. and Mikbel, Sh. 1992 structural analysis of the folds between Wadi El Yabis and the basalt plateau, northern Jordan. Dirasat 19B: 43-58.

Ben- Avraham, Z., Almagor, G., Garfunkel, Z.,1979. Sediments and structures of the gulf of Elat. Sediment. Geol. 23, 239- 267.

Bender, F., 1968. Geology of Jordan. Borntraeger, Berlin. 196 p.

Bott, M.H.P., 1959. The mechanism of oblique slip faulting. Geological Magazine 96, 109-117.

Burdon, D. J., 1959. Handbook of the Geology of Jordan: to accompany and explain the three sheets of 1: 250,000 Geological Map, East of the Rift, A. M.

Chu, D., Gordon, R. G., 1998. Current plate motions across the Red Sea. Geophys. J. Int. 135, 313- 328.

Delvaux, D. 1993. TENSOR program for paleostress reconstruction: examples from the East Africa and the Baikal Rift Zones. EUGVII Strassbourg, France , Terra Nova 5, 216.

Delvaux, D. 2006. WINTENSOR, VERSIO 1.3.75, Royal Museum for Central Africa, Tervuren, Belgium Dept. Geology – Mineraolgy.

Delvaux, D. Moeys, R., Stapel, G., Melnikov, A., and Ermikov, V. 1995. Paleostress reconstructions and geodynamics of the Baikal region, central Asia, Part I. Paleozoic and Mesozoic pre-rift evolution. Tectonophysics 252:61-101.

Delvaux, D. Moeys, R., Stapel, G., Petit, C., Levi, K., Miroshnichenko, A., Ruzchich, V., and San'kov, V. 1997. Paleostress reconstructions and geodynamics of the Baikal region, Central Asia, Part 2. Cenozoic rifting. Tectonophysics 282:1-38.

Diabat, A. 1999. Paleostress and strain analysis of the Cretaceous Rocks in the Eastern Margin of the Dead Sea Transform, Jordan. Unpublished Ph.D Thesis, University of Baghdad.

Diabat, A., 2002. Strain analysis of the Cretaceous rocks in the Eastern margin of the Dead Sea Transform, Jordan. Dirasat 29, 159-172.

Diabat, A., Salih, M., and Atallah, M., 2003. Magnitudes of the paleostresses at the Eastern Rim of the Dead Sea Transform Fault,Jordan. Dirasat, 30, 1-18.

Diabat, A. Masri, A.. 2005. Orientation of the principle stresses along Zarqa-Ma'in fault. Muta Journal for Researchs and studies 20: 57-71.

Diabat, A. Atallah, M., Saleh, M. 2004. Paleostress analysis of the Cretaceous rocks in the eastern margin of the Dead Sea transform, Jordan. Journal of African Earth Sciences 38: 449-460.

Dupin, G. M., Sassi, W., Angelier, J.., 1993. Homogeneous stress hypothesis and actual fault slip: a distinct element analysis. Journal of Structural Geology 15, 1033- 1043.

Eyal, Y. 1996. Stress fluctuation along the Dead Sea rift since the Middle Miocene. Tectonics 15:157-170.

Eyal, Y., Reches, Z., 1983. Tectonic analysis of the Dead Sea Rift region since the Late Cretaceous based on mesostructures. Tectonics 2:167- 185.

Eyal, Y., Gross, M., Engelder. T., Backer,A. 2001. Joint development during fluctuation of the region stress field in southern Israel. Journal of Structural Geology 23:279- 296.

Garfunkel. Z. 1981. Internal structure of the Dead sea leaky transform (rift) in relation to plate kinematics. Tectonophysics 80: 81-108.

Freund, R., Zak, I., Garfunkel, Z., 1968. Age and rate of the sinistral movement along the Dead Sea rift. Nature 220, 253- 255.

Garfunkel, Z., 1981. Internal structure of the Dead Sea leaky transform (rift) in relation to plate kinematics. Tectonophysics 80, 81- 108.

Joffe, S., Garfunkel, Z., 1987. Plate kinematics of the circum Red Sea. A re- evaluation. Tectonophysics 141, 5- 22.

Klinger, Y., Avouac, J.P., Abou Karaki, N., Dorbath, L, Bourles, D., Reyss, J. L., 2000a. Slip rate on the Dead Sea transform fault in northern Araba valley. Geophys. J. Int. 142, 755- 768.

Klinger, Y., Avouac, J.P., Dorbath, C, Abou Karaki, N., Tisnerat, N., 2000b. Seismic behavior of the Dead Sea fault along Araba valley, Jordan. Geophys. J. Int. 142, 769- 782.

McKenzie, D., Davies, D., Molnar, P., 1970. Plate tectonics of the Red Sea and East Africa. Nature 226, 243- 248.

Mikbel, Sh., 1986. Some relevant tectonical and geotechnical considerations of south Amman area/ Jordan.. Dirasat 7, 215-225.

Mikbel, Sh., Zacher, W., 1981. The Wadi Shueib structure in Jordan. Neues Jaharbuch fuer Geologie und Paleontologie Monatshefte 9, 571-576.

Pollard, D. D., Saltzer, S. D., Rubin, A., 1993. Stress inversion methods: are they based on faulty assumption ?. Journal of Structural Geology 15 (8) , 1045- 1054.

Quennell, A.M., 1983. Evolution of the Dead Sea Rift. A review, First Jordanian Geologic Conference 460-482.

Ron, H., Eyal, Y. 1985. Intraplate deformation by block rotation and mesostructures along the Dead Sea transform, northern Israel. Tectonics 4 :85-105

Salameh, E. Zacher, W. 1982. Horizontal stylolites and paleostress in Jordan. N.Jb, Geol.Palaont, Mh. 1982: 509-512.

Shapira, A., Hofstetter, H., 1993. Source parameters and scaling relationships of earthquakes hn Israel. Tectonophysics 217, 217-226.

Wallace, R.E., 1951. Geometry of shearing stress and relation to faulting. Journal of Geology 59, 118- 130.

Zain Eldeen, U. Delvaux, D. and Jacobs. J. 2002. Tectonic evolution in the Wadi Araba segment of the Dead Sea rift, southwest, Jordan. EGU Stephan Mueller special publication series, 2: 63-81.

JJEES

Volume 3, Number 1, June, 2010
ISSN 1995-6681
Pages 37- 48

Jordan Journal of Earth and Environmental Sciences

Mechanical Properties of Natural Building Stone: Jordanian Building Limestone as an Example

Nart Mawloud Naghoj [a,*], Nafi Abdel Rahman Youssef [b] and Omar Nawaf Maaitah [c]

[a,b] *Assistant Professor, Civil Engineering Department, Faculty of Engineering Technology, Al Balqa' Applied University, Marka 11134, Amman, Jordan*

[c] *Associate Professor, Civil and Environmental Department, P. O. Box 7, Karak, Jordan*

Abstract

This experimental investigation is intended to study the mechanical properties of natural building stone usually used in the construction of load-bearing concrete backed stone masonry walls and columns used in the construction of the majority of buildings in Jordan and some middle-eastern countries. Six types of building limestone, brought from different quarries in Jordan, were used in this study. The characteristics studied were the stress-strain curves, the modulus of rupture, the modulus of elasticity, the Poisson ratio and the compressive strength. An experimental method is suggested to determine the modulus of elasticity of limestone; the results were compared with those obtained from stress-strain curves carried out on prisms. The results indicated that there are remarkable differences in strength and behavior of stone specimens loaded parallel to the bedding (or rift) and perpendicular to it in both dry and wet conditions. It is also indicated that the differences in results of the modulus of elasticity obtained by the suggested method and the stress-strain curves are not significant. On the basis of the test results a new formula is suggested for estimating the modulus of elasticity of limestone when compressive strength is known.

Keywords: Building stone; mechanical Properties; prisms; cubes; compressive strength; limestone.

1. Introduction

Concrete-backed stone masonry is one of the most important construction method used in Jordan and the Middle East. Until the nineties of the last century, most of Jordan's low rise buildings are constructed from the assemblage of dimension stone, mortar and concrete constructed as structural walls; namely, stone masonry bearing walls where stone thickness varies from 40 to more than 80 mm (Abdel-Halim et al., 1989). The thickness of the stone at the edges is usually smaller than in the center, backed by 200-250 mm of concrete with total wall thickness of 300 - 350 mm for the buildings raising up to four stories; higher buildings usually have thicker bearing walls. For the 300 - 350 mm thickness wall, strengthening columns are concentrated at the corners of the wall usually 200 × 400 mm in dimension, reinforced by six vertical bars and confined by stirrups each 200 mm, the steel reinforcement area usually kept to minimum.

Other strengthening columns 200 × 200 mm in dimension, reinforced by four vertical bars and confined by stirrups each 200 mm are concentrated at a distance about four meters from each other.

2. Materials

Six different types of building limestone with 14 varieties were brought from different quarries in Jordan. A location map showing the position of each quarry is given in fig. 1.

The stone were sawed to appropriate dimensions. Among the large number of stone specimens, three different kinds of limestone were used: soft, hard and very hard. According to ASTM C 568-89 (1992) limestone may be classified into three categories. These are, *I* (*Low-Density*), for limestone having a density ranging from 1760 through 2160 kg/m^3; *II* (*Medium-Density*) for limestone having a density greater than 2160 and not greater than 2560 kg/m^3 and *III* (*High Density*) for limestone having density greater than 2560 kg/m^3. At least one type of each category was chosen to be included among the tested specimens.

[*] Corresponding author. nartnaghoj@yahoo.com

Fig. 1 Map showing the limestone quarry locations of the tested samples (the quarry names are underlined

3. Experimental Program

3.1. Testing Procedure

Water absorption and specific gravity were carried out in accordance with ASTM C 97-90 (1992). For determining the compressive strength 60 × 60 × 60 mm cubes were tested by axial compression in accordance with ASTM C 170-90 (1992). More than twenty sawed cubes from each type of stone were tested: ten specimens in dry conditions and ten in wet conditions. Each group of specimens was tested with load direction parallel to bedding (or rift) and perpendicular to it.

The modulus of rupture was carried out on specimens approximately 101 × 203 × 57 mm in size. For each type of stone, twenty specimens were prepared, ten specimens were tested in dry conditions where specimens lift in the oven at temperature of 60° C for 48 hours. The other ten specimens after being lift in water tank for 48 hours at temperature of about 22° C. For each test condition, five specimens were tested with load direction parallel to bedding (or rift). The other five specimens were tested with load direction perpendicular to bedding (or rift). The test was carried out in the accordance with ASTM C 99-87 (1992). A suggested technique based on the standard test method on specimens used to determine the modulus of rupture (ASTM C 99-87, 1992), was used to determine the modulus of elasticity of building limestone. The results were compared with test results obtained from stress-strain curves of stone prisms tested with strain measurements. In this method which is specified in ASTM C 120-90 (1992) Standard as methods of flexure testing of slate, and is under the jurisdiction of ASTM Committee C-18 to be applied on dimension stone, the modulus of elasticity was determined in conjunction with the modulus of rupture test (ASTM C 120-90, 1992). The deflection was measured at mid-span of the specimens by a deflection scale capable of reading 0.01 mm. The loading was stopped at each 222 N increment, and the corresponding deflections readings were taken.

To study the relationships between compressive stress and strain, modulus of elasticity and Poisson ratio, a set of more than three prisms 100 × 100 × 200 mm were prepared for each type of stone. At least two of the prisms were fitted with demec points for measuring vertical and horizontal strains at the middle of the stone face; the gauge length was 50 mm. The demec points were glued on identical positions on two opposite sides of the chosen prisms at least 72 hours prior to testing. For each type of stone, a set not less than three prisms were tested with load direction parallel to bedding (or rift). Another set of each stone type not less than three prisms was tested with load direction perpendicular to bedding (or rift). All specimens were tested at a loading rate of 10 N/mm^2 per minute in accordance with BS 6073: Part 1: 1981 (1981).

4. Results and Discussion

Table 1 gives the results of specific gravity, water absorption and compressive strength for studied limestones. Compressive strength ranges from 9.4 N/mm^2 for soft stones tested in wet conditions when load direction was perpendicular to rift, to 116.3 N/mm^2 for very hard stones tested in dry conditions when load direction was parallel to rift. The results show that the decrease of stone absorption has great significance in increasing the compressive strength of the stones (Abdel-Qader, 2002; Akroush, 1994). It also shows that the specimens tested with loading parallel to rift possess higher compressive strengths. The table clearly reveals that the compressive strength for specimens tested in dry conditions is higher than those in wet conditions.

The results also show that some specimens with smaller percentage of water absorption i.e., Ma'an Sateh 1 and Ma'an Sateh 2, have little difference in compressive strength compared to specimens with higher percentage of water absorption like Hayyan Soft.

Table 1 Results of average compressive strength of specimens loaded parallel and perpendicular to bedding (or rift).

Type of Stone	Specific Gravity	Water Absorption (%)	Average Compressive Strength (N/mm^2) of 60 × 60 × 60 (mm) Cubes			
			Dry		Wet	
			Load parallel to rift	Load perpendicular to rift	Load parallel to rift	Load perpendicular to rift
Ma'an Sateh 1 (first class)	2.51	0.81	56.2	51.3	55	47.9
Ma'an Sateh 2 (second class)	2.55	0.59	64.4	51.9	67.8	65.4
Ma'an Jazeerah	2.47	1.71	65.1	48.7	57	50.3
Ma'an Onizah	2.42	1.07	82	58.7	67.7	51.5
Ruwaished Hard	2.58	0.55	116.3	83.1	87.4	68.8
Ruwaished Medium	2.39	3.11	100.2	Not tested	79	Not tested
Ruwaished Soft	2.31	3.71	79.4	71.5	70.9	49
Hayyan Hard	2.49	1.96	64.5	54.2	55.1	45.7
Hayyan Medium	2.32	3.59	62.6	47.2	50.7	45.7
Hayyan Soft	1.99	9.43	16.3	15.5	11.3	9.4
Azraq Reddish	2.48	1.71	61.2	53.0	57.2	45.7
Sahrawi Yallowish	2.37	2.00	58.6	39.5	45.6	37.9
Qatranah	2.25	4.66	63	66.5	51.5	40.2
Qatranah Reddish	2.35	2.89	69	39.4	38	32.4

Note: Stone types are ranging between soft, for type Hayyan Soft, and very hard for Ruwaished Hard. All remaining types are hard stones.

Table 2 summarizes the results of the modulus of rupture and the modulus of elasticity of limestone specimens loaded parallel and perpendicular to bedding (or rift) for average of dry and wet conditions. The results indicated that the modulus of rupture perpendicular to the rift is slightly greater than that parallel to it. Modulus of elasticity parallel to the rift is greater than that perpendicular to it.

Table 2 Results of the modulus of rupture and the modulus of elasticity of limestone loaded parallel and perpendicular to the bedding (or rift).

Type of Stone	Modulus of Rupture (N/mm^2) Average of dry and wet conditions		Modulus of Elasticity (N/mm^2) Average of dry and wet conditions	
	Loading parallel to rift	Loading perpendicular to rift	Loading parallel to rift	Loading perpendicular to rift
Ma'an Sateh 1 (first class)	11.5	13.6	39431	36038
Ma'an Sateh 2 (Second class)	Not tested	Not Tested	41179	38212
Ma'an Jazeerah	Not tested	12.4	46292	33335
Ma'an Onizah	10.5	12.3	Not tested	37125
Ruwaished Hard	14.7	15.7	49873	43821
Ruwaished Medium	11.3	12.2	47457	40577
Ruwaished Soft	10.5	11.9	39010	36038
Hayyan Hard	12.1	13.1	38810	36038
Hayyan Medium	5.9	6.7	43931	37840
Hayyan Soft	1.85	2.0	21623	18435
Azraq Reddish	9.8	11.8	Not tested	35317
Sahrawi Yallowish	8.5	10.5	36857	313372
Qatranah	Not tested	11.35	41725	37840
Qatranah Reddish	9.14	8.64	Not tested	37179

In the standard test carried to determine the modulus of rupture, the specimen which is supported by two knife edges of the rocker type, is subjected to flexure using a center-point loading until failure. The maximum tensile stress is referred to as the modulus of rupture, occurred at the bottom fiber of the test specimen. The rift is defined as a consistent direction or trend in rock body along which the rock is most easily split or broken (ASTM C 119-91, 1992). The split indicated that the layers that contained the rift are weaker than the surrounding layers. Since the test is flexure test, the values of the modulus of rupture of the specimens tested with the load direction parallel to the rift are lower than those tested with the load direction perpendicular to it.

Table 3 gives the results of tested 100 × 100 × 200 mm prisms. Initial modulus of elasticity was obtained from stress-strain curves; values of Poisson ratio relied also upon initial strain. The results show that the modulus of elasticity parallel to the rift is greater than perpendicular to it.

Table 4 shows a comparison between the results of some physical and mechanical properties obtained from the current study and a previous one (Akroush, 1994). It shows close agreement between the two results. Notable differences in the physical and mechanical limestone properties are expected from stone brought from nearby locations within the same quarry.

Table 3 Results of the compressive strength and the modulus of elasticity of dimensioned limestone prisms loaded parallel and perpendicular to the bedding.

Type of Stone	Compressive Strength(N/mm^2) Average of dry and wet conditions 100 × 100 × 200 (mm) prisms		Modulus of Elasticity (N/mm^2) and Poisson ratio Average of dry and wet conditions			
			Load parallel to rift		Load perpendicular to rift	
	Load parallel to rift	Load perpendicular to rift	Modulus of Elasticity	Poisson Ratio	Modulus of Elasticity	Poisson Ratio
Ma'an Sateh 1	52.2	46.2	42533	0.17	37675	0.2
Ma'an Sateh 2	54.5	47.5	44147	0.14	38212	0.17
Ma'an Jazeerah	51.3	49	39234	0.14	32660	0.17
Ma'an Onizah	67.3	46	50545	0.18	------	------
Ruwaished Hard	103	not tested	42428	0.18	------	------
Ruwaished Medium	71.7	46	41284	0.15	39421	0.19
Ruwaished Soft	47	44	40077	0.14	35610	0.17
Hayyan Hard	59.2	47	43133	0.17	32435	0.25
Hayyan Medium	54	42.4	38110	0.2	30303	0.19
Hayyan Soft	8	9.5	28407	0.2	11645	0.26
Azraq Reddish	60.8	47.2	42692	0.16	40363	0.15
Sahrawi Yallowish	46	38.3	39481	0.15	33193	0.22
Qatranah	41	not tested	40993	0.16	-----	-----
Qatranah Reddish	43	39.8	35318	0.16	31533	0.18

Table 4 Comparison of some physical and mechanical properties obtained from the current study and previous one (Akroush, 1994).

Type of Stone	Specific Gravity		Water Absorption (%)		Compressive Strength (N/mm^2)				Modulus of Rapture (N/mm^2)			
					Load parallel to rift Average of Dry and Wet		Load perpendicular to rift Average of Dry and Wet		Load parallel to rift Average of Dry and Wet		Load perpendicular to rift Average of Dry and Wet	
	Current Study	Ref. 3	Current Study	Ref. 3	Current Study	Ref. 3	Current Study	Ref. 3	Current Study	Ref. 3	Current Study	Ref. 3
Ma'an Sateh 1	2.51	-----	0.81	-----	55.6	-----	49.6	-----	11.5	-----	13.6	-----
Ma'an Sateh	-----	2.59 2.63*	-----	0.69 0.57*	-----	48.56	-----	47.9	-----	8.60	-----	9.64
Ma'an Jazeerah	2.47	2.61 2.58*	1.71	0.58 1.18*	61.05	68.18	49.5	50.3	-----	12.20	12.4	12.63
Hayyan Hard	2.49	-----	1.96	-----	59.8	-----	49.98	-----	12.1	-----	13.1	-----
Mafraq	-----	2.46	-----	2.51	-----	51.86	-----	53.85	-----	8.74	-----	13.06

*Note: Hayyan quarries are within Mafraq area.

*Results of renewed study carried by the Building Research Center (Ref. 3, Akroush, 1994).

Table 5 shows a comparison between the compressive strength of cubes and prisms loaded parallel and perpendicular to rift. The table also gives a correction factor for converting from prism to cube and vice versa

The results show higher compressive strength for the cubes than for prisms. This is due to the frictional forces between the end surfaces of the limestone specimen and the adjacent steel platens of the testing machine. The platen restrains the lateral expansion near the top and bottom surfaces of the specimen. The effect of restraining decreases when the distance from the contact surfaces is increased; at the same time, the lateral forces reached its maximum in the middle of the specimen. This explains the pyramid mode of failure.

In case of prisms; the effect of restraining is limited to the upper and lower contact surfaces and the middle part of the prism is free from the restraining effects. Prisms failed by splitting due to the lateral tensile strains caused by the effect of the Poissions ratio which is 0.18 in average.

The specimens tested with the load direction parallel to the rift, exhibited higher compressive strength than those tested with the load direction perpendicular to the rift. This is explained by the nature of the rift that defines a consistent direction in rock body along which the rock is most easily broken. Furthermore, the grain orientation in stone, i.e. that shows how the stone was originally bedded, offers further explanation. The thin layers of solid materials bedded over each other, forming together the stone, have different properties e.g. grain size, voids and hollow; making one layer weaker than the other. When the specimen is tested with the loading parallel to the rift, two stress elements are likely to occur, tri-axial compression and bi-axial lateral tensile with uni-axial compression stresses. The bi-axial lateral tensile stresses tend to split the specimen. Wet Specimens have higher lateral tensile stresses than dry ones; this is related to the additional lateral tensile stresses of the moisture inside the voids.

Table 5 Comparison between the compressive strength of cubes and prisms.

Type of Stone	Compressive Strength (N/mm^2) 60 × 60 × 60 (mm) Cubes		Compressive Strength (N/mm^2) 100 × 100 × 200 (mm) Prisms		Correction Factor Conversion from Prism to Cube (Multiple by) Conversion from Cube to Prism (divide by)	
	Average Dry and wet		Average Dry and wet		Average Dry and wet	
	Load parallel to rift	Load perpendicular to rift	Load parallel to rift	Load perpendicular to rift	Load parallel to rift	Load perpendicular to rift
Ma'an Sateh 1	56.2	51.3	52.2	46.2	1.08	1.11
Ma'an Sateh 2	64.4	51.9	54.5	47.5	1.18	1.09
Ma'an Jazeerah	65.1	48.7	51.3	49	1.27	0.99
Ma'an Onizah	82	58.7	67.3	46	1.22	1.28
Ruwaished Hard	116.3	83.1	103	Not tested	1.13	-----
Ruwaished Medium	100.2	Not tested	71.7	46	1.40	-----
Ruwaished Soft	79.4	71.5	47	44	1.69	1.62
Hayyan Hard	64.5	54.2	59.2	47	1.09	1.15
Hayyan Medium	62.56	47.2	54	42.4	1.16	1.11
Hayyan Soft	16.3	15.5	8	9.5	2.03	1.63
Azraq Reddish	61.2	53.02	60.8	47.2	1.15	1.12
Sahrawi Yallowish	58.6	39.5	46	38.3	1.27	1.03
Qatranah	63	66.5	41	Not tested	1.54	-----
Qatranah Reddish	69	39.4	43	39.8	1.6	0.99

For specimens tested with the load direction perpendicular to the rift, the thin layers are bedded horizontally. Two stress elements are likely to occur; bi-axial lateral tensile with uni-axial compression in the stiffer layers and tri-axial compression stresses in the weaker layers confined by two stiffer ones. Frictional forces occur in the contact surface of the two adjacent layers; it also occurs between the upper and lower surfaces of the specimen and the adjacent machine platens.

The relationship between the compressive strength and the modulus of elasticity is suggested by the following formula for each case of loading:

$$E_{stone} = k \times (f_{cube})^{0.5} \quad (N/mm^2) \tag{1}$$

Where:

E_{stone} = Modulus of elasticity (average of dry and wet conditions).

f_{cube} = The compressive strength of sawed limestone cubes not less than 50.8 × 50.8 × 50.8 mm in dimensions.

$k = k_1$ load direction factor (loading parallel to rift).

$k = k_2$ load direction factor (loading perpendicular to rift).

Plotting best fit line representing the data, k_1 and k_2 , the mentioned factors could be taken as 5.47×10^3 and 4.88×10^3, respectively.

Figure 2 shows the stress-strain curves for Ruwaished Stone where a very hard stone specimen is compressed parallel to the rift. When compared to other types of stone specimens with parallel and perpendicular loading, the curves show a steady increase in strength with stress and vertical strain values higher than all other types of stones. Also, a sudden increase in the vertical strain values at around 90 N/mm^2 is observed. This is caused by the tendency of the prism to increase its stiffness after a lateral deformation.

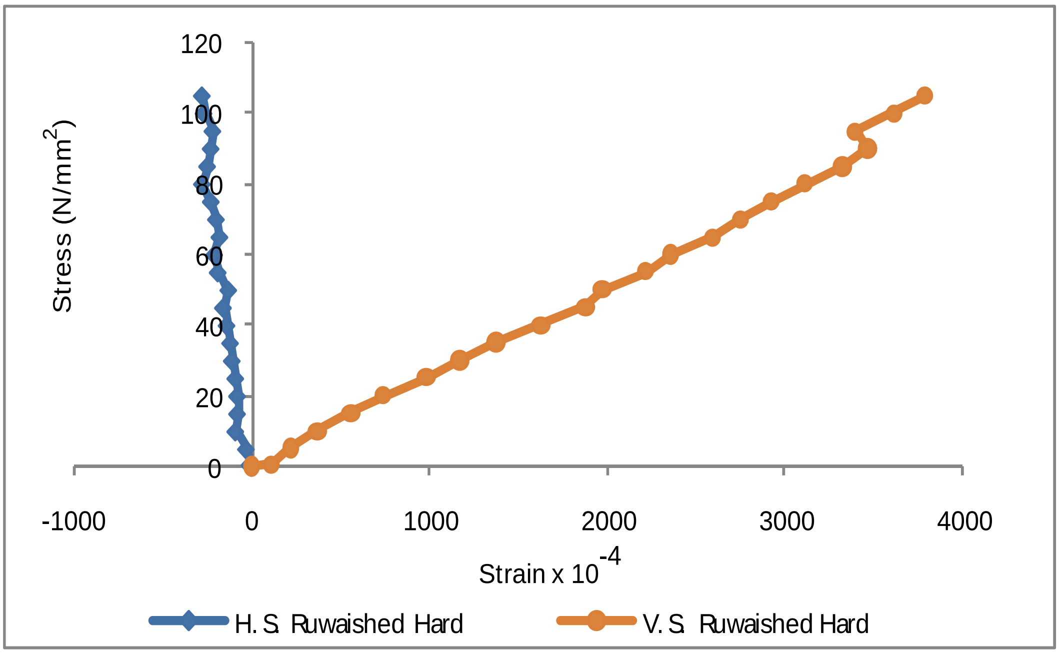

Fig. 2 Compressive stress-strain curves for very hard stone tested parallel to rift in dry conditions.

All the stress-strain figures show the relationship between the compressive stress and both compression and tension strains. For this reason the compression and the tension strain graphs are plotted in two opposite sides, namely the +ve and the –ve sides of the X axis.

Comparing the stress-strain curves for hard stone compressed parallel to rift in dry conditions (Fig. 3) to these for hard stone compressed perpendicular to rift under the same conditions (Fig. 4), two curves exhibited a sudden reduction in stiffness and increase in the lateral strain values near failure when load direction was perpendicular to the rift.

Comparing the stress versus strain curves for hard stone compressed parallel to rift in dry conditions (Fig. 3) to those in wet conditions (Fig. 5), a reduction in stiffness and rapid increase in lateral strains was found when the load direction was parallel to rift in wet conditions.

The stress-strain curves for hard stones compressed perpendicular to rift in wet conditions are given in Fig. 6. Two curves exhibit increase in stiffness occurred near failure; this was caused by the deformation of the stone layers where loading direction was perpendicular to stone rifts, and the deformation also caused high lateral strain values near failure.

Figure 7 shows a comparison between compressive stress-strain curves for soft stone tested parallel and perpendicular to rift in dry conditions. The curves exhibit a decrease in stiffness and high values of both vertical and lateral strains when load direction was perpendicular to rift.

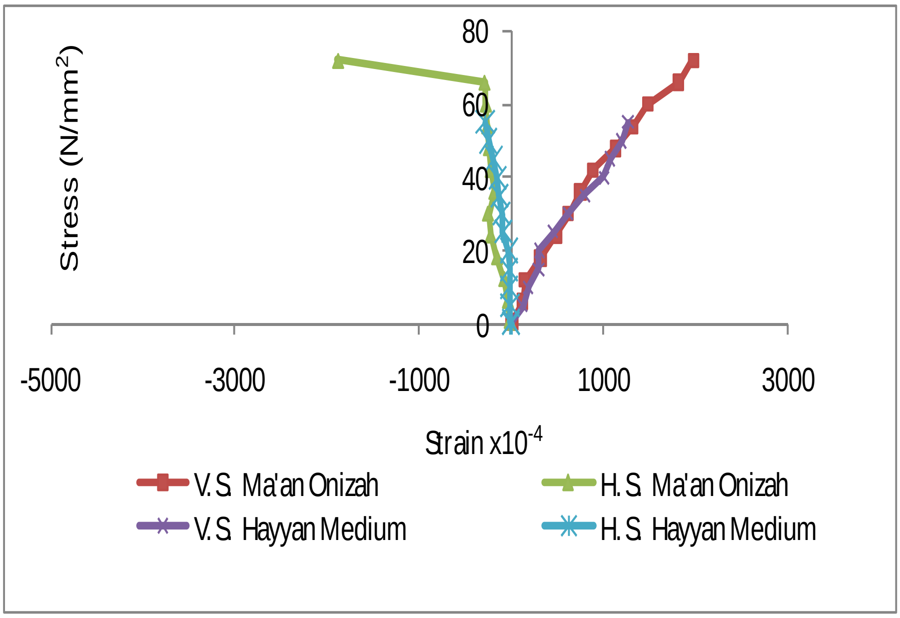

(a)

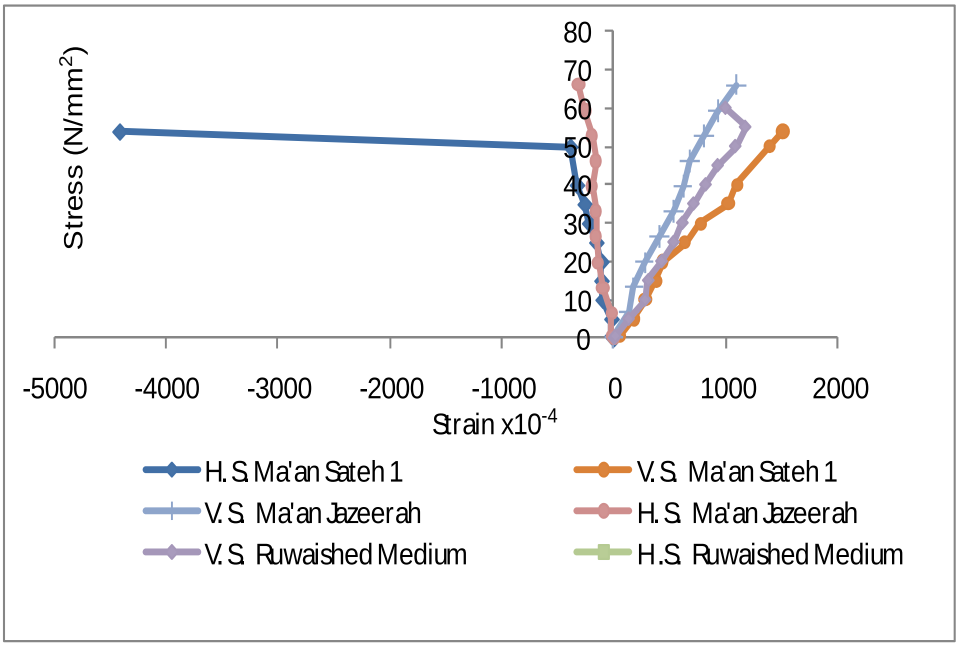

(b)

Fig. 3. a,b: Compressive stress-strain curves for hard stone tested parallel to rift in dry condition.

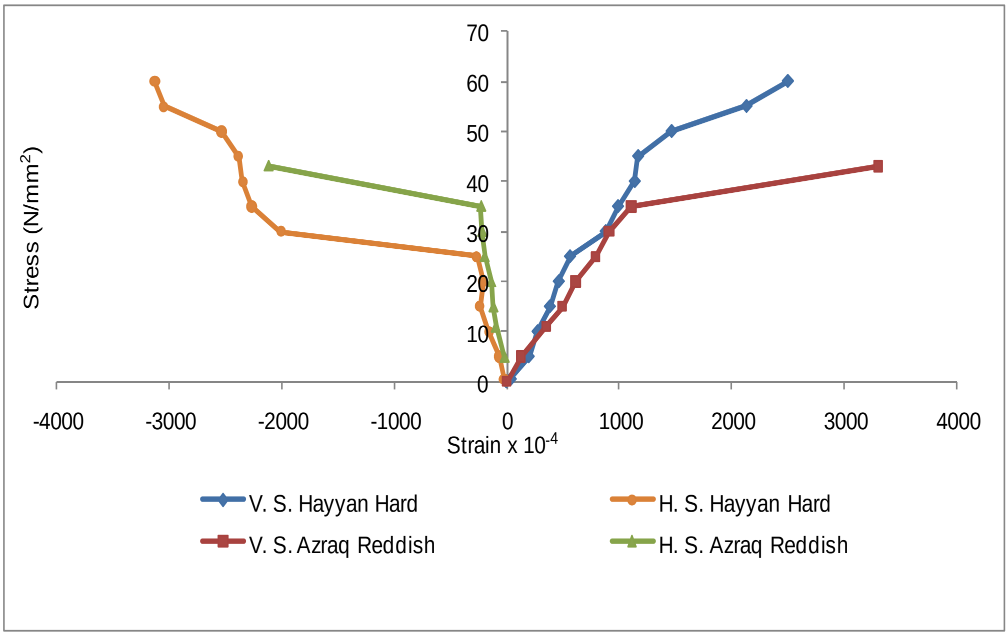

Fig. 4 Compressive stress-strain curves for hard stone tested perpendicular to rift in dry conditions.

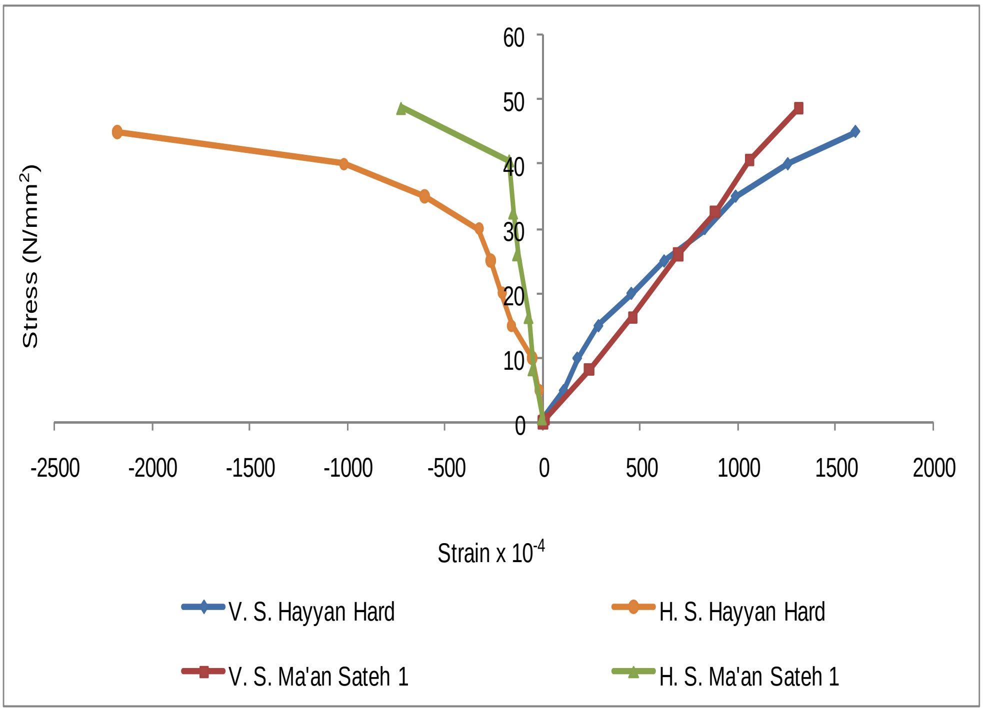

Fig. 5 Compressive stress-strain curves for hard stone tested parallel to rift in wet conditions.

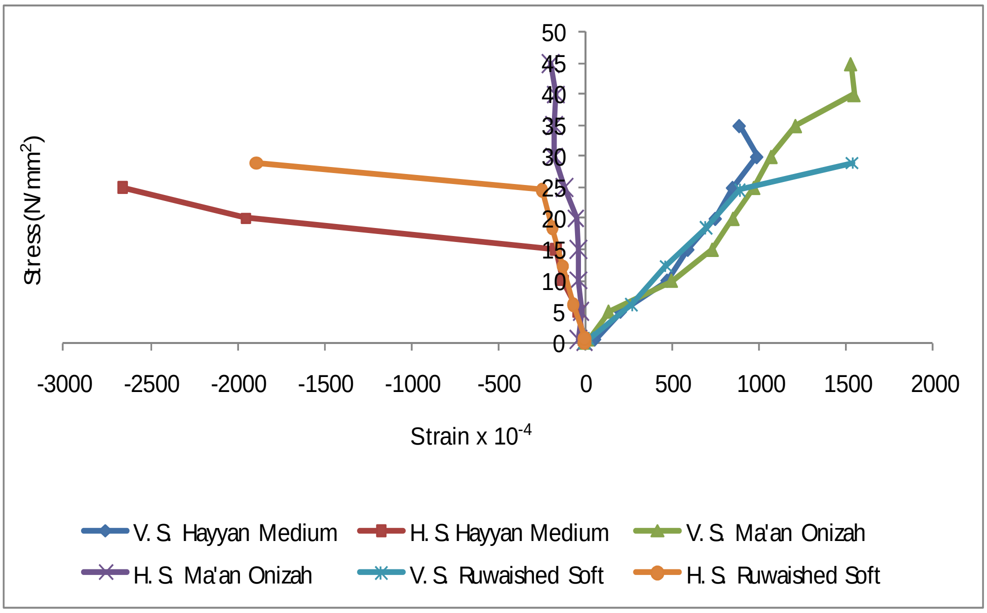

Fig. 6 Compressive stress-strain curves for hard stone tested perpendicular to rift in wet conditions.

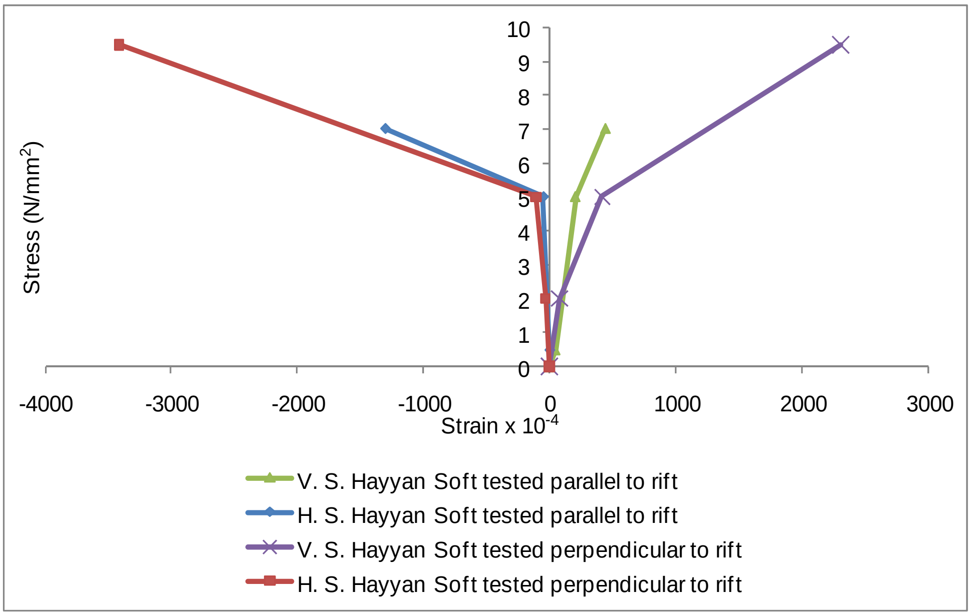

Fig. 7 Comparison between compressive stress-strain curves for soft stone tested Parallel and perpendicular to rift in dry conditions.

5. Conclusion

1. Higher specific weight and lower water absorption contribute to higher strength of the stones, and their elasticity and rupture moduli.
2. The modulus of rupture of limestone with load direction perpendicular to rift is higher than parallel to rift, whereas the modulus of elasticity obtained from the suggested method is higher for specimens tested with load direction parallel to rift.
3. The compressive strengths for limestone cubes tested in dry conditions are higher than limestone cubes tested in wet conditions. Compared to the limestone cubes, the tested limestone prisms exhibited higher decrease in compressive strength.
4. There are slightly differences between the values of the modulus of elasticity obtained from tested stress-strain curves and that obtained by the suggested method.
5. Based on test results, a new formula (equation 1) was suggested to estimate the modulus of elasticity of limestone from compressive strength.
6. The modulus of elasticity of prisms tested in dry conditions with loading parallel to rift is higher than that perpendicular to rift. Poisson ratio perpendicular to rift is higher than that parallel to it.

References

Abdel-Halim M. A. H., Basoul M. R., and Abdel-Karim R. A., 1989. Structural Evaluation of Concrete-Backed Stone Masonry, ACI Structural Journal, V. 86, No. 5, pp. 608-614.

Abdel-Qader N. M., 2002. Compressive Strength of Concrete-Backed Stone Masonry Prisms, The 6th International Conference on Concrete Technology for Developing Countries, Amman, Jordan, pp. 595-604.

Akroush M., Building Research Center, Royal Scientific Society, 1994. Building Natural Stone Specifications and Methods of Testing, Proc. of the Stone Scientific Day, Jordan Engineers Association, Amman, Jordan.

American Society for Testing and Materials, ASTM C 97 - 90, Standard Test Methods for Absorption and Bulk Specific gravity of Dimension Stone, Vol. 04.08, 1992.

American Society for Testing and Materials, ASTM C 99 - 87, Standard Test Method for Modulus of Rupture of Dimension Stone, Vol. 04.08, 1992.

American Society for Testing and Materials, ASTM C 119 – 91, Standard Terminology Relating to Dimension Stone, Vol. 04.08, 1992.

American Society for Testing and Materials, ASTM C 120 – 90, Standard Test Method of Flexure Testing of Slate (Modulus of Rupture, Modulus of Elasticity), Vol. 04.08, 1992.

American Society for Testing and Materials, ASTM C 170 - 90, Standard Test Method for Compressive Strength of Dimension Stone, Vol. 04.08, 1992.

American Society for Testing and Materials, ASTM C 568 - 89, Standard Specification for Limestone Dimension Stone, Vol. 04.08, 1992.

British Standards Institution BS: 6073: Part 1: 1981, Precast Concrete Masonry Units, BS 6073: Part 1 and 2.

JJEES

Volume 3, Number 1, June, 2010
ISSN 1995-6681
Pages 49 - 62

Jordan Journal of Earth and Environmental Sciences

Uranium distribution in the Upper Cretaceous-Tertiary Belqa Group, Yarmouk Valley, northwest Jordan

Basem K. Moh'd [a,*] and John H. Powell [b]

a. Civil Engineering Department, Tafila Technical University (TTU), Tafila, Jordan

b. British Geological Survey, Nottingham, NG12 5RA UK

Abstract

Uranium distribution has been studied in the outcropping Upper Cretaceous-Tertiary rocks (Belqa Group) in northwest Jordan. Representative samples of phosphorite, chert, silicified limestone, chalk, marl, fossiliferous limestone and glauconitic limestone were collected and chemically analyzed using XRF techniques. Uranium values range between less than 1 ppm and 70 ppm. The highest U concentration (52-70 ppm) was encountered in the phosphatic rocks. Uranium values in other lithologies are up to 19 ppm. The lowest values were encountered in fossiliferous limestone (<1 ppm), chert (2 ppm), silicified limestone, almost pure chalk and silicified chalk (4 ppm). Uranium concentrations in northwest Jordanian chalks are higher than Cretaceous chalks of the USA and Europe (North Sea). Uranium is positively related with P_2O_5 (francolite in phosphorite). Organic matter could be related to elevated levels of uranium in highly bituminous marl (average of 25 ppm). Uranium is positively associated with Cr, Zn, Mo, As, Sc and V (correlation coefficients r> 0.80). When U is cross-plotted against other variables, aggregation based on lithology became clear and the importance of other factors (with r>0.80) such as alumina, total iron oxides, P_2O_5, LOI (loss on ignition) Ni, Cl, As, Mo, Cd, La became evident. Factor analysis showed that uranium is distributed in clay and carbonates, formation water and organic matter, and phosphorite. Weak loadings are observed with factor 2 in comparison to factors 1 and 3. Uranium concentrations in Jordanian and similar chalks can be predicted from the knowledge of alumina, total iron oxides, P_2O_5, and LOI.

Keywords: uranium distribution, Jordan, Cretaceous-Tertiary, Belqa Group.

1. Introduction

Jordan faces two main challenges: lack of conventional energy resources and scarcity of water. The increasing cost of oil and gas imports, that currently supply most of the country's energy needs, severely affects its economic growth and security of supply. Hence, the development of a secure alternative energy supply is a top priority for Jordan. Jordan established the Jordan Atomic Energy Commission (JAEC), early in 2008, to lead the national efforts and implement Jordan's nuclear energy program. Dr. Khaled Toukan, the chairman of the Jordan Atomic Energy Commission, announced in an invited talk to the Symposium on the Technology of Peaceful Nuclear Energy, Yarmouk University-Jordan (Oct. 14-16, 2008) that 'following assessment of exploration and extraction of the proven uranium ore reserves, including domestic phosphate deposits, Jordan will sign mining agreements later this year, and we expect uranium production to begin by 2012. Jordan's plan is to generate electric power from its nuclear power reactors by 2016 and to export electricity by 2030'.

Uranium and its natural series radionuclides Th, ^{226}Ra and ^{222}Rn are widely distributed in a number of geological settings in Jordan. Uranium occurrences in phosphorite, oil shale (bituminous limestone), limestone, marble, sandstones, and thermal waters of Jordan were studied by many workers mainly during regional mapping and mineral exploration projects (Abu Ajamieh, 1974, 1981, 1987; Phoenix Corp., 1980; Abed and Khalid, 1985; Abu Ajamieh et al, 1988; Helmdach et al, 1985; Healy and Young, 1998; Wriekat et al, 1987; NRA, 1997; Smith et al., 1996a, b). The present work aims at examining the association of uranium with major, minor, and other trace elements in the chalk-dominated Belqa Group succession in northwest Jordan. It includes a comparison of uranium content with similar chalk-dominated successions worldwide, including 'average' limestone, and regional phosphate, oil shale and marble occurrences. In addition, geochemical proxies useful for uranium exploration are suggested.

* Corresponding author: mohdbk@yahoo.com

Groundwater pollution by natural radionuclides has been reported from local aquifers in the Amman area (Smith et al., 1996a,b); the source of the radiological hazard ^{222}Rn and elevated levels of uranium exceeding 1 mg/l is thought not to be from primary leaching of U from phosphorite deposits, but the result of carbonate groundwater mixing, at depth, with uranium mineralization of Cretaceous aquifers (Ajlun Group; Table 1) along the Amman-Hallabat fault (Smith et al.,1995). In addition, high levels of uranium have been reported from Late Cretaceous to Neogene phosphorites (Abed and Khaled, 1985). Other uraniferous geological terranes are the Ordovician-Silurian marine sandstones and mudstones of the southern Desert (Abu Ajamieh et al., 1988) and Late Cretaceous to Palaeogene oil shales (oil-saturated marls) (Abu Ajamieh, 1981, 1988; Wriekat et al., 1987).

High levels of U, Th, ^{226}Ra and ^{222}Rn have also been reported elsewhere in the Mediterranean Basin from ground waters derived from middle Miocene age carbonate-gypsum aquifers (Discospirina beds) of the Maroni region, Cyprus (Smith et al., 1997).

2. Geological Setting

The study area (Figure 1), situated 90 km north-northwest of Amman, was mapped at 1: 50 000 scale (Moh'd, 2000). The lithostratigraphy and lithology of the Late Cretaceous to Tertiary (Neogene) succession of the area is presented in Table 1 (after Powell, 1989). Superficial deposits, comprising calcrete, travertine, alluvium, alluvial fans and soil, are also present. The sampled rock units are briefly described here after Moh'd (2000).

The **Maestrichtian Al-Hisa Phosphorite Formation** is 10-15 m thick and consists of phosphate, phosphatic chert, limestone, coquina and marl. Mega-fossils include ammonite *Baculites* and bivalves. There are 16 species and subspecies of the microfossil *Globotruncana* (Abed and Ashur, 1987). Trace fossils are represented by Thalassinoides burrows. Phosphate was deposited as phosphate mud and then reworked and deposited as phosphate sands in shallow marine environment.

The **Umm Rijam Chert-Limestone Formation** (Eocene) is 220 m thick and consists of the alternation of chalky limestone, marly limestone and kerogenous limestone in its lower massive member and with appreciable amount of chert (beds and concretions) in its upper bedded member.

Tayyiba Limestone Formation consists of 2 informal members: a lower glauconitic and an upper 'cliffy' limestone. The lower glauconitic member consists of glauconitic sandstone, calcareous siltstone and marly limestone with shells of brachiopods and molluscs and tube-like fossils and trace fossils. The upper member consists of 3 cliffs of massive fossiliferous limestone. Nodular thinly bedded limestone is occasionally common at the base of these cliffs.

3. Clay mineralogy of the Belqa Group

Apart from Abed and Amireh (1985) and Shadfan et. al. (1985) there are no detailed studies on the clay mineralogy of the Belqa Group in north Jordan. The former authors reported that the clays constitute about 7% of the oil shale (bituminous marl) and are almost totally made of kaolinite with traces of illite whereas the latter authors where the first to report palygorskite in the Umm Rijam Limestone. More detailed work has been carried out west of the Jordan River (Shoval, 2004). Illite/smectite is almost the only clay mineral except in the Danian Lower Taqiye Formatin where kaolinite is present. Palygoskite accompanies illite-smectite in the Ladenian Upper Taqiye and Lower Eocene Mor Formation. In the present work clay mineralogy was not studied but the presence of clays is indicated by alumina contents which range from less than 1% to almost 11.74%.

4. Samples

16 representative samples from the dominant lithologies of the Late Cretaceous-Tertiary Belqa Group (Table 1) were collected at outcrop from Shallala (URC) and Wadi Tayiba (AHP and TL). These range from non-bituminous to slightly bituminous chalk, silicified chalk, marl, phosphorite, chert, glauconitic and fossiliferous limestone. The samples are summarized, along with their major oxides, in Table 2. Loss on ignition at 450°C reflects the organic matter content of the samples.

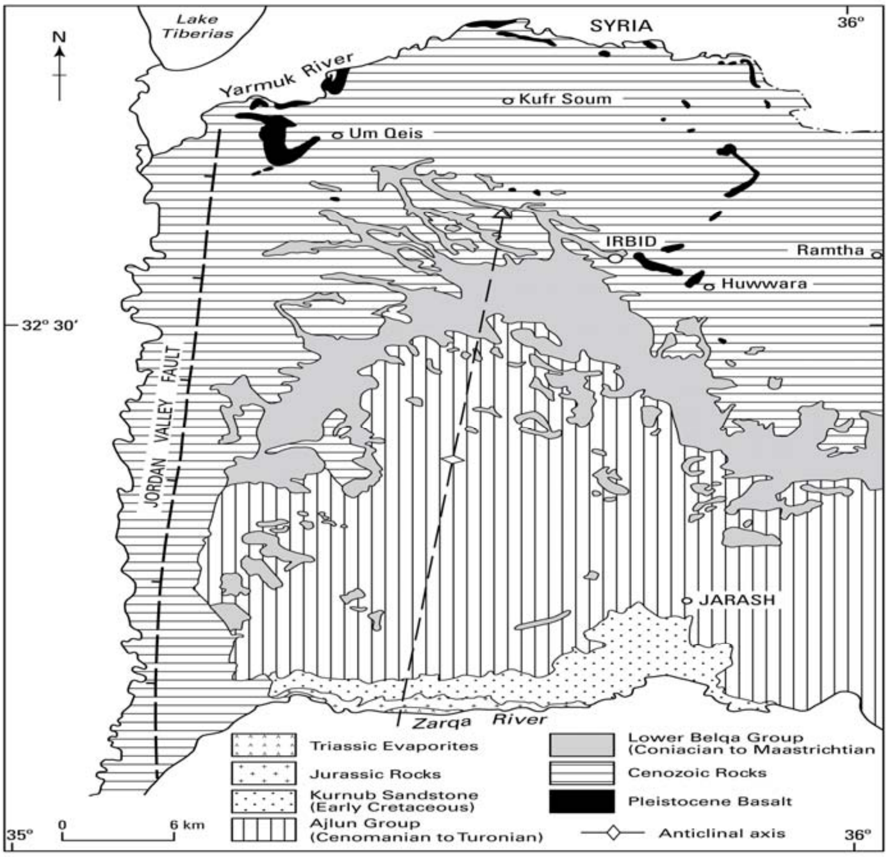

Figure 1 A simplified geological map of north Jordan. Study area is north of Irbid-Ramtha line (Abdelhamid et al., 1991).

Table 1. Stratigraphy of Belqa Group in the study area (Powell, 1989; Moh'd, 2000)

Age		Group	Stage	Formation	Symbol	Main lithologies
Tertiary (Neogene)		Belqa	Oligocene	Tayiba*	TL	Limestone, fossiliferous, glauconitic
			Eocene	Shallala	WSC	Chalk
				Umm Rijam*	URC	Chalk, chert, limestone
			Paleocene	Muwaqqar*	MCM	Chalk, marl, limestone concretions
Cretaceous	Late		Maastrichtian	Al Hisa*	AHP	Phosphorite, limestone, chert
			Santonian/ Campanian.	Amman	ASL	Chert, limestone, dolomite
				Umm Ghudran	WG	Chalk (massive and fossiliferous) *Unconformity*
			Coniacian			
	Early	Ajlun	Turonian	Wadi As Sir	WSL	Limestone, dolomite

*Units sampled for the present study

5. Analytical Procedures

Samples were analyzed using X-ray fluorescence (XRF) techniques at the Analytical Geochemistry Laboratories, British Geological Survey. In the present work oxides were analyzed using WD-XRFS fused glass beads, and most trace elements by WD-XRFS pressed powder pellets except Ag, Cd, In, Sn, Sb, Te, I, Cs, Ba, La and Ce which were analysed by ED(P)-XRFS pressed powder pellets. The samples were dried overnight at 105°C and pre-ignited with the temperature being ramped up from 200°C to 450°C, over the course of an hour and then for a further hour at 1050°C before analysis. Loss on ignition was determined after 1 hour at 1050° C and 1 hour at 450°C. Fe_2O_3t represents total iron expressed as Fe_2O_3. SO_3 represents sulphur retained in the fused bead after fusion at 1200C.

6. Results

The analytical results are presented in Tables 2 and 3. Correlation coefficients (r) between uranium and other analyzed elements are given in Table 4, and factor analysis is given in Table 5. The relationship between uranium and selected major and minor elements, and LOI are presented in cross-plots (Figures 2-12).

Table 2 Major oxides, LOI@450°C, and uranium concentration in the studied samples.

#	Lithology	Rock Unit	U ppm	SiO_2	Al+Fe	CaO+ LOI	MgO	P_2O_5	LOI@ 450°C
1	Slightly bituminous Chalk	URC	8	5.31	0.79	88.53	1.14	1.55	5.35
2	Slightly bituminous Marl	URC	6	23.39	15.14	58.17	0.93	1.11	1.87
3	Slightly bituminous silicified Chalk	URC	19	14.65	2.58	79.54	0.76	1.24	3.05
4	Slightly bituminous silicified Chalk	URC	12	13.92	3.40	74.52	2.3	0.30	5.49
5	Chalk	URC	4	2.64	0.94	95.59	0.40	0.96	0.86
6	Chalk	URC	4	2.81	0.86	94.96	0.40	0.93	0.95
7	Slightly silicified Chalk	URC	10	10.63	1.13	86.19	0.67	0.84	1.80
8	Limestone, fossiliferous	TL	<1	1.86	0.39	97.39	0.29	0.28	0.36
9	Slightly silicified Chalk	URC	11	8.66	1.45	87.00	0.80	0.93	1.52
10	Glauconitic Limestone	TL	10	6.26	3.48	86.60	0.78	2.27	0.65
11	silicified Chalk	URC	4	46.41	0.66	51.53	0.15	1.08	0.38
12	Chalk	URC	8	1.60	0.49	95.96	0.28	1.63	0.72
13	Phosphorite	AHP	70	1.83	0.46	81.00	0.35	14.49	1.16
14	Phosphorite	AHP	52	14.35	0.08	69.11	0.36	14.58	0.72
15	Chert	URC	2	95.32	0.16	3.77	0.05	0.26	1.95
16	Silicified Limestone	URC	4	64.51	0.43	34.00	0.08	0.55	1.96

Table 3. Average and standard error of the major, minor and trace elements.

	Average	Std error		Average	Std error		Average	Std error
SiO_2	19.63	6.67	Cl	1531.00	495.96	Sn	0.59	0.07
TiO_2	0.06	0.02	Sc	3.00	1.22	Sb	1.06	0.20
Al_2O_3	1.39	0.70	V	54.50	10.24	I	3.44	0.57
Fe_2O_3t	0.86	0.23	Cr	132.00	17.31	Cs	1.31	0.18
Mn_3O_4	0.01	0.00	Co	2.19	0.75	Ba	512.00	146.29
MgO	0.61	0.14	Ni	73.25	15.60	La	12.25	2.55
CaO	42.10	3.81	Cu	28.13	5.25	Ce	9.00	3.09
Na_2O	0.07	0.01	Zn	194.69	49.54	Nd	15.00	2.11
K_2O	0.10	0.04	Ga	2.06	0.75	Sm	3.06	0.06
P_2O_5	2.69	1.16	As	3.38	0.93	Cd	4.58	2.82
SO_3	0.46	0.13	Se	6.44	2.65	Yb	1.31	0.15
Cr_2O_3	0.02	0.00	Br	5.63	1.31	Hf	1.75	0.23
SrO	0.10	0.01	Rb	6.75	2.15	Ta	1.06	0.06
BaO	0.02	0.01	Sr	787.31	103.62	W	1.63	0.15
NiO	0.05	0.00	Y	22.75	3.87	Pb	1.94	0.62
ZnO	0.01	0.01	Zr	13.19	3.26	Bi	1.13	0.09
LOI	32.13	2.84	Nb	1.56	0.50	Th	1.38	0.26
Total	100.06	0.12	Mo	3.5	0.75	U	14.06	4.79
LOI@450	1.80	0.40	Ag	0.76	0.09			

Table 4 Correlation coefficients (r) between uranium and other components.

	r		r		r
SiO_2	-0.36	Cl	-0.12	Sn	0.63
TiO_2	0.15	Sc	0.83	Sb	-0.17
Al_2O_3	0.07	V	0.83	I	0.79
Fe_2O_3t	0.28	Cr	0.87	Cs	-0.13
Mn_3O_4	-0.08	Co	0.11	Ba	0.03
MgO	0.56	Ni	0.81	La	0.10
CaO	0.28	Cu	0.77	Ce	0.44
Na_2O	0.13	Zn	0.84	Nd	0.04
K_2O	0.38	Ga	0.09	Sm	0.35
P_2O_5	0.37	As	0.89	Cd	-0.08
SO_3	0.49	Se	0.63	Yb	0.22
Cr_2O_3	0.91	Br	0.71	Hf	0.14
SrO	0.50	Rb	0.42	Ta	-0.20
BaO	0.05	Sr	0.50	W	0.22
NiO	0.78	Y	0.66	Pb	0.06
ZnO	0.84	Zr	0.19	Bi	-0.12
LOI	0.35	Nb	-0.05	Th	0.03
Total	0.08	Mo	0.86		
LOI@450	0.46	Ag	0.18		

Table 5. Factor analysis, rotated component matrix, extracted by Principal Component Analysis.

	Factor 1	Factor 2	Factor 3
Explaining % variation	50.02	25.46	24.52
SiO_2	-0.657		-0.749
TiO_2	0.986		
Al_2O_3	0.988		
Fe_2O_3t	0.988		
MgO	0.976		
CaO	0.416		0.905
Na_2O	0.260	0.962	
K_2O	0.982		
P_2O_5	0.479		0.863
SO_3		0.988	
LOI	0.552		0.827
Total	0.402	0.478	0.781
LOI@450	0.365	0.537	-0.76
Cl	-0.364	0.932	
Sc	0.790	0.599	
V	0.955		0.292
Cr	0.595		0.768
Ni		0.977	
Cu	-0.276	0.960	

Table 5 Continues next page…..

Zn	0.475	0.875	
Br	-0.427	0.887	
Rb	0.988		
Sr	0.283	0.318	0.905
Y	0.922		0.384
Zr	0.990		
I	-0.497		0.862
Ba	0.985		
Nd	0.984		
U	0.739	0.283	0.612

7. Uranium

The average uranium value in the samples is 14 ppm and the range is <1-70 ppm. Phosphatic samples (13 and 14) show a higher range (52-70 ppm). Other samples have a range from <1-19 ppm. Uranium is positively correlated with the following oxides: Cr_2O_3 (0.91), ZnO (0.84), and MgO (0.56). It also has positive correlation with many trace elements. The strongest correlations being with As (0.89), Cr (0.87), Mo (0.86), Zn (0.84), V (0.83), Ni (0.81), and Sb (0.79).

7.1. U/SiO$_2$

SiO_2 shows a weak negative correlation (R=-0.36) with U (Figure 2). Figure 2 shows that the two phosphatic, as well as, siliceous samples (with SiO_2 >20%) have a linear inverse relationships with uranium with the former having higher gradient than the latter

(Uranium= -0.052 (SiO_2) + 6.9858 (R^2=0.94).

Of the siliceous samples in which uranium concentration is less than 10 ppm, chert has the lowest concentration of uranium, followed by silicified limestone, then siliceous chalks. On the other hand, pure and impure chalks (SiO_2<20%) have a positive relatively strong relationship with uranium (r>0.80) as follows:

Uranium= 0.8912 (SiO_2) + 2.6097 (R^2=0.75)

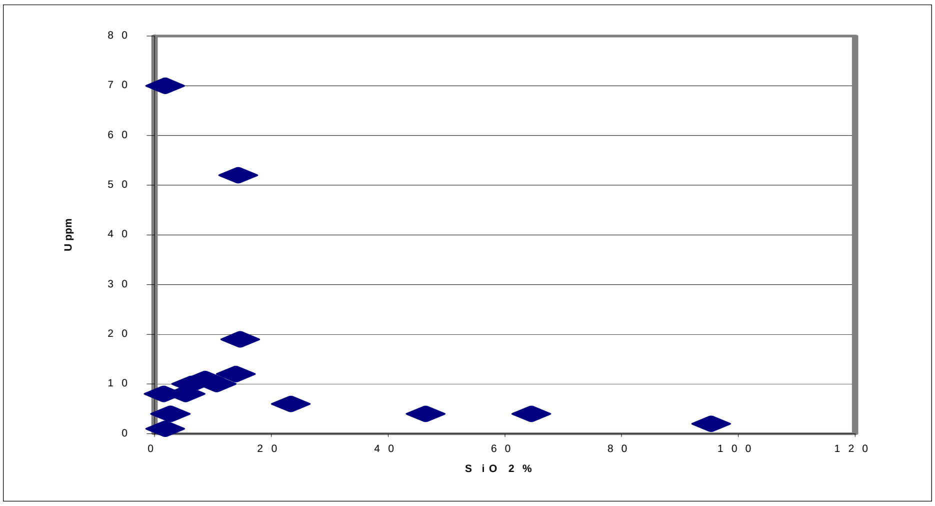

Figure 2. Correlation between U and SiO_2.

7.2. U/CaO

When CaO<35% (e.g. chert, silicified limestone, marl, highly siliceous chalk) uranium is less than 10 ppm. Non-phosphatic and low silica samples can be fit with a negative linear relationship as follows:
Uranium= -0.819 (CaO) + 49.25 (R^2=0.64)

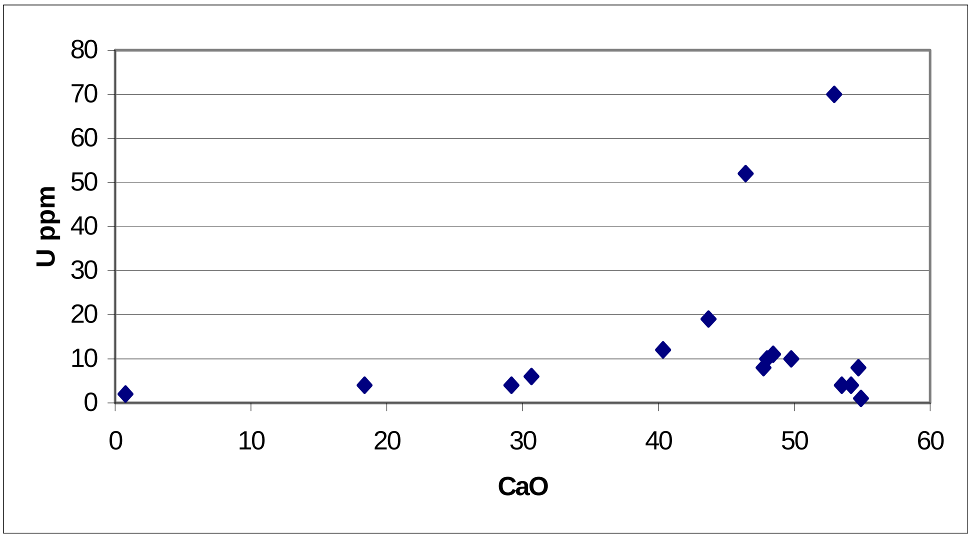

Figure 3. Correlation between U and CaO.

7.3. U/ P2O5

Uranium has a very strong positive relation with P_2O_5 (Figure 4) as shown in the following equation
Uranium= 791.67 (P_2O_5) + 35.75 (R^2=0.92)

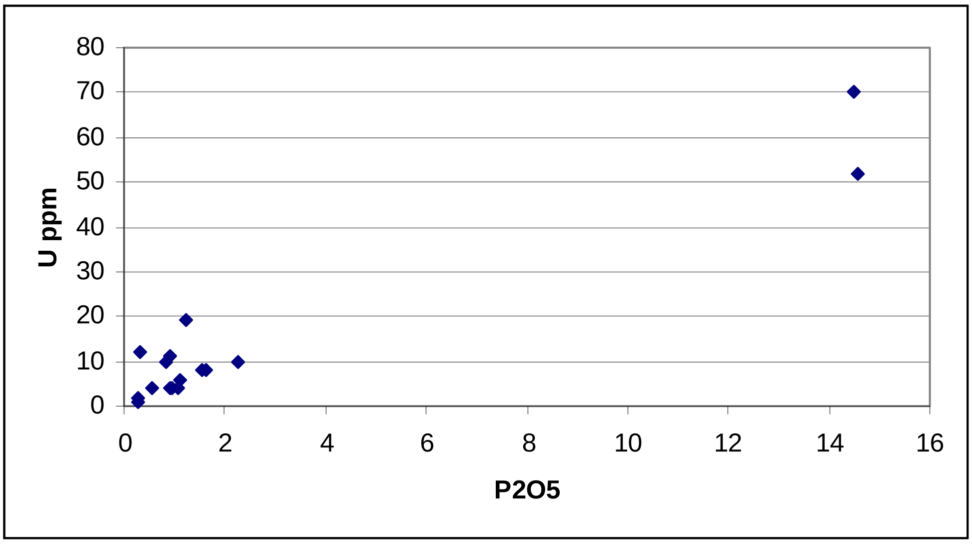

Figure 4. Correlation between U and P_2O_5.

  - Volume 3, Number 1 (ISSN 1995-6681)

7.4. U/ Cr

The positive high correlation coefficient (r=0.87) between uranium and Cr is shown in Figure 5. The figure consists of two almost parallel separate lines. When taken separately, the upper line represents phosphorites.

Uranium= 0.261 (Cr) + 34.78 (R^2=1.00)

The lower line represents the rest of the samples

Uranium= 0.058 (Cr) – 0.56 (R^2=0.92)

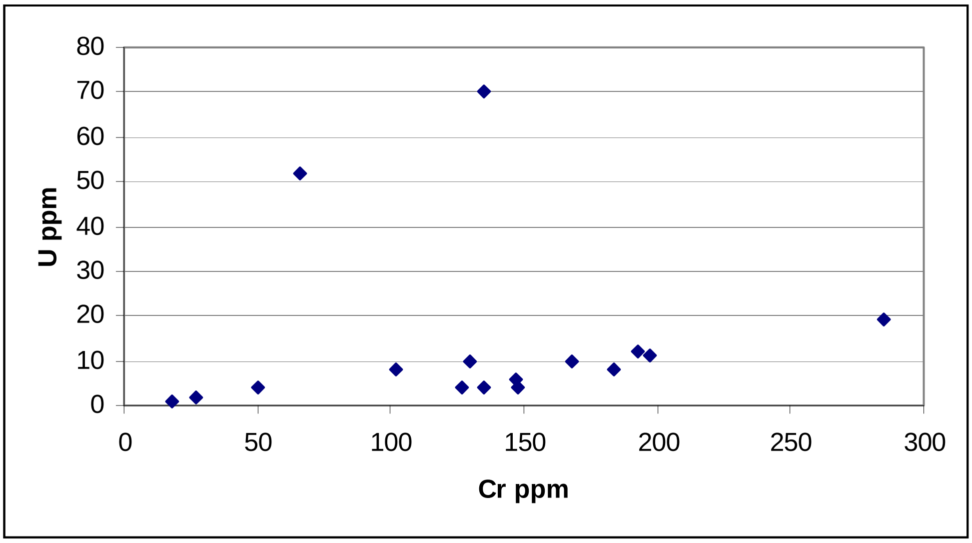

Figure 5: Correlation between U and Cr. U/SrO

The best fit between uranium and SrO and including all samples (Figure 6) is an exponential one as shown in the following equation:

$$\text{uranium} = 1.699\ e^{14.84\ (SrO)}$$

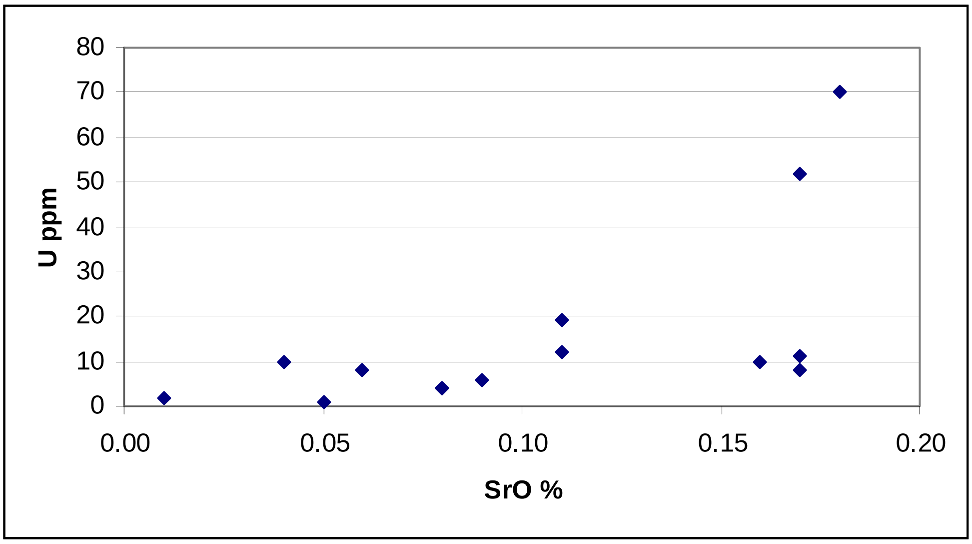

Figure 6: Correlation between U and SrO.

7.5. U/Zn

Zn (Figure 7) has positive linear relations with uranium when phosphatic samples are excluded.

Uranium= 0.026 Zn + 3.33 (R^2=0.70)

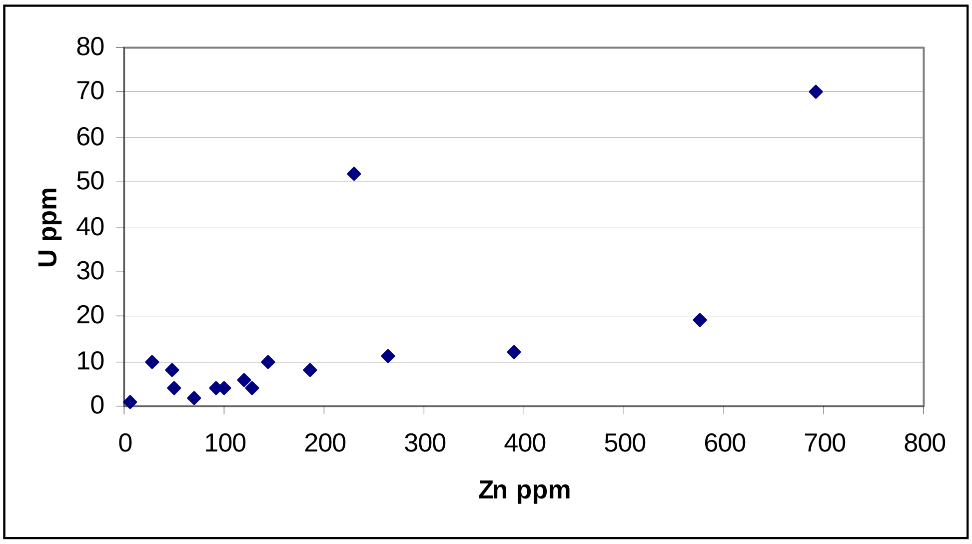

Figure 7: Correlation between U and Zn.

7.6. U/V

Vanadium (Figure 8) has a strong positive linear relationship with uranium when phosphate samples are excluded. This relationship has the following equation

Uranium= 0.099 V + 2.48 (R^2=0.70)

Uranium and vanadium are characteristically negatively related in the phosphate samples

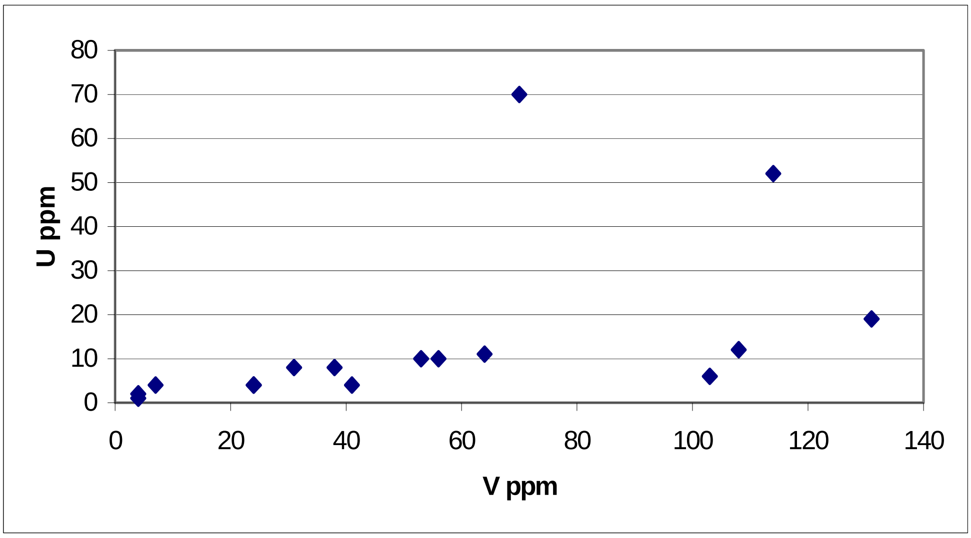

Figure 8: Correlation between U and V.

7.7. U/Mo

Mo (Figure 9) has also a positive linear relationship with uranium when phosphates are excluded. This relationship has the following equation

Uranium= 1.255 Mo + 3.144 (R^2=0.74)

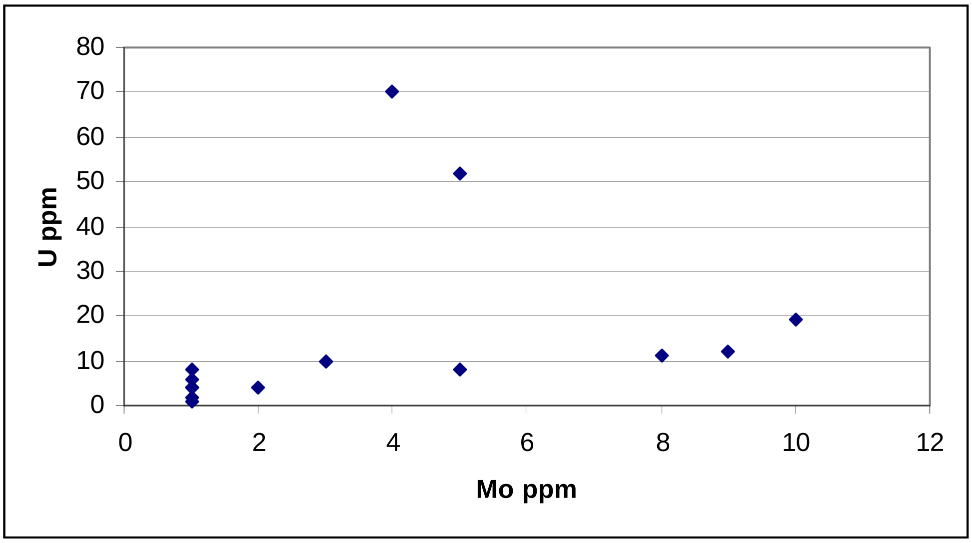

Figure 9. Correlation between U and Mo.

7.8. U/Loss on Ignition (LOI)

Three straight lines can fit the LOI (Figure 10) in the different samples with uranium. The first line being with phosphate samples where a positive relationship with uranium is evident. The second line includes chert, silicified limestone, highly siliceous chalk and marl which show a positive linear relationship

$$\text{Uranium} = 0.1455\ \text{LOI} + 1.51 \quad (R^2=0.89)$$

The rest of the samples show a negative relationship with uranium as shown in the following equation

$$\text{Uranium} = -2.011\ \text{LOI} + 88.13 \quad (R^2=0.81)$$

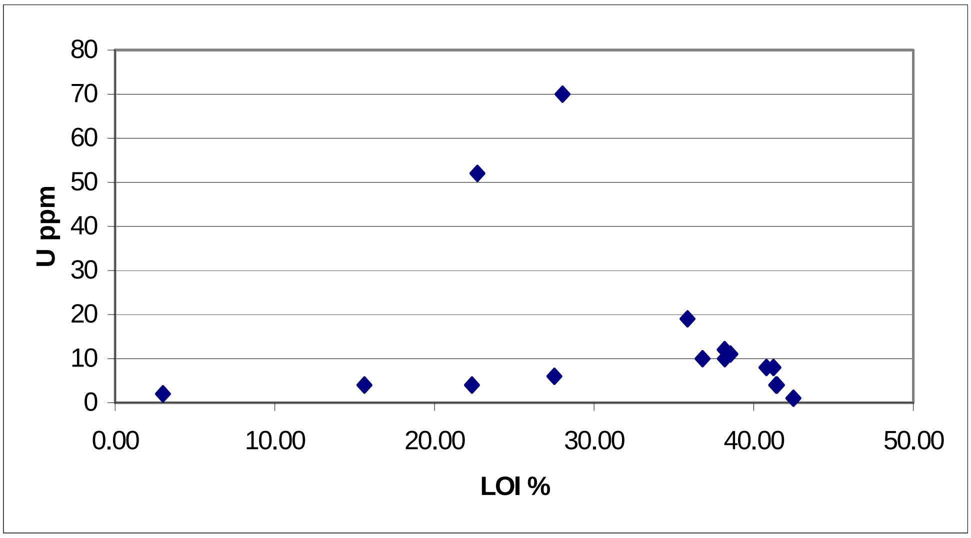

Figure 10: Correlation between U and LOI.

An approximate estimate of uranium content can be derived from the knowledge of the total chemical analysis (including all oxides and LOI) (Figure 11) using the following equation

$$\text{Uranium} = -30.4\ \text{Total} + 3056.2 \quad (R^2=0.57)$$

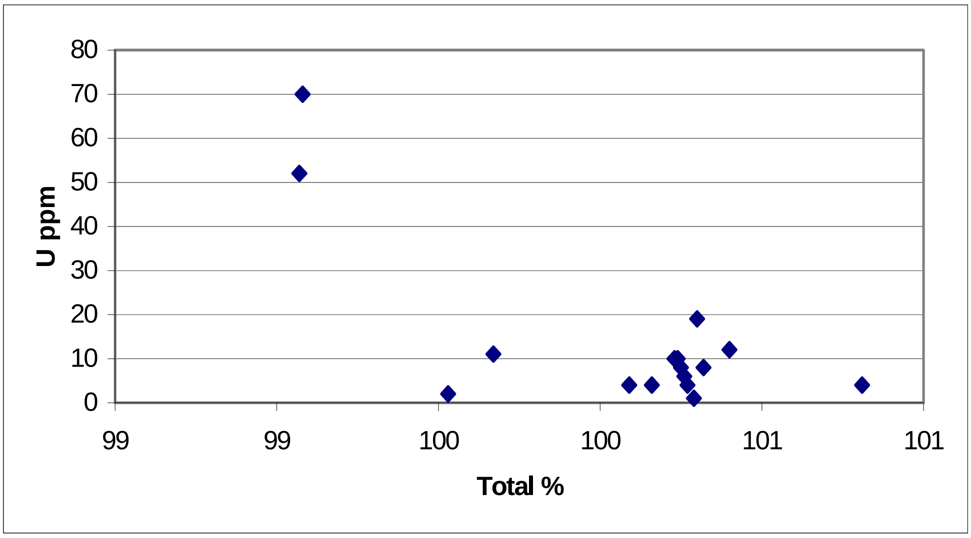

Figure 11: Correlation between U and total components.

LOI@450C is related to carbonates, organic matter and clay minerals and shows at least three trends or fields with uranium. The first is a negative trend that includes slightly bituminous samples. The second trend is also negative and includes chert, silicified limestone, marl and highly siliceous chalks. The third field includes the rest of samples.

8. Discussion

Uranium in Late Cretaceous to Early Tertiary rocks (Jordan)

Turekian and Wedepohl (1961) reported the following average uranium concentrations (in ppm) in the main types of sedimentary rocks: shale 3.7, sandstone 0.45 and limestone 2.2. These compare with 2.7 ppm in igneous rocks. In non-bituminous Upper Cretaceous chalk of the United States, Gale et. al., (2008) reported less than 2 ppm of uranium. Similarly, Kuzendorf and Sorensy (1989) and Stemmerik et. al. (2006), reported concentrations of less than 2 ppm for Upper Cretaceous chalks of the North Sea and of Stvens Klint, Denmark. However, along the southern margin of the Late Cretaceous to Neogene Tethys Ocean uranium concentrations are higher. For instance, Ilani et al (2006) reported the following figures for U concentrations from formations penetrated by a well drilled in the vicinity of the western shores of Tiberia lake: 4.6 ppm from Timrat (Eocene), 8.9ppm from Taqiya (=Muwaqqar Chalk Marl, in part), 5.5ppm from Ghareb (=Muwaqqar Chalk Marl, in part), and 8-23.6ppm from En Zetim (=Umm Ghudran to Al Hisa Phosphorite), with high concentrations being associated with oil shale horizons. Furthermore, Late Cretaceous to Neogene shallow marine phosphorites in the Tethyan belt including Egypt and the Levant, commonly have high uranium contents compared to the world average for phosphates (120 ppm; Altschuler, 1980). Uranium contents of 90-150 ppm of U have been reported in Negev Phosphorites (Nathan et. al, 1979; Gross and Ilani, 1987; Gill and Shiloni, 1995) and 50-357 ppm in Egypt (El-Arabi and Khalifa, 2002). Uranium content in the economic Cretaceous to Neogene phosphorite belt of Jordan ranges from 65 -170 ppm (Abu Ajamieh et al, 1988; Smith et al., 1996b).

Uranium in the Upper Cretaceous to Lower Tertiary oil shales was first reported from the Lajjun deposit in central Jordan by Hufnagel et. al. (1980) as 26 and 24 ppm in Boreholes 86 and 97, respectively. More recent work on oil shale of Jordan has been carried out by Abu Murad (2008) who reported the following uranium concentrations from oil shale deposits in central Jordan: Lajjun 31.4, Sultani 12.3, Jurf 9.8, Attarat 16.7, Wadi Maghar 12.5, Siwaqa 9.7, Khan Az-Zabib 28.1, and Eth Thamad 41.6 ppm.

The analytical results (Tables 2-3) and statistical analysis (Tables 4-5, and Figures 2-12) from this study demonstrate the close association of U with other major and minor elements in Late Cretaceous to Early Tertiary samples (full analytical results, not included for brevity, are available for the authors). Uranium is most strongly associated with phosphorite deposits where the metal is present together with other trace elements in the phosphate mineral francolite $Ca_5(CO_3\ P0_4)_3(F,OH)$ lattice where U partially substitutes for calcium in the mineral lattice (McClellan and Van Kauwenbergh, 1990; Wriekat et al., 1987). A positive correlation between uranium and phosphorite deposits has been recognized in the region (Gill and Shiloni, 1995; Abed and Khaled, 1985). In Jordan, the Late Cretaceous Campanian to Maastrichtian phosphorite belt shows a general decrease from north to south in the mean concentration of both phosphate and associated uranium from the Zarqa (Ruseifa) area, immediately south of the study area, (29.7% P_2O_5; 145 U ppm) to Esh Shidiya (24.85% P_2O_5; 80 U ppm (Saadi and Shaban, 1981; Smith et al, 1996b). This trend is attributed to a southward decrease in the purity of the phosphate rock, and hence in the proportion of uranium substituting in the francolite lattice. The relatively low U content (52-70 ppm) in the samples analyzed in this study from northwest Jordan indicate a lower phosphate, and hence uranium, content. This trend is attributed to the palaeoenvironmental setting of the studied rocks in more basinal (offshore) locations during deposition of the Belqa

Group sediments on a pelagic ramp at the southern margin of the Tethys Ocean (Powell, 1989).

The presence of U contents ranging from 8 ppm to 19 ppm in chalk lithologies from Umm Rijam Chert-Limestone reflects the presence of uranium in slightly bituminous chalks. The organic matter in these chalks is associated with minor amounts of similar organic fish and marine vertebrate fragments that make up much of the original source of francolite in these phosphorite lithologies. A similar relationship can be seen in the higher than average phosphate and uranium concentrations in the marine glauconitic marl from the Oligocene Tayiba Formation (Table 2).

Trace metals such as Mo, Zn,V, Ni, Cr, As and Mo have strong (r>0.80) positive correlation with uranium, and are mostly associated with organic matter (bitumen and francolite).

Factor analysis (Table 5) resulted in deriving 3 factors explaining 100% of the variations of the data. Factor 1 explains 50% of the data variation and is controlled by clay minerals, and to less extent, by carbonate. Factor 2, explaining 25% of the variation, is controlled by both depositional/diagenetic water and organic matter content. Factor 3, explaining also 25% of the variation, is controlled by phosphorite beds. Uranium was found to be associated with the three factors but with different loadings. Association of uranium with factor 2 (organic matter and ground water) is weak in comparison to association with factors 1 and 3.

9. Conclusions

Uranium concentrations in Jordanian Late Cretaceous to Tertiary (Neogene) chalks are higher than those of the standard limestone and equivalent 'pure' chalk (98% $CaCO_3$) of USA and northwest Europe. High uranium concentrations are closely associated with phosphorite deposits, in which uranium substitutes for calcium in the francolite lattice. Higher than average levels of uranium, in slightly bituminous chalks and glauconitic limestone are attributed to minor amounts of organic matter found in these samples.

Uranium Association with organic matter and formation water is weak in comparison to association with the clays and carbonates (factor 1), and P_2O_5 (factor 3). Trace elements (Cr, Mo, Zn, V, Ni, Cl, As, and Mo) have strong positive relations with Uranium (with r>0.80).

The correlation matrix should not be relied upon totally as it gives average correlation coefficients (assuming linear relationships between variables) when dealing with different lithologies. Cross-plotting results may emphasize the effect of different lithologies and different curves may be used to fit the data. Cross-plotting may reveal relationships with lithologies that are not clear in the correlation matrix.

Exploration for uraniferous deposits of economic value should focus on phosphorite and/or associated phosphorite/high bituminous sedimentary rocks, especially where these lithofacies reach high levels of P_2O_5 in the Late Cretaceous to Neogene Tethyan phosphorite belt.

Acknowledgements

The authors thank Charles Gowland and Mark Ingham of the BGS Analytical Laboratories for chemical analyses and discussion of the results. BKM would like to thank Tafila Technical University for a travel grant to the UK during 2008 summer. JHP publishes with permission of the Executive Director, British Geological Survey (NERC). The authors would like to thank the two anonymous reviewers of this paper for their comments.

References

Abdelhamid, G., Moh'd, B., and Barjous, M.,1991, The geology of northwest Jordan 'to accompany the preliminary 1: 100 000 geological map', *Internal Report*, Amman.

Abed, A., and Amireh, B., 1983, Petrography and geochemistry of some Jordanian oil shales from north Jordan. *Journal of Petroleum Geology*, **5**(3): 261-274.

Abed, A., and Khaled, H., 1985, Uranium in Esh-Shediya phosphates, *Dirasat* **8**: 57-66.

Abu Ajamieh, M., 1974, Uranium in the Jordanian phosphates, *Unpublished Report,* Natural Resources Authority, Amman, Jordan.

Abu Ajamieh, M., 1981, Radioactive minerals in Jordan, *The 4TH Arab Mineral Resources Conference*, Amman, 2: 16p.

Abu Ajamieh, M., 1987, Mineral resources of Jordan, *Unpublished Report*, Natural Resources Authority, Amman, Jordan.

Abu Ajamieh, M., Bender, F.K. and Eicher, R. N. 1988. *Natural Resources in Jordan*, pp. 224. Natural Resources Authority, Amman, Jordan.

Abu Murad, K., 2008, Determination of uranium concentration in Jordanian oil shale using fission fragments technique with cx-39, 24th International Conference on Nuclear Tracks in solids, 1-5 Sep., 2008, Bologna, Italy.

Altschuler, Z.S. 1980. The geochemistry of trace elements in marine phosphorites, Part 1: Characteristic abundances and enrichment. *SEPM Special Publication* , **575-B**, 19-30.

El-Arabi, A.M. and Khalifa, I.H., 2002. Application of multivariate statistical analyses in the interpretation of geochemical behaviour of uranium in phosphatic rocks in the Red Sea, Nile Valley and Western desert, Egypt. *Journal of Environmental Radioactivity*, **61**, 169-190.

Gale, A., Hancock, J., Kennedy, W., Petrizzo, M., Lees, J., Ireneusz Walaszczyk, I., and Wray, D. 2008, An integrated study (geochemistry, stable oxygen and carbon isotopes, nannofossils, planktonic foraminifera, inoceramid bivalves, ammonites and crinoids) of the Waxahachie Dam Spillway section, north Texas: a possible boundary stratotype for the base of the Campanian Stage, Cretaceous Research 29: 131-167.

Healy, R. and Young, J. 1998, Mineralogy of U-bearing marls from the Jordanian Desert, Unpublished Report for Cameco Corporation, Canada.

Gill, D., and Shiloni, Y. 1995. Abundance and distribution of uranium in Senonian phosphorites, Arad basin, southern Israel. *Journal of African Earth Sciences* , **20**, 17-28.

Gross, S., and Ilani, S. 1987. Secondary uranium minerals from the Judean Desert and northern Negev, Isreal. *Uranium*, **4**, 147-158.

Helmdach, F., Khoury, H., and Meyer, J. 1985, Secondary uranium mineralization in the Santonian-Turonian, near Zarqa, north Jordan, *Dirasat*, **12**: 105-111.

Hufnagel, H., Schmitz, H., and El-Kaysi, K., 1980, Investigation of the El-Lajjun oil shale deposit, Technical Cooperation Project No. 78.2165.5, Bundesanstalt fur Geowissen-Schaften und Rohstoffe, Hannover, Germany.

Ilani, S., Minster, T., Kronfeld, J., and Even, O., 2006, The source of anomalous radioactivity in the springs bordering the Sea of Galilee, Israel, *Journal of Environmental Radioactivity,* **85**: 137-145.

Kunzendorf, H. and Sorensey, P., 1989, Geochemical criteria for reservoir quality variations in chalk from North Sea, Riso National Laboratory, Roskilde, Denmark, 99p.

McClellan, G.H. and Van Kauwenbergh, S.J. 1990. Mineralogy of sedimentary apatites. In: Phosphorite Research and Development, Notholt, A.J.G. and Jarvis, I. Eds. *Geological Society Special Publication,* **52**, 23-31.

Moh'd, B., K., 2000, The geology of Irbid and Ash Shuna Ash Shamaliyya (Waqqas) map sheets, *Geology Directorate, Bulletin* **46**, Natural Resources Authority, Amman, Jordan .

Nathan, Y., Shiloni, Y., Roded, R., Gal, I., and Deutch, Y., 1979, The geochemistry of the northern and central Negev phosphorites, *Israel Geological Survey Bulletin* 73: 41p.

NRA, 1997, Uranium exploration in Siwaqa area, Unpublished Report, in Arabic.

Phoenix Corp., 1980, A comprehensive airborne magnetic /radiation survey of the Hashemite Kingdom of Jordan, Internal Report, NRA, Amman.

Powell, J H. 1989. Stratigraphy and sedimentation of the Phanerozoic rocks in central and southern Jordan. *Bulletin 11, Geology Directorate, Natural Resources Authority (Ministry of Energy and Mineral Resources) Amman, H K of Jordan.* Part B : Kurnub, Ajlun and Belqa Groups, 161pp, 12 figs., 17 tables.

Saadi T.A. and Shaban, M.R.1981. *Arab Mining Journal*, **1**, 70-70.

Shadfan, H., Dixon, J., and Kippenber, L., 1985, Palygorskite distribution in Tertiary limestone and associated soils of northern Jordan. *Soil Science*140 (3): 206-212.

Shoval, S., 2004, Clay sedimentation along the southeastern neo-Tethys margin during the oceanic convergence stage, *Applied Clay Science* 24: 287-298.

Smith, B, Powell, J H, Bradley, A D, Gedeon, R, and Amro, H. 1995. Naturally occurring uranium pollution in Jordan. *Mining Environmental Management***,** **3**, 7-10.

Smith, B, Powell, J H, Gedeon, R, and Amro, H. 1996a. Radiological and chemical hazards associated with natural series radionuclides in the Amman-Zarqa basin, Jordan: a case study. 449-464, In: *6th Spanish Congress and International Conference on Environmental Geology and Land-Use Planning*, *Natural Hazards, Land-use Planning and Environment*, Vol. III, Chacon, J and Irigaray, C (eds).

Smith, B, Powell, J H, Gedeon, R, and Amro, H. 1996b. Groundwater pollution by natural radionuclides: an evaluation of natural and mining contamination associated with phosphorite (Jordan). 375-394, In: *Minerals, Metals and the Environment II*, Prague. Conference Proceedings. Institution of Mining and Metallurgy, London.

Smith, B, Hutchins, M.G., Powell, J H, Talbot D, Trick, J K, Gedeon, R, Amro, H, Kilani, S, Constantinou, G, Afrodisis, S, and Constantinou, C. 1997. The distribution of natural radioelements in groundwaters and Cretaceous-Neogene sediments from the south-east Mediterranean region. *Presented at the 4th International Environmental Geochemistry Symposium, Vail, Colorado*, Oct. 1997.

Stemmerik, L., Surlyk, F., Klitten, K., Rasmussen, L., and Schovsbo, N., 2006, Shallow core drilling of the Upper Cretaceous chalk at Stevns Klint, Denmark, *GEUS Geological Society of Denmark and Greenland Bulletin* **10**: 13-16.

Turekian, K. and Wedepohl, K., 1961, Distribution of the elements in some major units of the earth crust, *Geological Society American Bulletin* **72**: 175-192.

Wriekat, A., Abdullah, M., and Saffarini, G., 1987, The determination of U and Th in some Jordanian mineral deposits using natural gamma ray spectroscopy, *Dirasat* **14**: 187-191.

الجامعة الهاشمية

المملكة الأردنية الهاشمية

المجلة الأردنية

لعلوم الأرض والبيئة

JJEES

مجلة علمية عالمية محكمة

http:// jjees.hu.edu.jo/

ISSN 1995-6681

المجلة الأردنية لعلوم الأرض والبيئة

مجلة علمية عالمية محكمة

المجلة الأردنية لعلوم الأرض والبيئة : مجلة علمية عالمية محكمة أسستها اللجنة العليا للبحث العلمي في وزارة التعليم العالي والبحث العلمي، الأردن، وتصدر عن عمادة البحث العلمي والدراسات العليا، الجامعة الهاشمية، الزرقاء، الأردن.

ترسل البحوث إلى العنوان التالي:

رئيس تحرير المجلة الأردنية لعلوم الأرض والبيئة
عمادة البحث العلمي والدراسات العليا
الجامعة الهاشمية
الزرقاء ١٣١٣٣ - الأردن
فرعي: 4147 هاتف : 3903333 (5) 962+
Email: jjees@hu.edu.jo
Website: www.jjees.hu.edu.jo